NISTIR 4433

Performance of 1/3-Scale Model Precast Concrete Beam-Column Connections Subjected to Cyclic Inelastic Loads

Geraldine S. Cheok
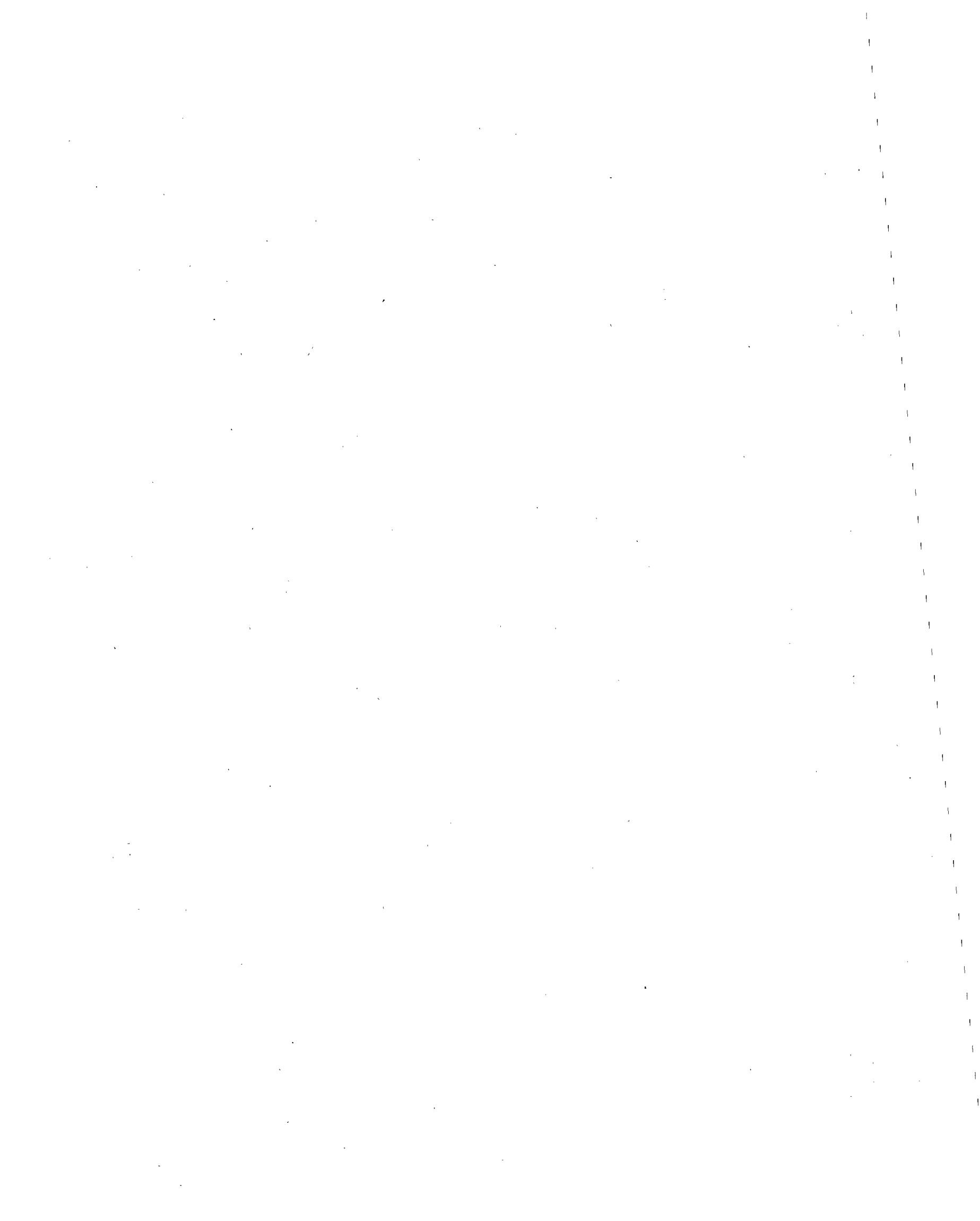H. S. Lew

October 1990

ABSTRACT

An experimental study of the behavior of precast concrete beam-column connections subjected to cyclic inelastic loading was initiated at the National Institute of Standards and Technology. The study was initiated to provide data for the development of a rational design procedure for such connections in high seismic regions. The objective of the study is to develop a moment resistant precast concrete connection that is economical and easily constructed. Results of the experimental tests of both monolithic and precast beam-column connections are described. The monolithic concrete specimens were designed to 1985 UBC Seismic Zone 2 and 4 criteria. The design of the precast concrete specimens was similar to that for the monolithic specimen designed to UBC seismic zone 4. The results from the monolithic specimens provide a benchmark for comparison with the results from the precast tests.

The experimental program is divided into three phases. This report presents the findings of the first phase of the test program. Comparisons of the performance of the monolithic beam-column joints with that of the precast joints in which the beam-to-column connection is provided by post-tensioning bars are presented. The effects of fiber reinforced grout between the beam and column are described. Comparisons are made between the energy dissipation, ductility, and failure mode for the two types of beam-column joints.

KEYWORDS: beam-column; buildings; connections; cyclic loading; interior joint; joints; moment resistant; precast concrete; post-tensioned; reinforced concrete.

ACKNOWLEDGEMENT

TABLE OF CONTENTS

List of Tables

List of Figures

1.0   INTRODUCTION

1.1   General

Many experimental and analytical studies have been conducted in the past on the performance of reinforced monolithic concrete beam-column connections subjected to cyclic inelastic loadings. However, there have been only a limited number of studies on the performance of precast concrete connections and to a lesser extent moment resistant precast concrete beam-column connections. This is true even though precast concrete construction has been in use in the U. S. since the 1950's.

Due to the limited data available, it has been presumed that precast structures tend to be less ductile and tend to have a less stable inelastic response than cast-in-place structures. This is primarily because the inelastic strains are concentrated in the connections. As a result, only general provisions for the design of precast structures have been included in the U.S. building codes. This is illustrated in Section 5004 of the UBC [12] which states that the design of connections for prefabricated structures should be as required for monolithic or cast-in-place structures. The UBC is the code that is most commonly used or referenced in seismically active areas in the U.S and as a result, precast construction is not prevalent in these regions.

The need for a more comprehensive guideline for precast concrete structures has been recognized by both designers and researchers [1, 10, 7]. A workshop conducted by the Applied Technology Council on the design of prefabricated

1

concrete buildings for earthquake loads [1] was held in 1981 to determine current knowledge of precast structures and to identify research needs. Forty research areas were identified and the topic receiving the highest priority was one which called for the development of recommended practice for moment resistant beam-to-column connections [1].

In response to these needs, a study of the behavior of precast beam-column connections subjected to cyclic inelastic loading was initiated at the National Institute of Standards and Technology (NIST) in 1987. The goal of the test program was to develop recommended guidelines for the design of precast beam-column connections in seismically active regions. Emphasis is placed on an economical and constructible connection as economics is a key consideration in the undertaking of any construction project. A steering committee consisting of individuals from the precast industry, the private sector, and from academia agreed to work with NIST and to provide technical guidance throughout the project. This report details the experimental results of four monolithic concrete joint specimens designed to UBC Seismic Zones 2 and 4 criteria and two precast concrete connections designed to UBC Seismic Zone 4 criteria.

1.2   Scope of the Experimental Program

The overall test program involved the testing of 1/3-scale model interior beam-column connections. This scale was selected as a result of the size limitations imposed by the test facility at NIST. The experimental program consists of three phases and a report will be published at the end of each phase.

The first phase of the experimental program included the tests of two monolithic beam-column connections designed in accordance with 1985 UBC Seismic Zone 4 criteria and two monolithic beam-column connections designed in accordance with UBC Seismic Zone 2 criteria. The results from these tests were intended to provide a reference for comparison with later precast concrete connection tests. In addition to the monolithic specimens, two post-tensioned precast connections designed similarly to the monolithic zone 4 specimen were also tested. Zone 4 will be taken to mean UBC Seismic Zone 4 and zone 2 will be taken to mean UBC Seismic Zone 2 throughout this report.

The second phase of the project will involve the testing of three sets of post-tensioned beam-column specimens. Each set will consist of two replicates designed to investigate the effects of location and distribution of the prestressing bars and to determine if any difference in performance resulted when the post-tensioning bars were replaced by prestressing strands. Specimens in Set 1 are designed to zone 4 criteria. The only difference between the Phase II Set 1 specimens from the precast specimens in Phase I will be the location of the post-tensioning bars. The specimens in Set 2 are also designed to zone 4 criteria and the location of the post-tensioning force depends on the results of the first two sets of post-tensioned specimens. Prestressing strands are used instead of post-tensioning bars in the Set 2 specimens as the use of strands is more common in field practice. The third set of specimens will be designed to seismic zone 2 criteria and will be post-tensioned with strands.

Phase III of the program will consider the effects of high concrete strength, the presence of precast slabs, prestressed beams and the effects of member aspect

ratios (span/width). Some areas in this phase will be coordinated with the Precast Seismic Structural Systems (PRESSS) project. PRESSS is part of the U.S.-Japan large scale testing program and is a multi-year cooperative project involving several universities and the private sector. In brief, the intent of PRESSS is to develop comprehensive design recommendations based on research data for precast concrete construction in seismic zones. The first phase of PRESSS commenced in 1989.

2.0 LITERATURE REVIEW

In recent years, several studies have been conducted on the behavior of precast beam-column connections designed to resist earthquake loads. A summary of these studies is presented in following sections.

2.1 New Zealand Studies

A study on the behavior of four full-scale exterior post-tensioned precast beam-column connections (Units 1 to 4) was conducted by Blakeley and Park [3] at the University of Canterbury. The columns were prestressed and the beams were lightly prestressed. The joint between the beam and column was filled with mortar. Units 1 and 2 were designed so that plastic hinging occurred in the beams at the joint while Units 3 and 4 were designed so that plastic hinging occurred in the column immediately above or below the beam. The transverse reinforcement for Units 1 and 3 satisfied the shear requirements for prestressed concrete. The transverse reinforcement for Units 2 and 4 was increased to determine the effect of increased confinement on ductility. The mortar joints for Units 2 and 4 were internally bound with light wire while those for Units 1 and 3 were not. The beam and column details are shown in Figs. 2.1 and 2.2. Prestressing strands were used to connect the precast elements. The specimens were tested cyclically.
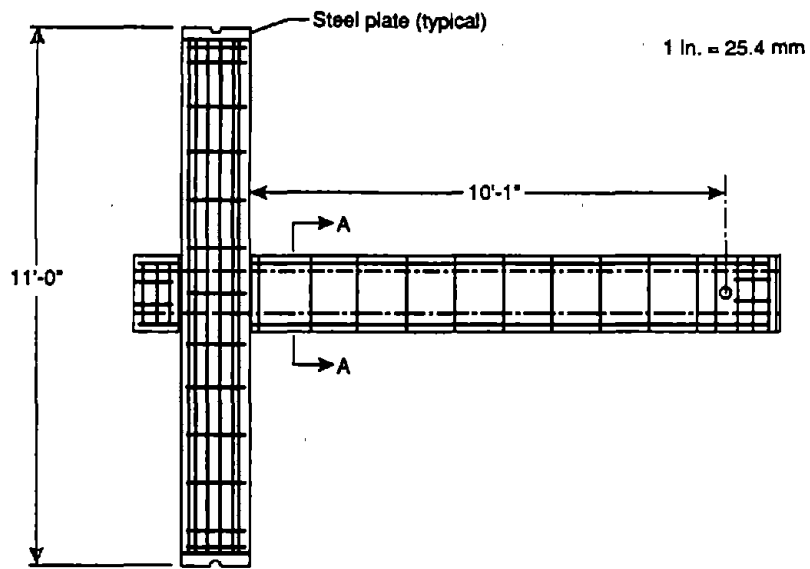
Fig. 2.1 Blakeley and Park's specimens [3].
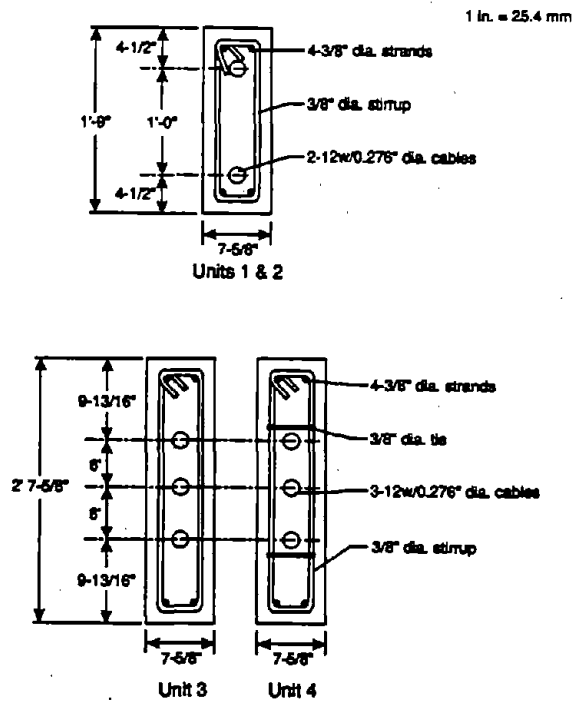
Fig. 2.2 Cross sections of Blakeley and Park's specimens [3].

6

The test results showed that the connections had low energy dissipation capacities prior to crushing of the concrete but showed a substantial increase in energy dissipation once concrete crushing occurred. Test specimens with the increased transverse reinforcement did not exhibit any significant improvement in performance. The mortar joints performed satisfactorily and it was recommended that corrugated metal ducts be used for the post-tensioning cables to prevent bond failure between the ducts and the column.

Bull and Park [4] tested 3 full scale exterior precast beam-column connections at the University of Canterbury. The specimens were composite connections consisting of a precast prestressed beam shell with a cast-in-place (CIP) concrete core as shown in Fig. 2.3. The CIP concrete was a two step process. The lower column was cast first up to where the precast beam shell would be seated. When the precast beam shell was placed on the lower column, the upper column and the beam core were then cast.

Specimens 1 and 3 were detailed for seismic loads while Specimen 2 was not. The difference between Specimens 1 and 3 was the bonding of the interface between the beam shell and the CIP concrete in the plastic hinge region. Specimen 3 was debonded over a length equal to the depth of the CIP beam core.

The specimens were loaded axially up to $0.1 \, f'_c \, A_g$. The loading history of the specimens was 2 cycles at $\pm 1 \, \Delta_y$, 4 cycles at $\pm 2 \, \Delta_y$, 4 cycles at $\pm 4 \, \Delta_y$, and 2 cycles at $\pm 6 \, \Delta_y$. The yield displacement, Δ_y, was defined as 1.33 times the displacement of the beam end measured at 75% of the theoretical ultimate

7

strength. Satisfactory behavior was defined as the retention of 80% of the specimen strength after 4 cycles at 4 Δ_y.
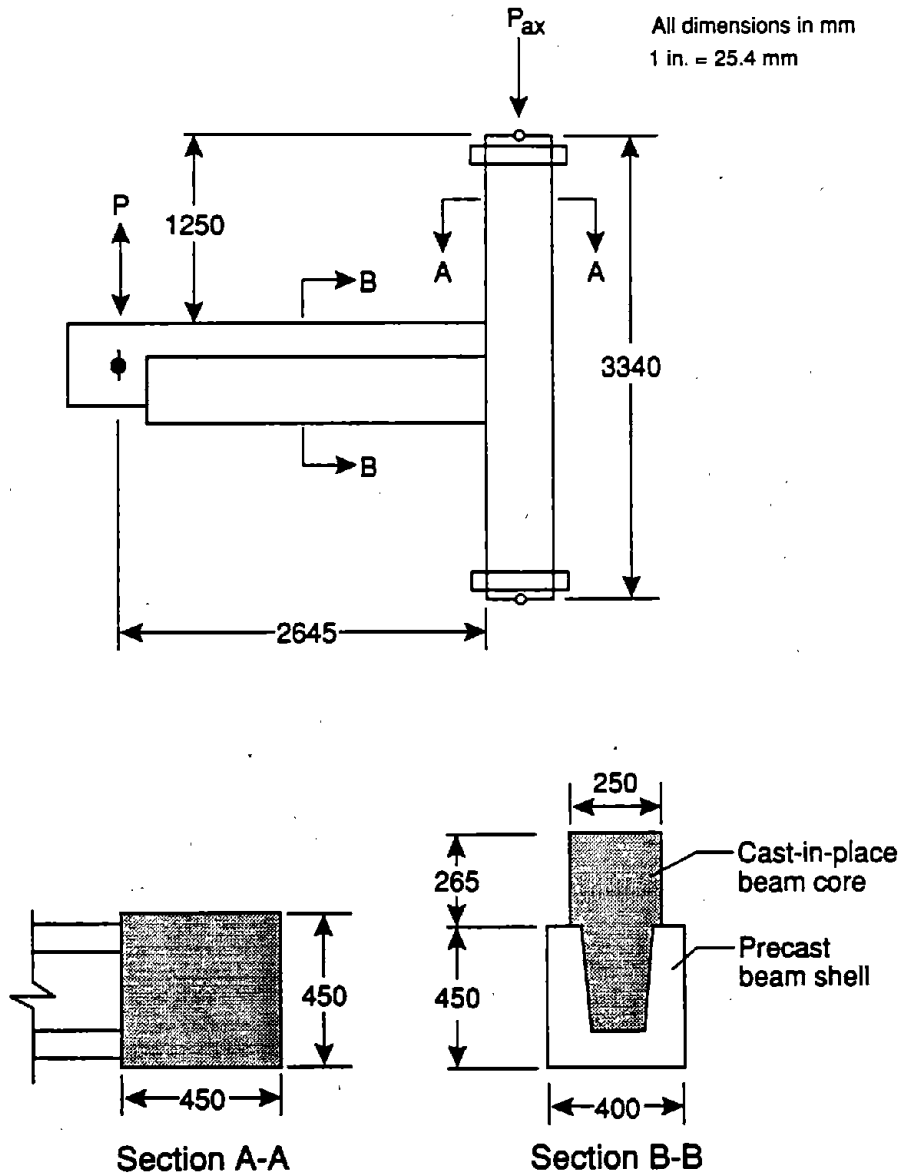
Fig. 2.3   Bull and Park's composite specimens [4].

Specimens 1 and 3 performed satisfactorily in terms of strength, ductility and energy dissipation and could, therefore, be used in ductile seismic moment

resisting frames. Specimen 3, the debonded specimen, had a longer plastic hinge length in the CIP concrete than Specimen 1. The precast shell in Specimen 3 sustained no damage while the precast shell in Specimen 1 sustained extensive cracking. Specimen 2 experienced sliding shear displacements in the beam at the column face and small energy dissipation.

2.2 Canadian Studies

Pillai and Kirk [15] tested 11 moment resisting exterior beam-column connections at the Royal Military College. Two of the eleven specimens were cast monolithically. All the precast connections were welded connections. The main variable in these tests was the shear span. The specimens were subjected to cyclic loads - one cycle at 0.75 θ_y, two cycles at 2 θ_y, one cycle at 0.75 θ_y, two cycles at 4 θ_y, one cycle at 0.75 θ_y, etc. The yield rotation, θ_y, was defined as the rotation of the beam relative to the column over a length of 15.75 in. assuming elastic behavior up to the theoretical ultimate strength. An axial load of 75.3 kips was applied to the columns. Satisfactory performance was defined as the ability of the connection to maintain 80% of its theoretical ultimate moment after 8 cycles of loading. The connection detail is shown in Fig. 2.4.

1 in. = 25.4 mm
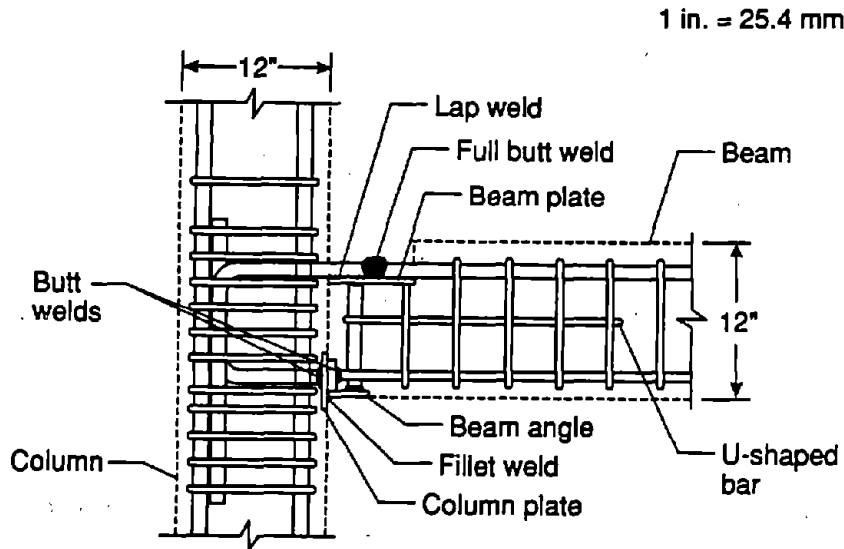
Fig. 2.4 Pillai and Kirk's welded exterior connection [15].

The tests indicated that the precast specimens with the welded connections performed as well as and in some cases better than the monolithic specimens and exhibited adequate ductility. Failure of the specimens was caused by the deterioration of the compression side of the beam. Some of the specimens experienced weld fracture. The specimens showed good energy dissipation characteristics. The connection detail was adequate to allow plastic hinging to occur in the beams.

In a subsequent study by Bhatt and Kirk [2], four precast connections with modified connection details were tested. The modifications were made to prevent weld fracture between the beam bars and column plate as experienced in the study by Pillai and Kirk. This was accomplished by increasing the weld length between the column anchorage and column plate by replacing the column plate (Fig. 2.4) with a T-section. Two of the specimens were exterior beam-column connections and two were interior beam-column joints. The test procedure was similar to

10

previous tests conducted by Pillai and Kirk. The modified specimens demonstrated ductile behavior with no weld fracture. The beams had not failed when the test was stopped once ductile behavior was demonstrated.

Another study conducted at the Royal Military College by Seckin and Fu [17] also examined the behavior of a welded precast connection. Four interior connections were tested in which one was a monolithic connection while the other three were precast connections. The specimens were loaded cyclically at the beam ends and the column was subjected to an axial load of 108 kips which is approximately 10% of the design axial strength of the column. The connections between the precast beam and column were made by welding plates embedded in the beam to plates embedded in the column. Two sets of plates were used; one set to resist flexural stresses and another to resist shear stresses. The flexural plates were located at the top and bottom of the beam while the shear plates were located vertically in the middle of the beam. Flexural reinforcement in the beams was welded to the flexural plates. Fig. 2.5a and Fig. 2.5b give an overall view of the connection.

1 in. = 25.4 mm

15 mm bar

Column shear plate

Beam shear plate

Beam flexure plate
20 mm bar

Column flexure plate
(not shown completely)
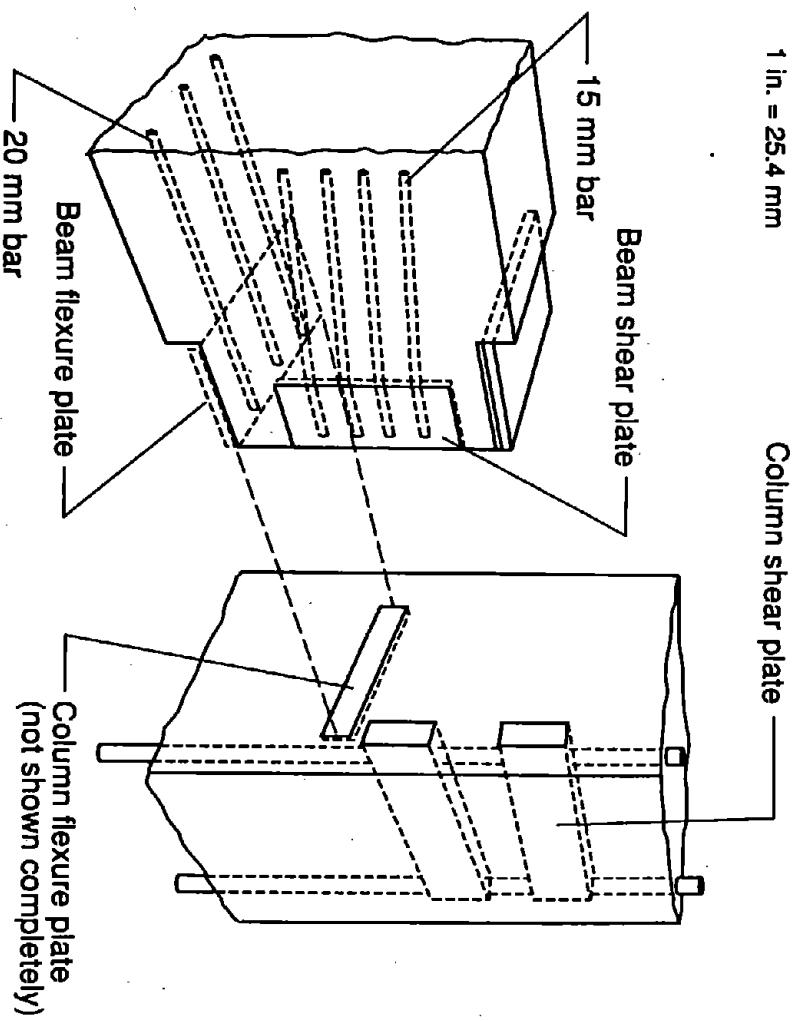
Fig. 2.5a Seckin and Fu's connection [17].
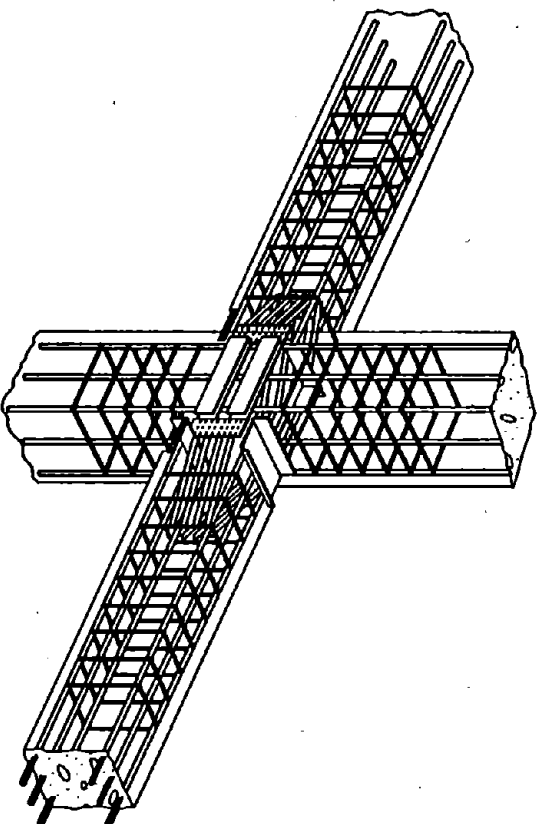
Fig. 2.5b Overall view of Seckin and Fu's test specimens [17].

12

Failure of one of the precast specimen was due to the fracture of the rebars in the beams and failure of the other two precast specimens was a result of weld fracture between the column shear plates and shear connector. No significant slippage of the beam bars occurred during the tests. Conclusions drawn from the test program were that the precast connections performed as well as the monolithic specimen in terms of ductility, energy dissipation, and stiffness.

2.3   U. S. Studies

Martin and Korkosz [14] compiled a report on the state-of-the-art of precast concrete connection technology. In the report, approximately 100 precast connections were evaluated by professionals and producers in the precast concrete industry and by members of PCI. Evaluations were based on usage, simplicity, and durability. These evaluations were subjective. Connection types included in the survey were column-to-foundation, column-to-column, beam-to-column, slab-to-beam, beam-to-girder, beam-to-beam, slab-to-slab, wall-to-foundation, slab-to-wall, beam-to-wall, and wall-to-wall.

In a study sponsored by the Prestressed Concrete Institute (PCI), eight moment resistant and eight simple connections were tested by Stanton, et. al. [19] at the University of Washington. The objective of the program was to identify economical and competitive methods in designing precast connections. Only the results of the moment resistant connections are applicable to seismic design.

13

The moment connections consisted of a welded connection (BC15), a combination of a cast-in-place topping and a welded connection (BC16A), a bolted column-to-column connection (BC25 & CC1), a precast beam constructed into a CIP column (BC26), a post-tensioned connection (BC27), a connection grouted or partially grouted to dowels (BC28 & BC29), and a composite connection consisting of a precast beam shell filled with CIP concrete using post-tensioning bars as a means of attachment (BC99). Overall views of the different connection types are shown in Fig. 2.6 as taken from Reference 19. More detailed information on each of the connection types may be found in Reference 19. The specimens were 2/3-scale models of prototype connections. Some of the specimens were tested monotonically and some were tested cyclically. A 0.04 radian rotation was defined as the minimum requirement for a ductile frame.
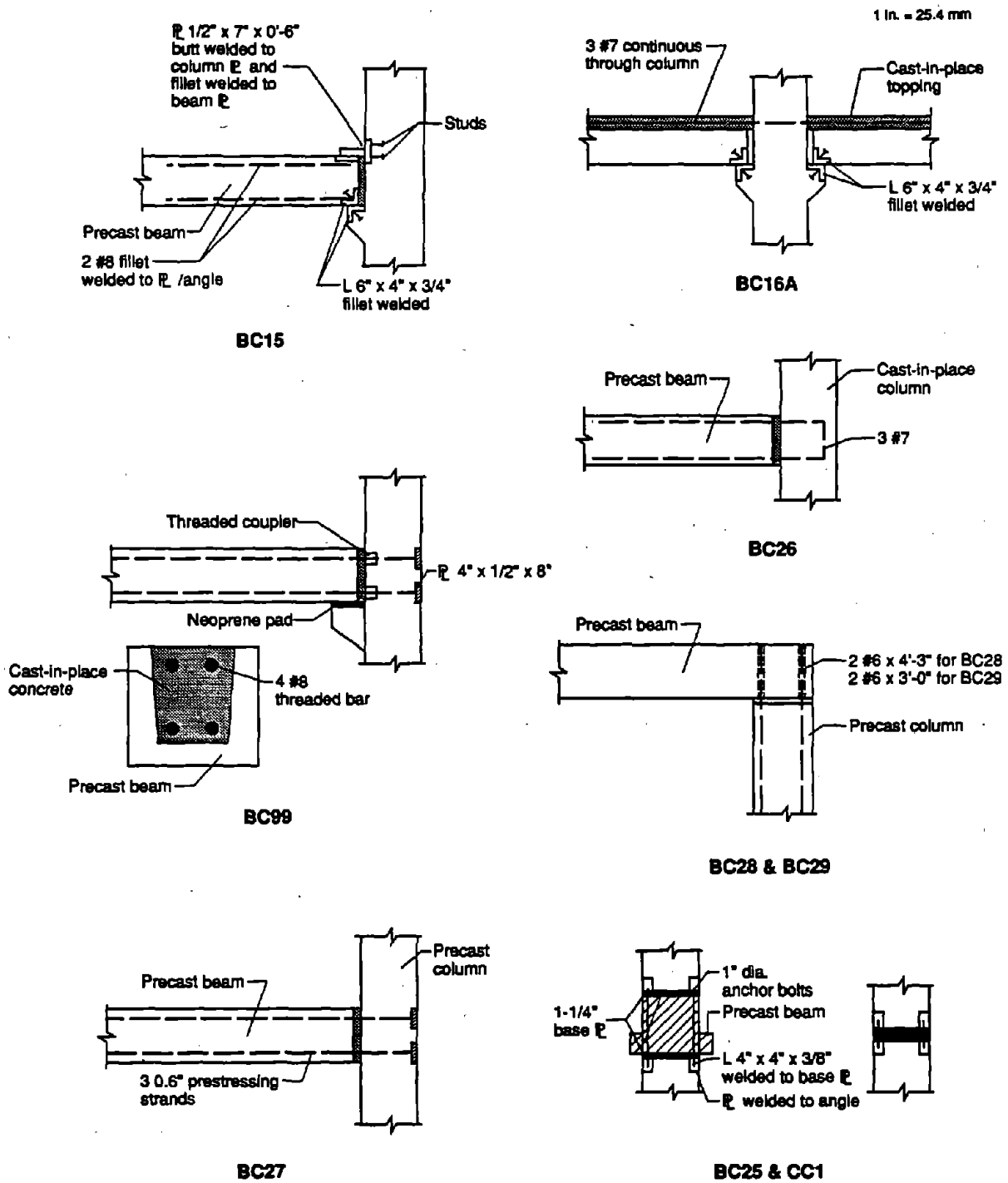
Fig. 2.6 Stanton's test specimens [19].

15

The results from these tests indicated that the dowel connections (BC28 and BC29) could not be classified as moment connections, specimens BC16A and BC27 could possibly be used in seismic zones 1 and 2, and specimens BC26 and BC99 could be used in seismic zones 3 and 4.

A series of 7 precast beam-column connections were tested at the University of Minnesota [8, 9]. The connection details varied from post-tensioning with two post-tensioning bars (BMA), a connection using four threaded rebars (BMB), a composite connection (BMC) consisting of a CIP topping and a precast beam connected with a post-tensioning bar, a welded connection (BMD), a bolted connection (BME), a connection with four threaded rebars which were threaded into couplers anchored in column (BMF), and a connection similar to connection BMF with the difference being the use of tapered-threaded splices (BMG). Specimens BMA - BMF were exterior connections and specimen BMG was an interior connection. Details of the connections are shown in Fig. 2.7.

All dimensions in inches
1 in. = 25.4 mm

Two 1-3/8" post-
tensioning rods

SECTION A-A

BMA

Four 1-3/8" post-
tensioning rods

Corrugated
duct

SECTION A-A

BMB

Cast-in-place topping

Three No. 9
threaded rebar

Duct (through column)

One 3/8" post-
tensioning rod

SECTION A-A

BMC

Weld

Four No. 11
rebar

Two No. 5
rebar

SECTION A-A   SECTION B-B

Weld

BMD

Fig. 2.7 French's beam-column connection details [8, 9].

17

Welded headed studs

1-1/4" anchor bolts

Four No. 6 rebar

Eight No. 3 rebar (tendons unbonded)

19

10

SECTION A-A   SECTION B-B

84

BME

35

10

Four No. 7 rebars

19

Threaded coupler

SECTION A-A

BMF

35   35

10

Four No. 7 threaded rebar

19

Detail A

BMG

℞ 3" x 7" x 1-1/4"

Fillet weld

Tapered coupler

Detail A

Fig. 2.7 (Cont.)   French's beam-column connection details [8, 9].

Specimens BMA - BMD were designed so that the plastic hinge was moved away from the connection region.   Specimens BME - BMG were designed so that the plastic hinge occurred in the connection region.   The beams were partially prestressed. The column was square with 14 in. sides and the beam dimensions were 19 in. deep by 10 in. wide.   The design compressive strength was 6000 psi.   The loading sequence was two cycles each at 0.75 Δ_y and 2 Δ_y, three cycles each at 3 Δ_y and at 4 Δ_y and to the full stroke of the actuator.   The yield displacement was

18

computed based on the dimensions and capacity of specimen BMB and using the effective moment of inertia of the beam and the gross moment of inertia of the column. The load was applied at the beam end.

The specimens with the plastic hinge occurring at the joint region showed better energy dissipation characteristics than those with the plastic hinge occurring in the prestressed beams. Specimens BMA - BMD achieved interstory drifts of at least 3.3% while specimens BME-BMG achieved interstory drifts greater than 4%. In general, the threaded rebar connection with the tapered splices and the composite connection appear to be the most likely candidates for use in seismically active regions.

A test program at the University of Michigan conducted by Soubra, et. al. [18] studied the characteristics of fiber reinforced concrete (FRC) composites and examined the use of FRC in the joint between two precast elements. The specimens were made up of two precast beams connected with a CIP joint to form a beam as shown in Fig. 2.8. The beam was loaded cyclically at the third points. In this study, the parameters included fiber type, volume of fiber and matrix type - mortar or concrete. Six specimens were tested cyclically. The performance of the FRC joints was measured against the performance of a joint constructed using regular concrete.
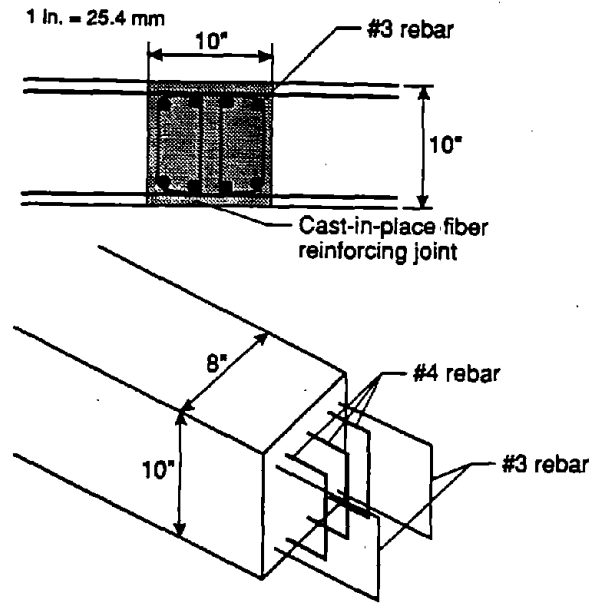
Fig. 2.8 Soubra's fiber reinforced concrete joint [18].

Failure of the specimens was initiated by a single flexure crack which led to the eventual fracture of one or more rebars in the CIP joint. Conclusions drawn from the study were that FRC joints performed better than joints cast with regular concrete and that FRC joints with steel fibers performed better than FRC joints with plastic fibers.

2.4 Other Studies

The Japanese permit the use of precast joints which have been proven to have acceptable levels of strength, rigidity, and ductility [11]. Joint acceptance is based on unit testing and member testing methods. Procedures for these test methods and classifications of the joints based on the results of these tests are outlined by the Building Center of Japan. As a result of this qualification method, much of the research on the precast framing system in Japan is funded

by the designer and/or contractor and is therefore proprietary. Some such systems are discussed in Reference 13.

The following European studies involve connections with embedded structural steel sections in the precast elements. The specimens were monotonically tested.

Precast joints using embedded structural steel and a CIP topping was investigated by Clarke [6]. Ten half-scale exterior beam-column joints and three half-scale interior beam-column joints were tested. In addition, three full-scale exterior joints were also tested. The joint consisted of a precast beam with an embedded U-shaped steel insert which rested on a projecting steel billet embedded in a precast column. Continuity between the beam and column was provided by steel bars threaded into couplers located in the column, by projecting stirrups in the beam and by a CIP topping. The connection details are shown in Fig. 2.9.

All dimensions in mm
1 in. = 25.4 mm
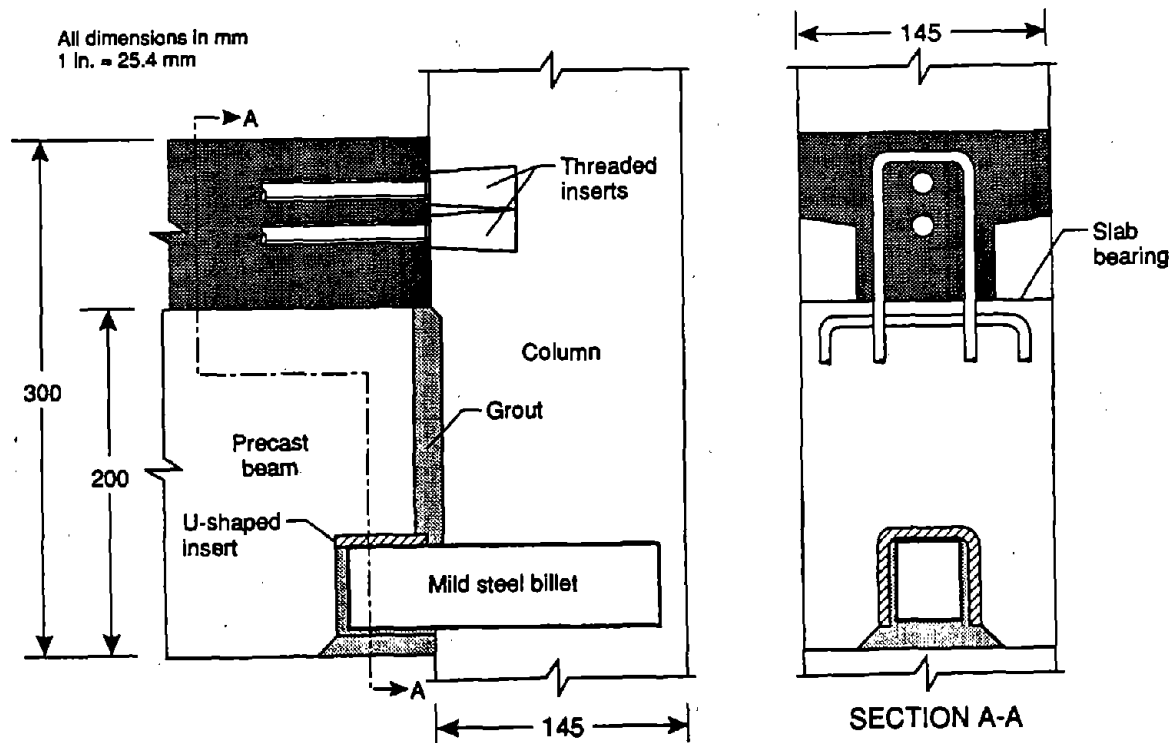
Fig. 2.9 Clarke's exterior connection [6].

Failure of the half-scale exterior connections was evidenced by splitting of the beam above the steel billet. This failure mode was prevented in the half-scale interior connections by the addition of horizontal links above the steel insert in the beams. Specimens constructed with intentional flaws simulating poor construction practices indicated that the design ultimate strength of the connection could be as much as 60% of the strength for a joint constructed without flaws. The average experimental strength of the properly constructed connections was 1.6 times the design ultimate strength. Of the three full-scale specimens, one failed at 1.5 times the design strength with the billet

punching through the beam while the other two achieved a strength of 1.8 times the design strength without any indications of distress. The test was stopped due to limits of the test equipment.

Wilby [20] tested twenty connections of which nine were monolithic and eleven were bolted connections. The specimens were two span continuous beams with the joint located to one side of the center support simulating an exterior beam-column joint. Both beams were then loaded at 1/3 points. The connection was made by bolting together a structural T-section embedded in one precast beam to two angles embedded in the other precast beam with a CIP topping poured over both beams. The bolts acted in double shear as shown in Fig. 2.10. The reinforcement was welded to the T-sections. The main variable in the test was stirrup arrangement. In one arrangement, stirrups were located over the supports and continuous through the joint. The second arrangement was similar to the first except for the discontinuity of the stirrups in the joint. The third arrangement consisted of stirrups spaced evenly over the entire specimen. The average concrete strengths for the beams, joints and topping were 5000 psi, 5195 psi, and 3719 psi, respectively.
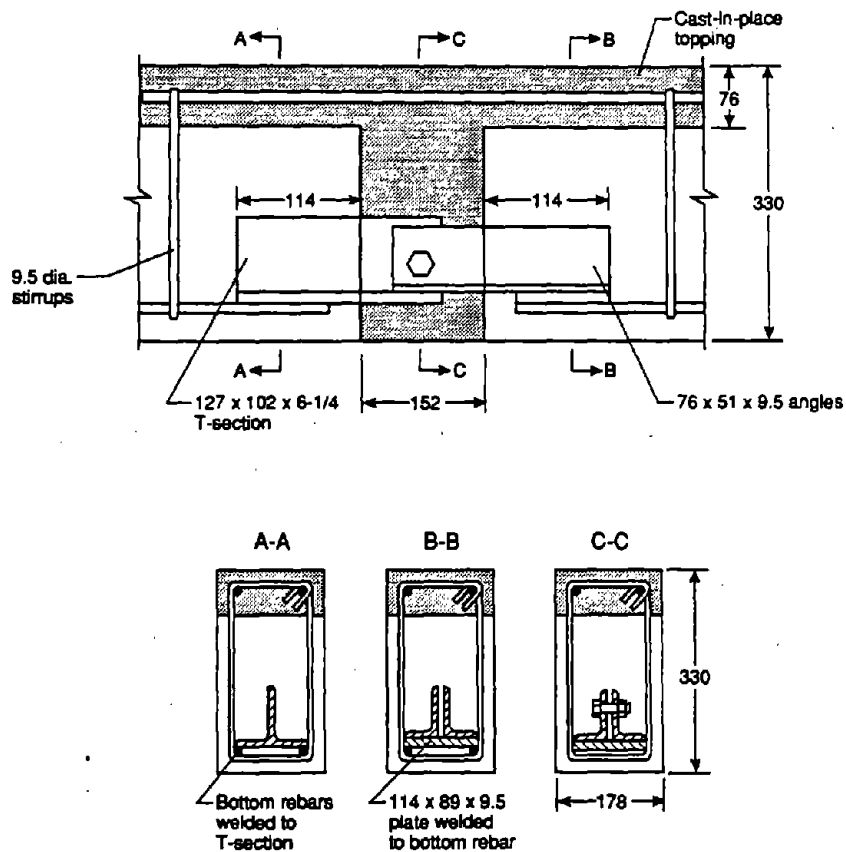
Fig. 2.10 Wilby's bolted connection [20].

The results of the tests indicated that the joints with the stirrups continuous over the joint performed as well as the monolithic joints. The performance appeared to be independent of whether the stirrups were evenly spaced over the beams or whether the stirrups were just located over the supports but at a closer spacing. The performance of joints where the precast surfaces were not roughened was poorer than for those in which the surfaces were roughened.

24

A study by Reinhardt and Stroband [16] dealt with precast joints where the shear and moment was transferred by embedded steel plates connected with dowels driven through slotted holes in the plates. The slotted holes were angled at 45° in one element and 145° in the other element. This permitted larger tolerances for fabrication and construction errors. The dowels were square, hardened and ribbed. The ribs caused the dowel to bite into the plates when driven in - thus forming a rigid connection. A schematic of the connection is given in Fig. 2.11. Variables in the test included moment/shear ratio, plate anchorage, steel strength, and grouted or ungrouted joint. The results indicated that the connection was capable of transferring shear and moment provided the joint was grouted and the plates were anchored properly. Proper anchorage included embedding the plate at least 18 in., connecting the upper and lower plates with four rebars, and having studs on both sides of the plates. Adequate transverse reinforcement in the joint region was also required to prevent beam splitting.
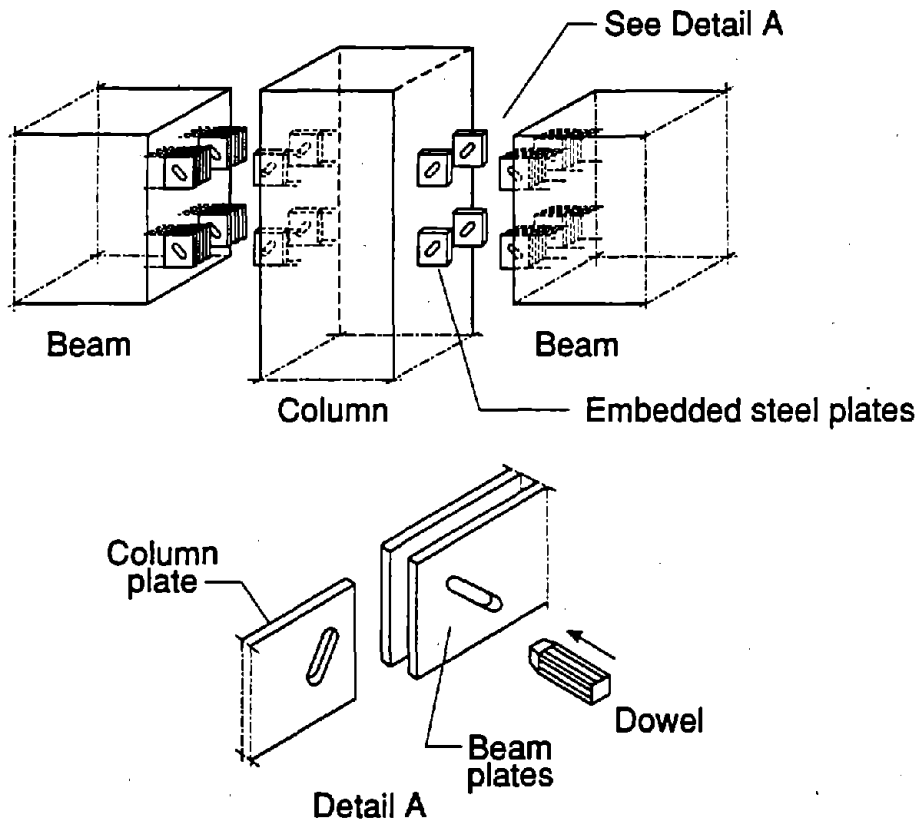
Fig. 2.11 Reinhardt and Stroband's connection [16].

NOTE:

1 in. — 25.4 mm

1 kip — 4.448 kN

1 k-in. — 112.98 N-m

1 ksi — 6.895 MPa

3.0 SPECIMEN DESIGN AND TEST PROCEDURE

3.1 Introduction

Through discussions with the advisory committee, it was determined that the precast details to be tested in this program should be typical of those that would be used for office buildings constructed in seismic zones 2 and 4. The prototype structure was a 15-story office building with a floor plan of 200 ft (8 bays) by 100 ft (4 bays) and a story height was 13 ft. The subassemblages selected for testing were typical of interior beam-column joints for this building.

The specimens consisted of a precast column and two precast beams. Post-tensioning bars were used to connect the precast elements. Several types of precast connections were considered among which were welded connections, connections with a cast-in-place topping, bolted connections, post-tensioned connections, or a combination of these types of connections. However, in keeping with the objective of the test program, a post-tensioned precast connection was considered to be the most economical as it would be easy to construct and enable rapid erection. Steel angles bolted to the precast column would be used in actual field practice as temporary supports for the precast beams until they were grouted and post-tensioned to column. Such temporary supports were not used for the model specimens as they were not needed in a laboratory environment.

3.1.1 Zone 2 Specimen Design

A 1/3-scale factor was dictated by maximum size that the test facility at NIST [7] can accommodate. The model beam was 6-2/3 in. wide by 10 in. deep while the model column dimensions were 8-2/3 in. wide by 10 in. deep. The corresponding dimensions for the prototype were a beam 20 in. wide by 30 in. deep and a column 24 in. wide by 30 deep. The compression steel in the beam consisted of 6 #4 and the tension steel consisted of 8 #3 rebars; resulting in a ρ_s of 1.3 % and a ρ'_s of 1.8 %. The beam stirrups were spaced at 2 in. The column steel consisted of 4 #3 rebars and 3 #4 rebars top and bottom with a tie spacing of 2 in. The reinforcement details are shown in Fig. 3.1. Both beam and column longitudinal reinforcement was ASTM Grade 60 steel. Smooth wire with a diameter of 0.207 in. was used to construct the ties and crossties for both beam and column. The actual material properties are given in Table 3.1.

The design concrete strength was 5000 psi. The concrete used to construct the specimens was ready-mixed concrete obtained from a local concrete plant. The maximum aggregate size was 3/8 in. A water reducer was added to the mix to increase the slump for easy placement. This was necessary due to the congestion of the steel in the column. The same design mix was used for all the specimens. Actual concrete strengths obtained from tests of 4 in. x 8 in. cylinders at the time of the specimen tests and strengths at 28 days are given in Table 3.2. The cylinders tested at the time of the specimen tests were cured in the same environment as the test specimens while the 28-day strengths were obtained from cylinders which were moist-cured.
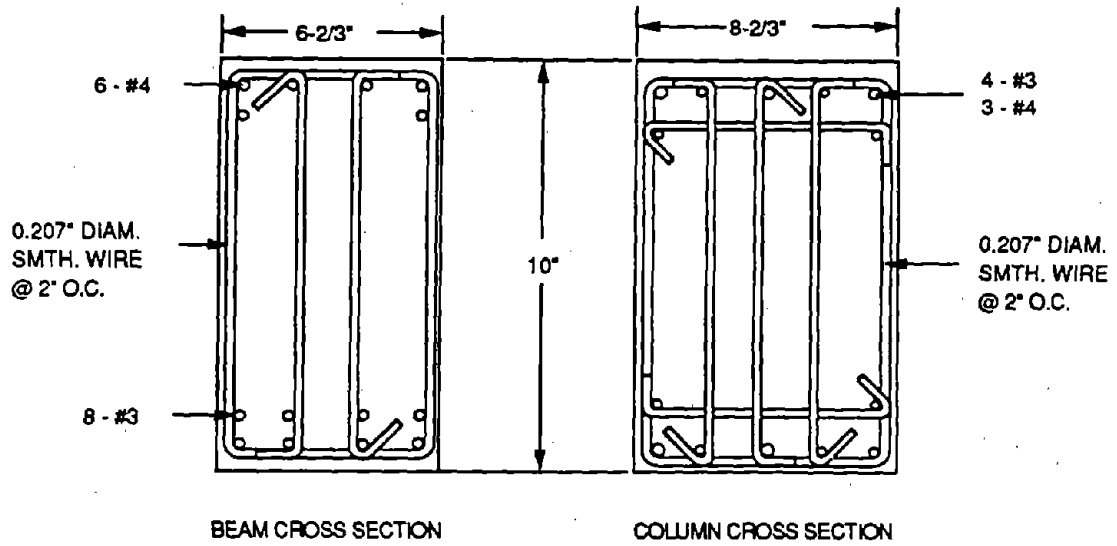
Fig. 3.1 Reinforcement details for the UBC zone 2 specimens.

Table 3.1 Reinforcement Properties.

Specimen	f_y (ksi)				f_u (ksi)			
	Wire	#3	#4	PT[1]	Wire	#3	#4	PT[1]
A-M-Z2	73.4	74.2	68.4	-	82.0	112.3	106.0	-
B-M-Z2	73.4	74.2	68.4	-	82.0	112.3	106.0	-
A-M-Z4	73.4	74.2	68.4	-	82.0	112.3	106.0	-
B-M-Z4	73.4	74.2	68.4	-	82.0	112.3	106.0	-
A-P-Z4	83.3	67.6	60.7	148.5	91.0	90.0	97.4	159.6
B-P-Z4	83.3	67.6	60.7	148.5	91.0	90.0	97.4	159.7

1   1 inch diameter post-tensioning bar.

Table 3.2 Concrete and Grout Strengths.

Specimen	f'_c (psi)		Duct Grout (psi)		Joint Grout (psi)	
	28-day	Test date[1]	28-day	Test date[1]	28-day	Test date[1]
A-M-Z2	5838	6314	-	-	-	-
B-M-Z2	5838	5962	-	-	-	-
A-M-Z4	4675	4452	-	-	-	-
B-M-Z4	4675	4675	-	-	-	-
A-P-Z4	5915	5891	9785	8687[2]	10721	10677
B-P-Z4	5915	6450	9785	9542	10721	11437

[1] These cylinders and cubes were stripped at the same time as the test specimen and allowed to cure in the same environment as the test specimen.

[2] Specimen A-P-Z4 was tested before the duct grout reached 28 days.

The specimens were pinned at the column bottom and roller supported at the beam ends and the column top as shown in Fig. 3.2. These boundary conditions were felt to best model actual conditions where the moments are approximately zero at mid-span of the beam and the column.

	ZONE 2	ZONE 4	
	A-M-Z2 & B-M-Z2	A-M-Z4 & B-M-Z4	A-P-Z4 & B-P-Z4
a	10"	18"	18"
b	10	16	16
c	40	41-3/4	37
d	46	47-3/4	43

Axial Load

Loading direction
North-South
(East-West for B-M-Z4)
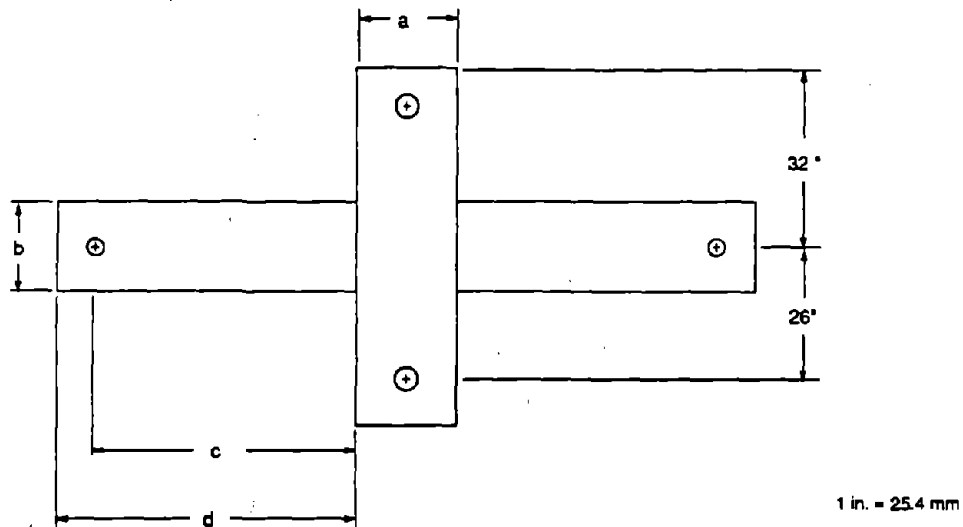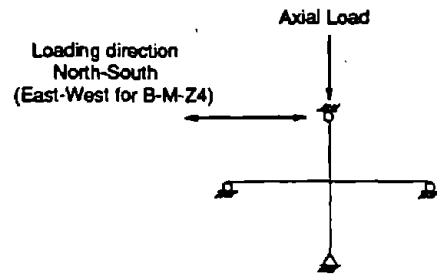

32 "

26"

1 in. = 25.4 mm

Fig. 3.2   Interior beam-column subassemblage.

3.1.2   Zone 4 Specimen Design

The model beam was 8 in. wide by 16 in. deep while the column dimensions were
10 in. wide by 18 in. deep.   The compression steel consisted of 9 #3 and the
tension steel consisted of 5 #3 and 2 #4.   This resulted in a ρ_s of 0.7% and a
ρ'_s of 0.8%.   The column steel consisted of 8 #3 and 4 #4 top and bottom.   The
monolithic zone 4 reinforcement details for both the beam and column are shown
in Fig. 3.3.   The reinforcement was ASTM grade 60 and the design concrete

31

strength was 5000 psi. Fig. 3.4 shows the tied column cage and the beam rebars during the construction process for the monolithic specimen.

The beam and column dimensions for the precast specimens were same as for the monolithic zone 4 specimens. The longitudinal reinforcement for the precast beams consisted of 4 #3 bars with one bar in each corner of the stirrup. The column steel was the same as for the monolithic specimen. The ties and crossties were made of smooth wire with a diameter of 0.207 in. Material properties are given in Table 3.1. No provisions were made to move the plastic hinge away from the column face.

1 in. = 25.4 mm

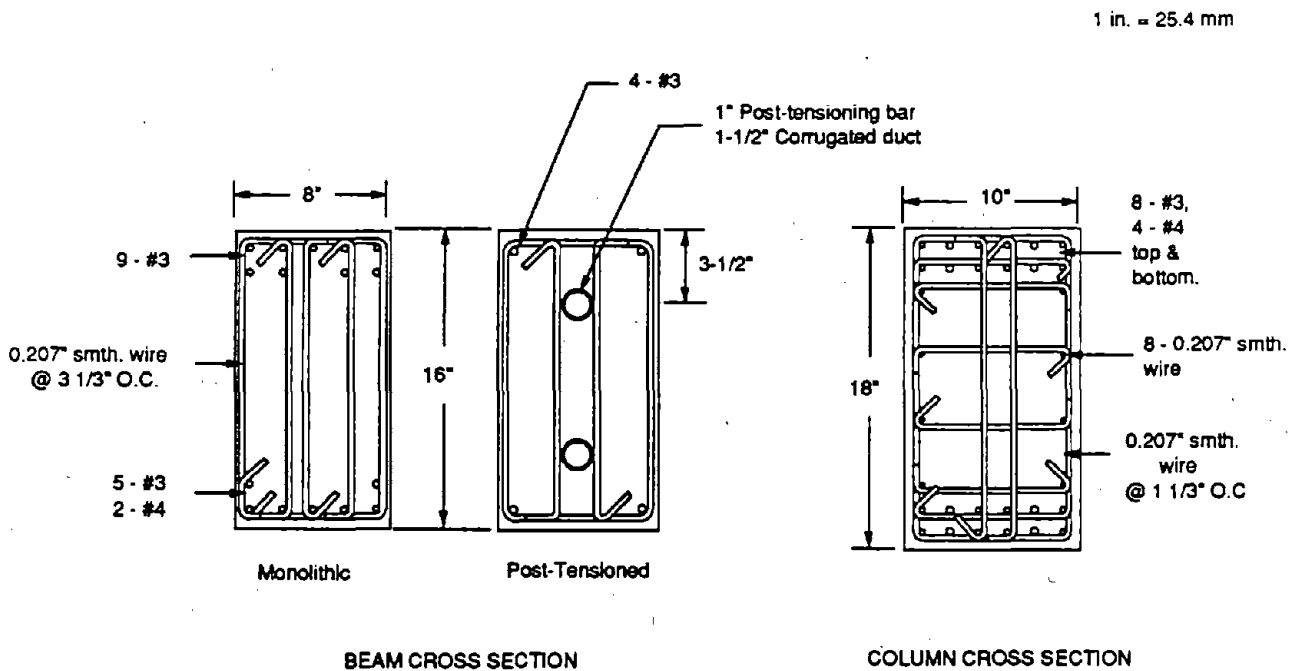BEAM CROSS SECTION   COLUMN CROSS SECTION

Fig. 3.3 Reinforcement details for the UBC zone 4 specimens.
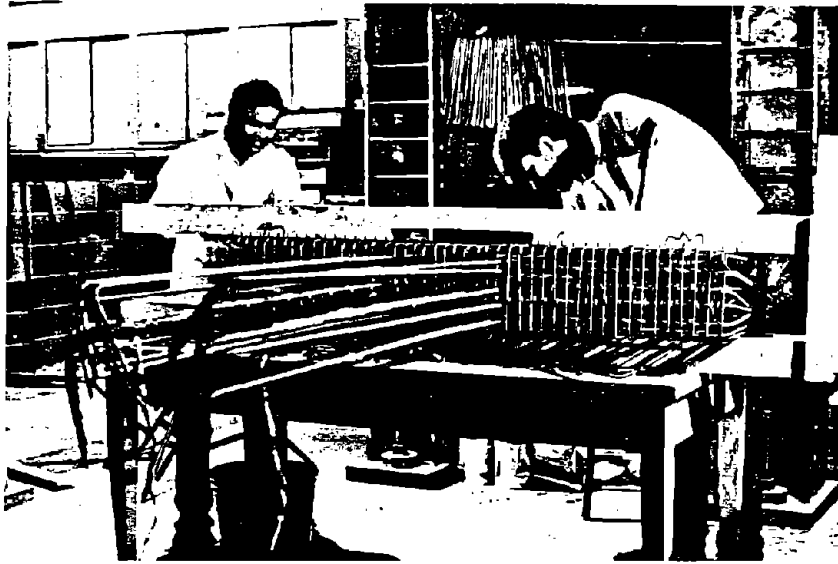
Fig. 3.4 Construction of the monolithic zone 4 specimens.

Two 1 in. diameter post-tensioning bars with an ultimate stress of 150 ksi were used to connect the precast beams to the precast column. The bars were located 3-1/2 in. from the top and from the bottom of the beam. The steel cages for the column and beam are shown in Figs. 3.5 and 3.6, respectively. In this first exploratory phase of the test program, post-tensioning bars were used instead of strands because prestress losses in short strands would be substantial due to seating losses. The initial post-tensioning load was 128.6 kips which resulted in an initial beam stress of 1008 psi. The losses in the post-tensioning bars would be minimal as the post-tensioning load was maintained while the nuts were tightened.
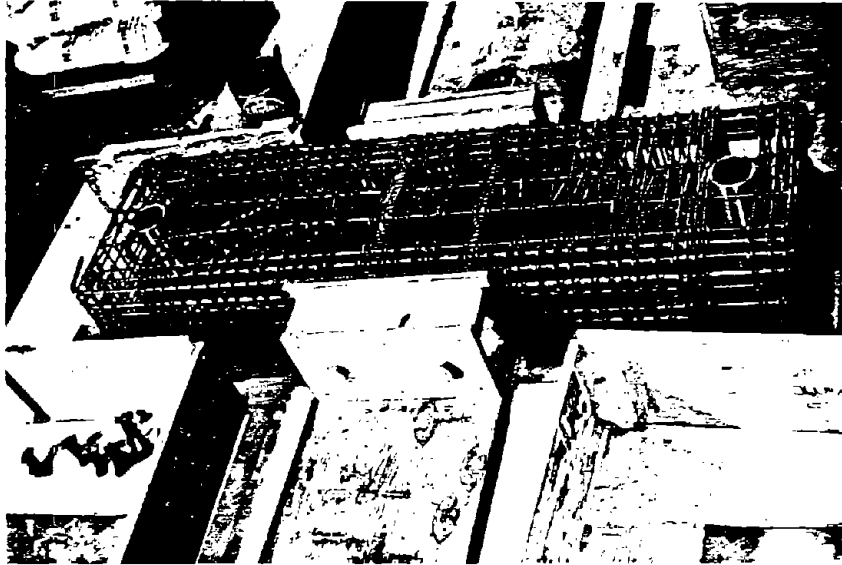
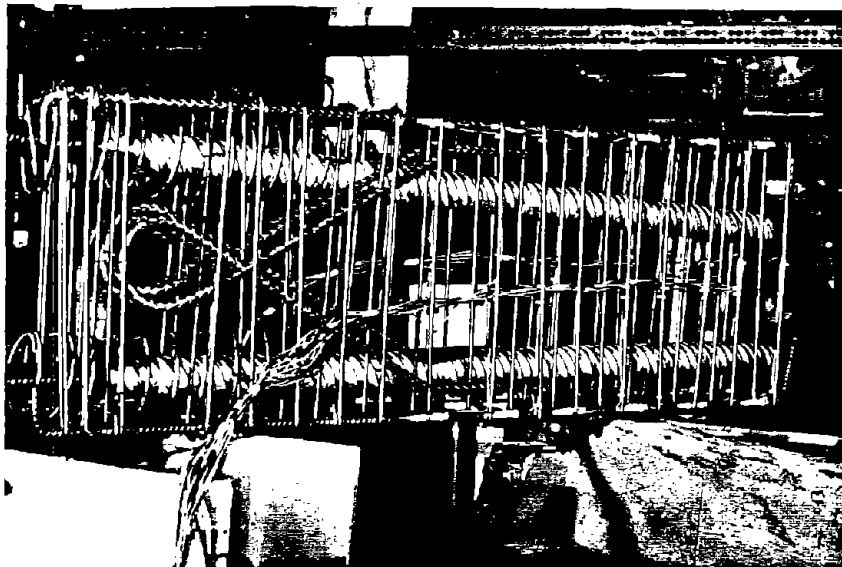Fig. 3.5 Column cage for the post-tensioned specimens.

Fig. 3.6 Steel cage for the post-tensioned beams.

34

The post-tensioning ducts were corrugated and were grouted with a grout having a design strength of 6000 psi. The inch wide construction joint was filled with a fiber reinforced grout. The joints were subjected to high compressive loads and it was felt that the fibers would hold the grout together. One and a half percent by volume of straight 3/4 in. long steel fibers were added to the grout mix. The design grout strength for the joint was 10000 psi. The actual grout strengths are given in Table 3.2. The grout used for both the ducts and joint was a pre-mixed non-shrink commercially available product. The faces of the beams and column were roughened to an amplitude of approximately 1/4 in. as required by the UBC [12] for placing concrete against hardened concrete.

3.2   Instrumentation and Test Procedure

Load cells were used to measure the applied loads to the beam and to the column. Strains in the beam and in the column were measured using resistance type strain gages. Beam curvature was measured at 3 locations along the beam using linear variable differential transducers (LVDT). Column rotation was measured at three locations using clinometers.

The vertical and lateral loads were applied as shown in Fig. 3.2. Each specimen was first loaded axially to $0.1 \, f'_c \, A_g$. The specimens were then laterally loaded in-plane to 75% of the calculated ultimate beam moment in the forward (south) direction and then in the reverse (north) direction. The top column displacements were recorded in each direction. The yield displacement, Δ_y, was then defined as the average of the two column displacements divided by 0.75.

35

Although this displacement is the displacement of the column top, it corresponds to yielding in the beam.

The specimen was then cycled twice at $\pm 2 \Delta_y$, $\pm 4 \Delta_y$, and three times at $\pm 6 \Delta_y$. The loading histories for the monolithic zone 2 and post-tensioned specimens varied slightly from this basic load sequence. Failure of a specimen was defined as the point at which the lateral load was less than 80% of the lateral load obtained for the first cycle at $2 \Delta_y$. The entire test was conducted under displacement control.

Displacement ductility, μ, is defined as the ratio of the maximum displacement attained at any cycle to the yield displacement. Ultimate ductility, μ_u, is defined as the ratio of the maximum displacement achieved for a specimen to the yield displacement.

NOTE:
1 in. = 25.4 mm
1 kip = 4.448 kN
1 k-in. = 112.98 N-m
1 ksi = 6.895 MPa

4.0   TEST OBSERVATIONS AND RESULTS

4.1   Monolithic Zone 2 Specimens

Two identical specimens, A-M-Z2 and B-M-Z2, detailed as shown in Fig. 3.1 were
tested. The loading sequence for the zone 2 specimens was one cycle at 0.75 Δ_y,
2 cycles at 2 Δ_y, 3 cycles at 4 Δ_y, and 2 cycles at 6 Δ_y as shown in Fig. 4.1.
Specimen B-M-Z2 underwent a third cycle at 6 Δ_y. Each column was loaded to 51.15
kips (0.1 f'_c A_g based on a 28-day concrete strength of 5900 psi). Both
specimens were loaded in-plane in the N-S direction.
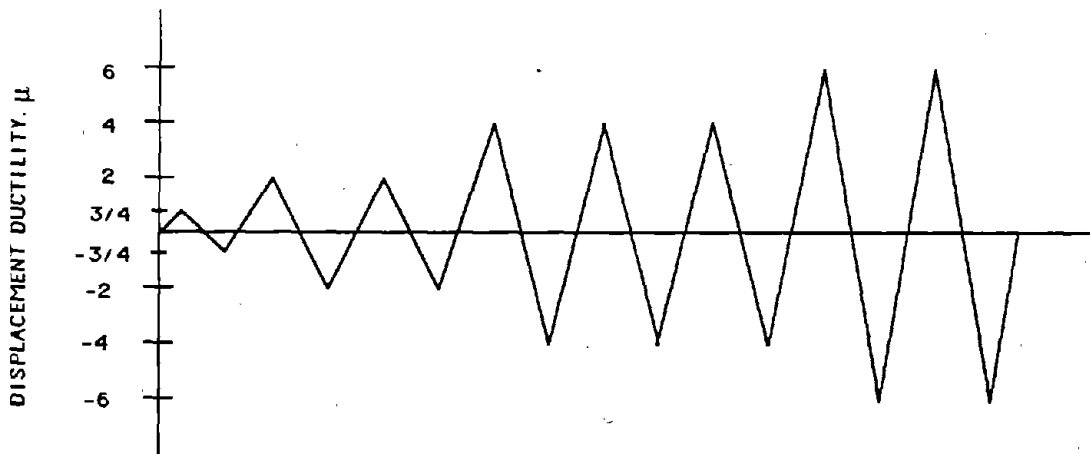
Fig. 4.1 Loading sequence for the monolithic zone 2 specimens.

Only hairline flexural cracks were observed in the beams at 0.75 Δ_y. Both
flexure and shear cracks were observed in the beams at 2 Δ_y. Shear and flexure
cracking of the column was also noted in the column joint region at this
ductility level. Fig. 4.2 shows the east face of specimen B-M-Z2 at 2 Δ_y.
Severe shear cracking followed by spalling of the concrete cover in the column

37

joint region occurred at 4 Δ_y. The column joint region of specimen B-M-Z2, Fig. 4.3, appeared to have sustained less damage than its companion specimen A-M-Z2, Fig. 4.4, at the same stage in the test. Propagation of existing cracks, formation of additional shear cracks and very minor crushing of one of the beams were also observed at 4 Δ_y. Crushing and severe spalling of the column occurred at 6 Δ_y. The joint regions of specimens A-M-Z2 and B-M-Z2 at the second cycle at 6 Δ_y are shown in Figs. 4.5 and 4.6, respectively. Figs. 4.4 and 4.5 show the same side of specimen A-M-Z2. Other than cracking, the beams did not experience any other damage at the end of the tests. The regions indicated by arrows in Figs. 4.4 through 4.6 were not spall zones. These regions were a result of the manner in which the specimens were constructed. The specimens failed predominantly in shear as evidenced by the shear cracks in the column joint region.

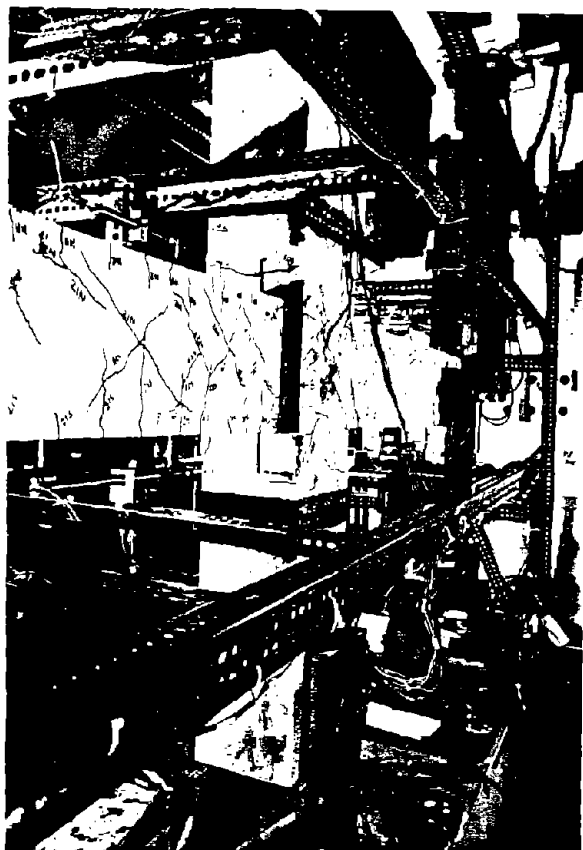Fig. 4.2 Specimen B-M-Z2 at 2 Δ_y.

38

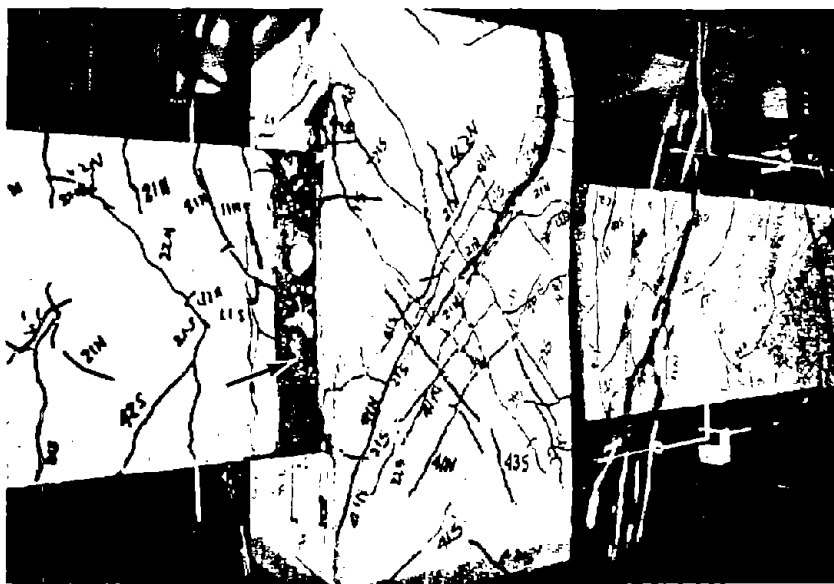Fig. 4.3 Joint region of B-M-Z2 at 4 Δ_y.

Fig. 4.4   Joint region of A-M-Z2 at 4 Δ_y - east face.

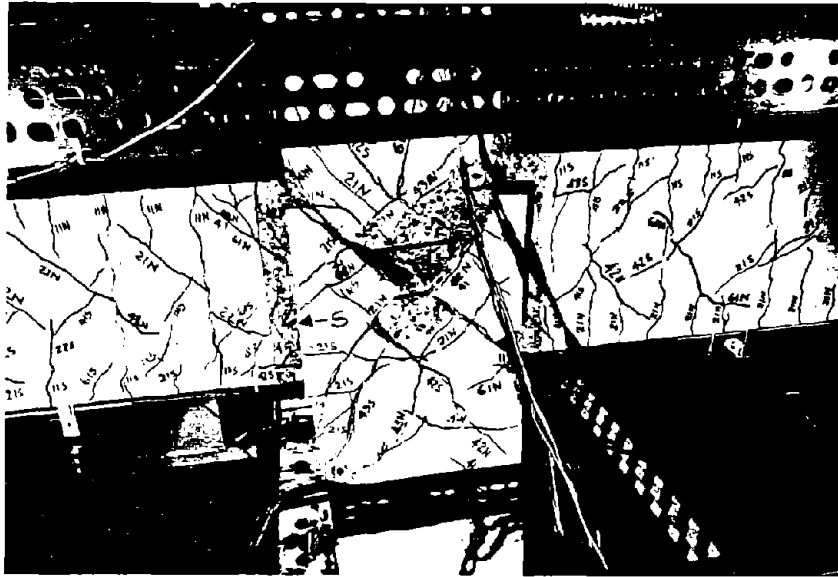Fig. 4.5   Joint region of A-M-Z2 at 6 Δ_y - east face.

Fig. 4.6   Joint region of B-M-Z2 at 6 Δ_y.

The load-displacement plots for both the monolithic zone 2 specimens, A-M-Z2 and B-M-Z2 are shown in Figs. 4.7 and 4.8, respectively. The load in the figures is the lateral load applied to the column top and the displacement is the lateral displacement of the column top. As seen in Figs. 4.7 and 4.8, the specimens exhibited stable behavior until failure occurred. The experimental yield displacements were 0.359 in. and 0.371 in. for A-M-Z2 and B-M-Z2, respectively. The ultimate displacement ductility of specimen A-M-Z2 was 4 and 6 for specimen B-M-Z2.
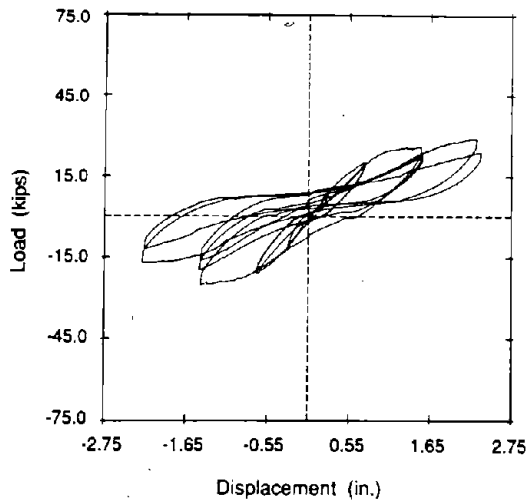
Fig. 4.7 Load displacement curves
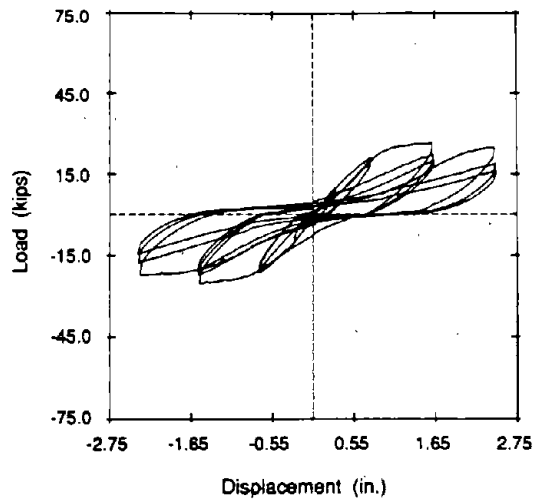   for specimen A-M-Z2.

Fig. 4.8 Load displacement curves
          for specimen B-M-Z2.

The experimental ultimate beams moments were 51 k-ft and 59 k-ft for A-M-Z2 and were 52 k-ft and 55 k-ft for B-M-Z2. These moments were measured at the column face and were obtained by multiplying the beam reaction as measured by the load cells by the lever arm. Three of these values were attained in the first cycle at 4 Δ_y while the fourth (59 k-ft for A-M-Z2) was attained in the first cycle at 6 Δ_y.

A comparison of the energy dissipated on a per cycle basis by the zone 2 specimens is given in Fig. 4.9. The energy dissipated was defined as the area enclosed by the load-displacement plot and was calculated using an in-house program written at NIST. In brief, each load-displacement cycle was plotted on a raster screen and the hysteresis curve was filled with a given color. The program then counted the number of pixels of this color. This number, modified by the appropriate conversion factors, represented the area within the hysteresis

42

curve. More detailed information on the computer program may be found in Reference 5

As shown in Fig. 4.9, the two zone 2 specimens exhibited similar behavior and low energy dissipation characteristics. The bar graph shown in Fig. 4.9 plots the energy dissipated per cycle. The cumulative energy dissipated up to failure was 77 k-in. and 204 k-in. for A-M-Z2 and B-M-Z2, respectively. Again, the lower energy dissipated by specimen A-M-Z2 is a result of earlier failure (failure as defined in Section 3.2) of the specimen.
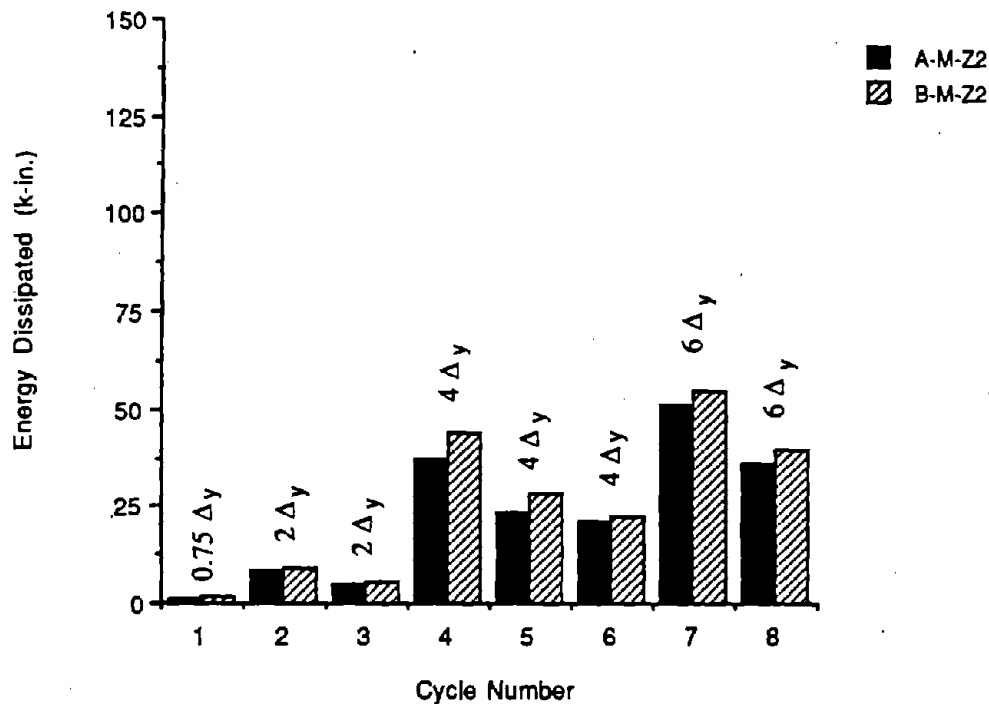
Fig. 4.9 Energy dissipated per cycle by the monolithic zone 2 specimens.

The extent of yielding the beam rebars is shown in Figs. 4.10 through 4.17. In these figures, "top" refers to the top of the beam and a negative numbers on

the x-axis indicate that the gage is located inside the column; zero datum corresponds to a gage located at the column face; and positive numbers represent gage distances away from the column face. The labels in the legend refer to the cycle and excursion. For example, 21S refers to the south excursion for the first cycle at 2 Δ_y. Not all cycles are plotted for purposes of clarity.

The average rebar yield length for the monolithic zone 2 specimens is 17.0 in. which is approximately 1.96 D where D is the depth of the beam. The average yield length was computed by taking the average of the yield lengths for all the rebars from both specimens. The yield lengths were determined graphically from Figs. 4.10 through 4.17 and were defined as the lengths over which the strain in the rebar was greater than yield strain, 2000 ϵ. As seen in Figs. 4.10 through 4.17 and from observations during the tests, the beams in these specimens did not experience much distress.
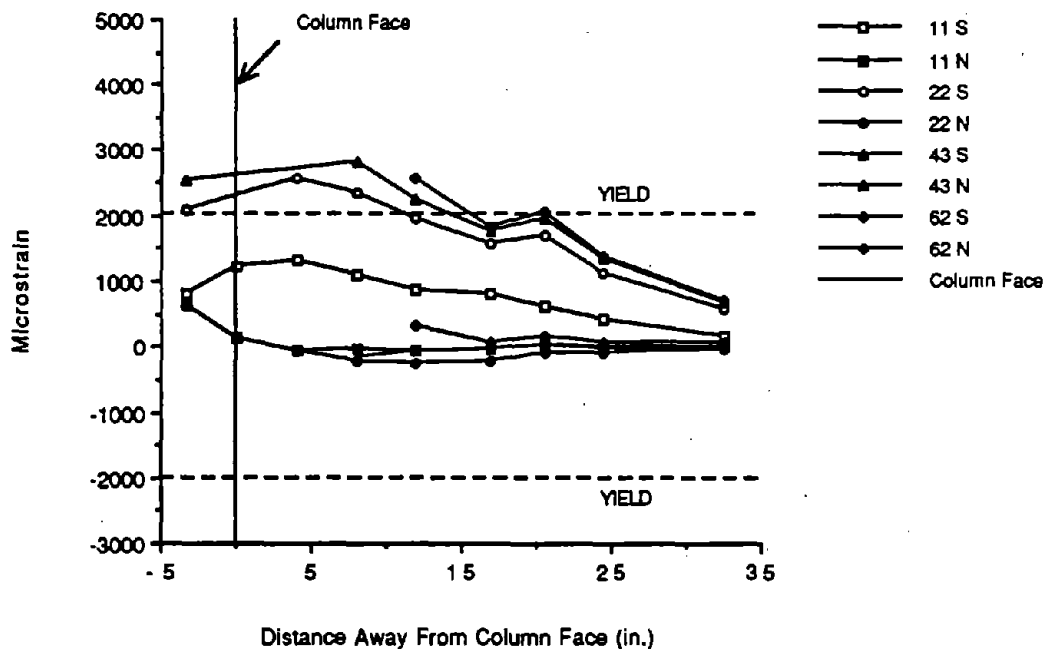

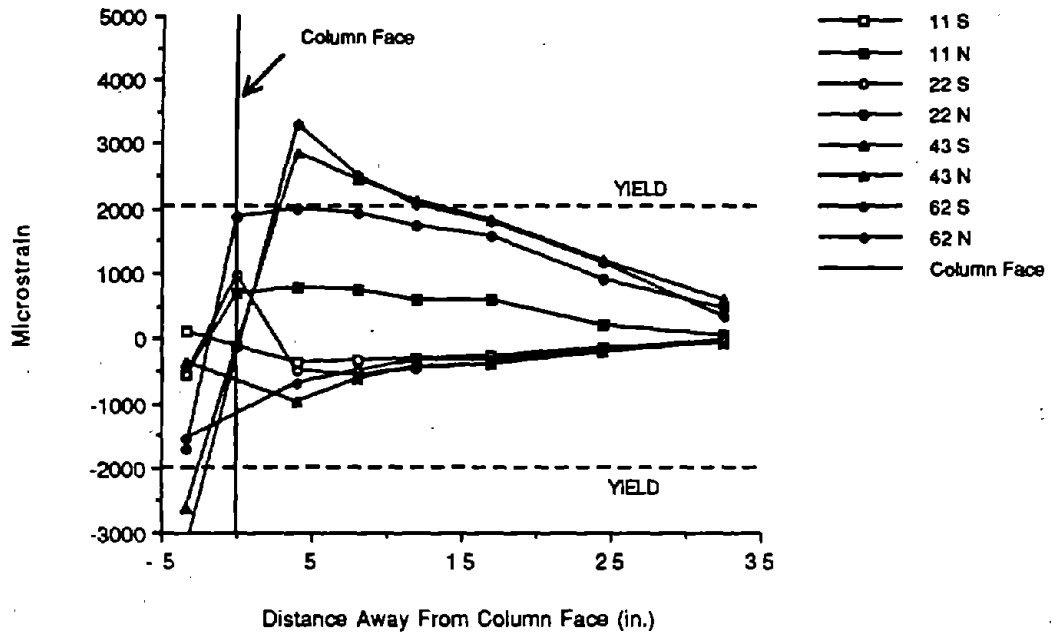Fig. 4.10   Top rebar strains in the north beam for A-M-Z2.

44

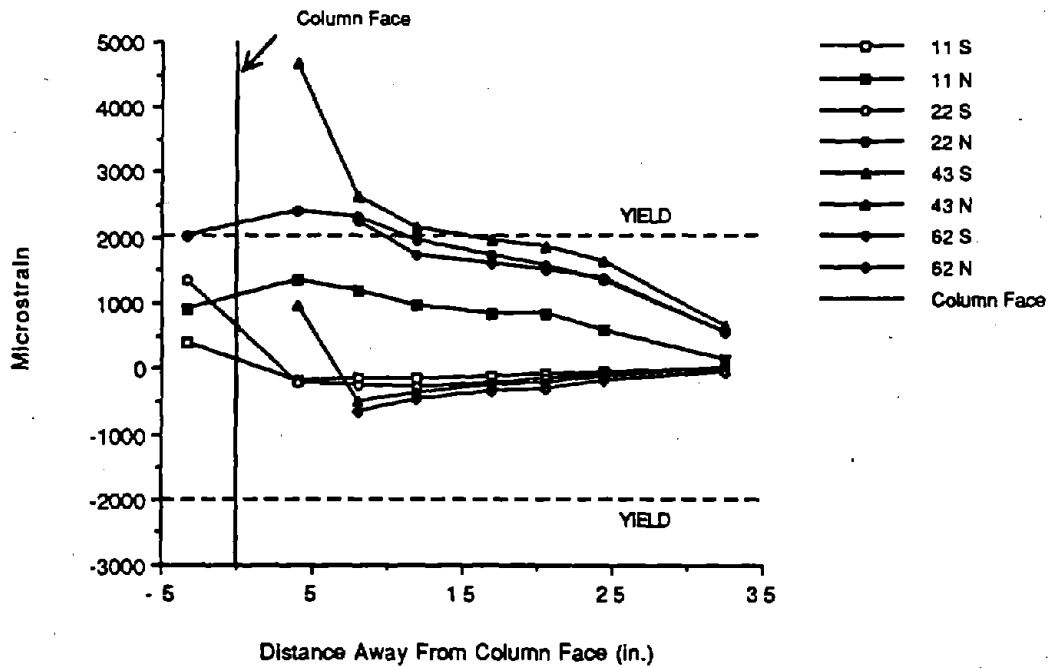Fig. 4.11 Bottom rebar strains in north beam for A-M-Z2.

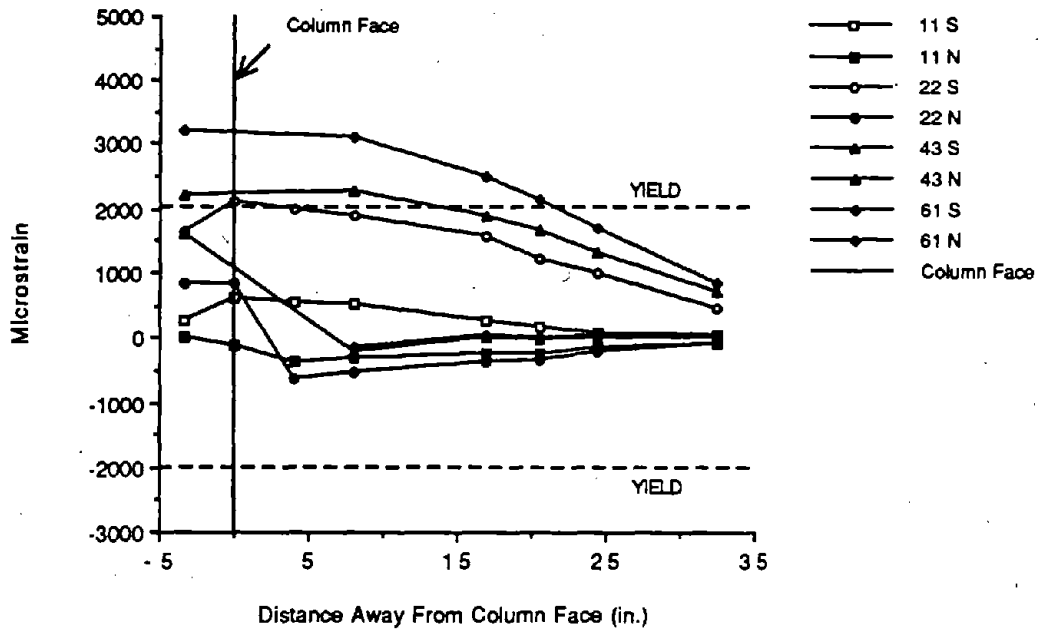Fig. 4.12 Top rebar strains in south beam for A-M-Z2.

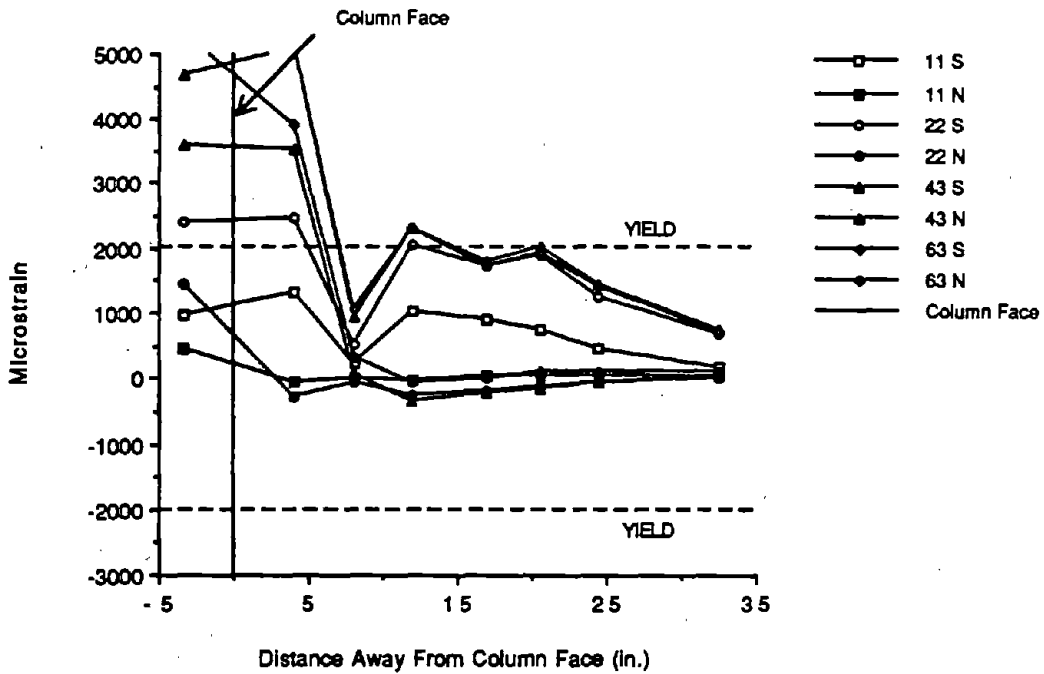Fig. 4.13   Bottom rebar strains in south beam for A-M-Z2.

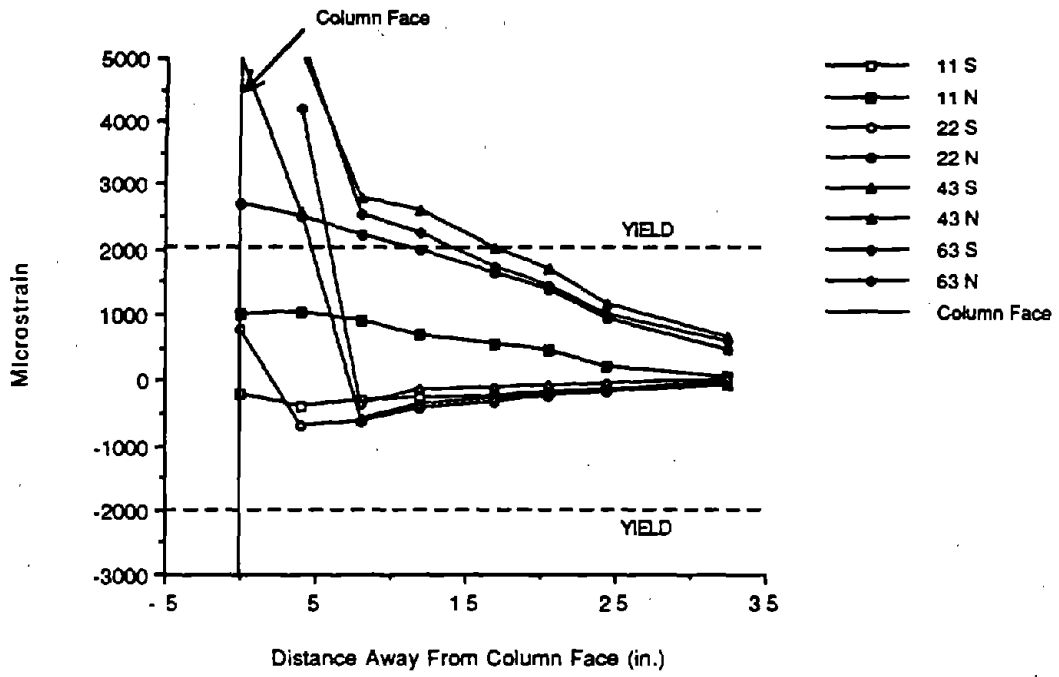Fig. 4.14   Top rebar strains in north beam for B-M-Z2.

46

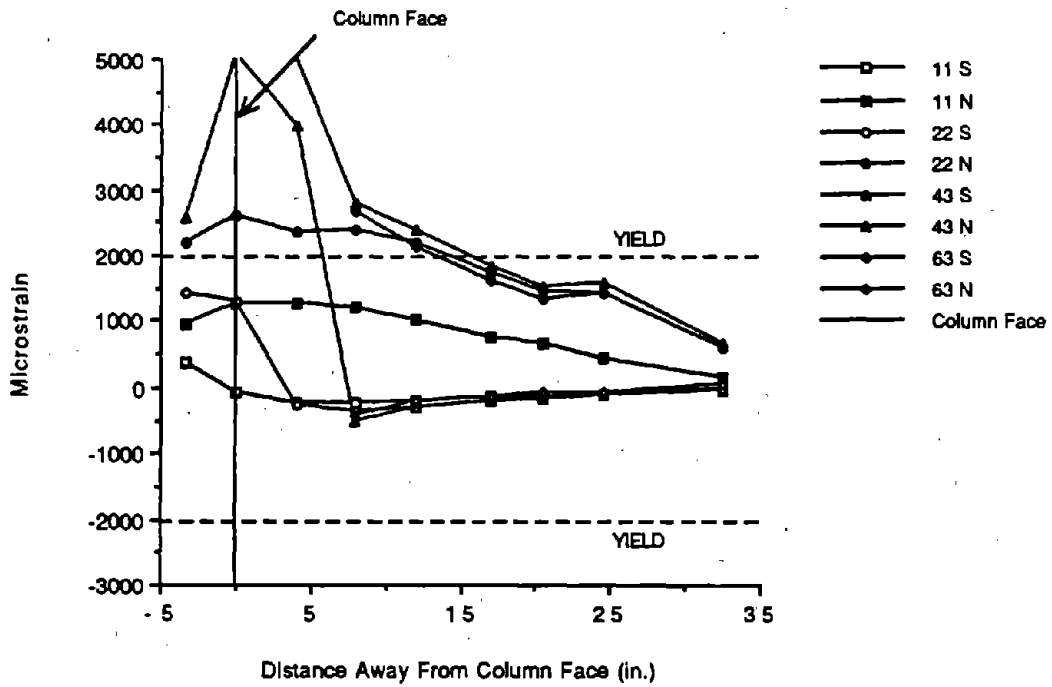Fig. 4.15 Bottom rebar strains in north beam for B-M-Z2.

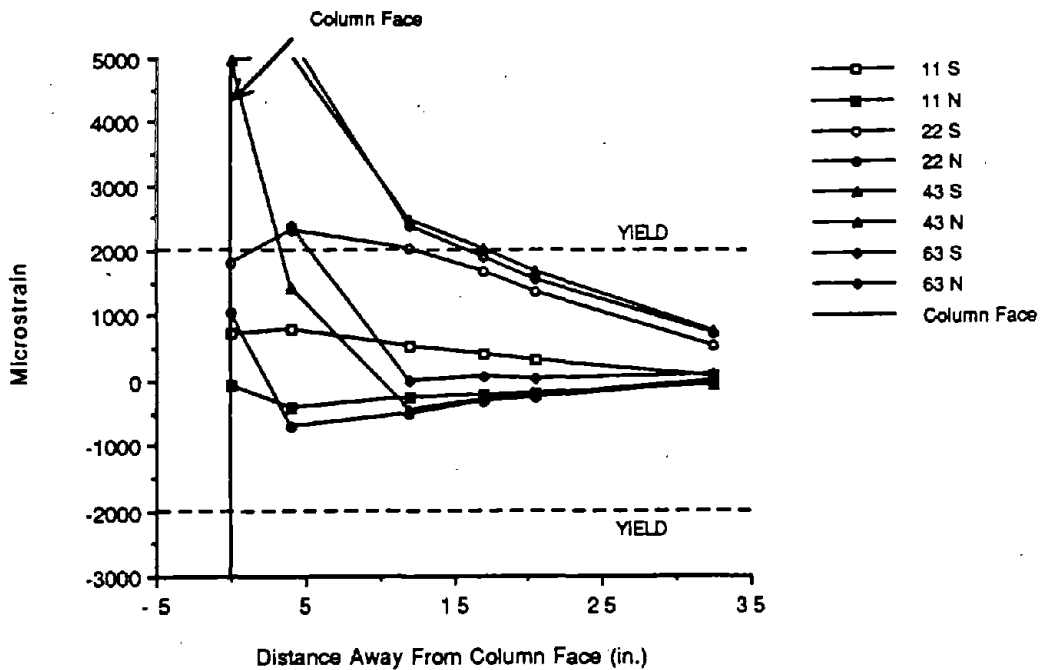Fig. 4.16 Top rebar strains in south beam for B-M-Z2.

Fig. 4.17 Bottom rebar strains in south beam for B-M-Z2.

4.2 Monolithic Zone 4 Specimens

Two identical specimens, A-M-Z4 and B-M-Z4, detailed as shown in Fig. 3.3 were

tested. The load history for the monolithic zone 4 specimens is as described

in Chapter 3 and shown in Fig. 4.18. The applied axial load on the column was

84.2 kips (0.1 $f'_c A_g$ based on a 28-day concrete strength of 4675 psi). Specimen

A-M-Z4 was loaded in-plane in the N-S direction while specimen B-M-Z4 was loaded

in-plane in the E-W direction. Specimen B-M-Z4 was tested first and the stroke

of the E-W actuator at 6 Δ_y was found to be close to its maximum limit. It was,

therefore, decided that specimen A-M-Z4 be tested in the N-S direction as the

maximum limits of the N-S actuators were twice that of the E-W actuator. In the

following sections and figures, "east beam" refers to the beam east of the

48

column; "south beam" refers to the beam south of the column; "north face of the

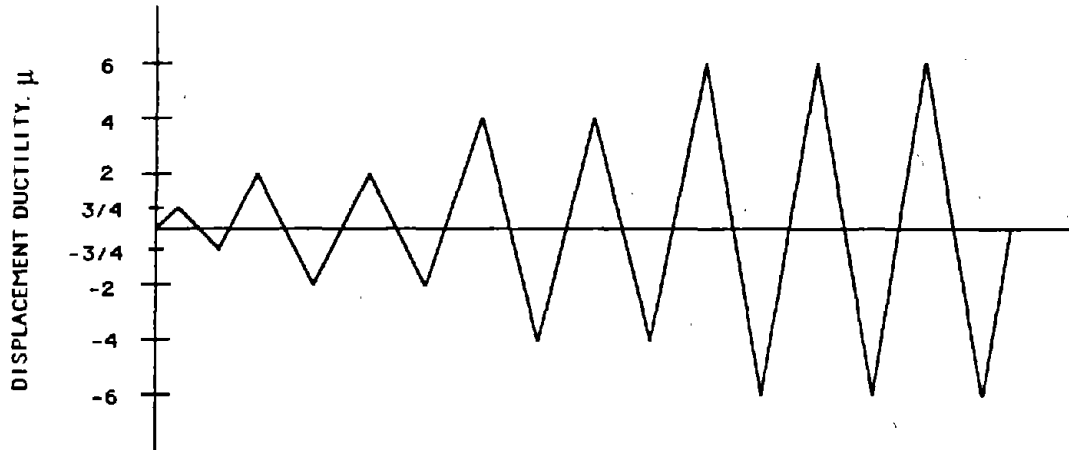east beam" refers to side of the east beam which faces north.

Fig. 4.18 Loading sequence for the monolithic zone 4 specimens.

Hairline flexure cracks in the beams were observed in the first cycle to 0.75 Δ_y and hairline diagonal cracks in both the beams and column were observed at 2 Δ_y. The crack pattern on the south face of specimen B-M-Z4 at 2 Δ_y, second cycle is shown in Fig. 4.19. Minor crushing of the beam compression zone at the connection and additional shear cracks in the beams and column were observed at 4 Δ_y. The crack pattern at 4 Δ_y for specimen B-M-Z4 is shown in Fig. 4.20. At 6 Δ_y, spalling of the beam concrete cover and buckling of the beam reinforcement were noted for both beams. Hinging of the beams at the column face was apparent at this ductility level. Also, at this ductility level, several shear cracks in the beams measured approximately 1/2 in. wide while the crackwidths in the column remained very fine. Both specimens failed predominantly in flexure with the formation of hinges in the beams and

49

deterioration of the beams. The progression of beam deterioration for specimen B-M-Z4 is illustrated in Figs. 4.21 through 4.23. Fig. 4.21 shows the north face of the west beam after the first cycle at 6 Δy; Fig. 4.22 shows the south face of the west beam after the second cycle at 6 Δ_y; and Fig. 4.23 shows the south face of both beams after the third cycle at 6 Δ_y. Figs. 4.24 and 4.25 show specimen A-M-Z4 at 6 Δ_y, second and third cycle, respectively. The 1/2 in. crack width is very clearly shown in Fig. 4.24. Both columns were intact and sustained only minor shear cracking. This failure mode was expected as a result of the design philosophy of employing "weak-beams" and a "strong-column".
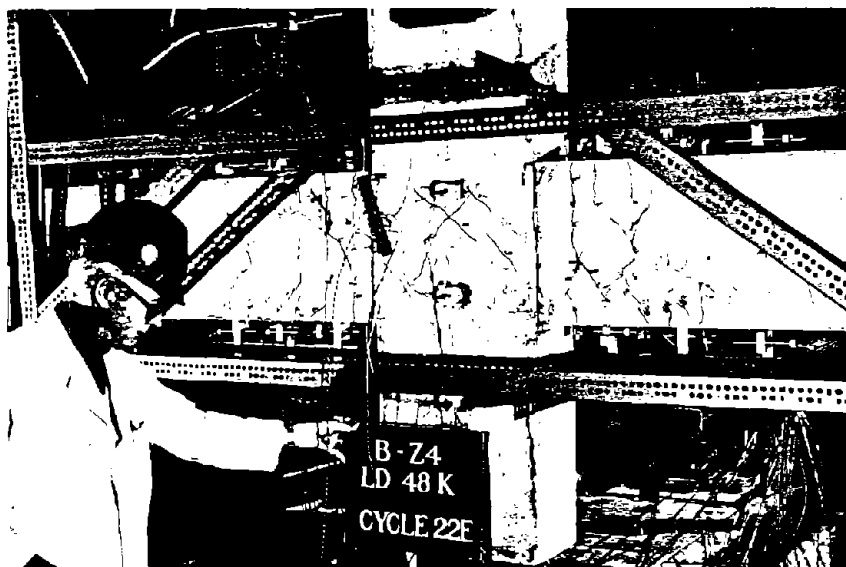

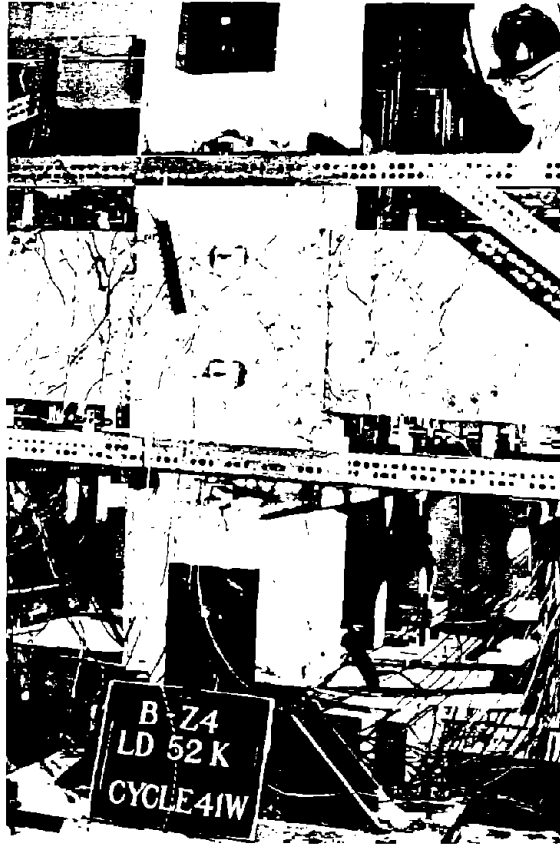Fig. 4.19 Specimen B-M-Z4 at 2 Δ_y, cycle 2.

Fig. 4.20 Crack pattern of B-M-Z4 at 4 Δ_y, cycle 1.

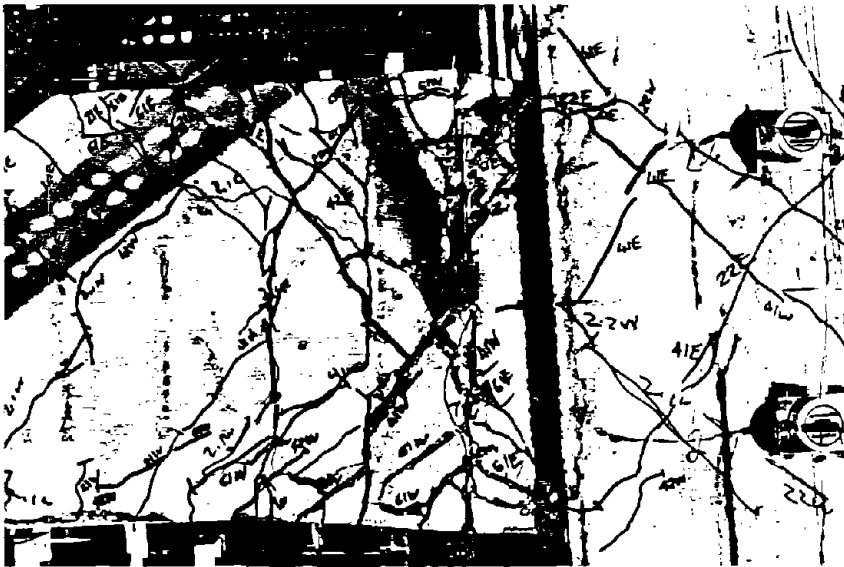Fig. 4.21   Crack opening in beam of B-M-Z4 at 6 Δ_y, cycle 1.

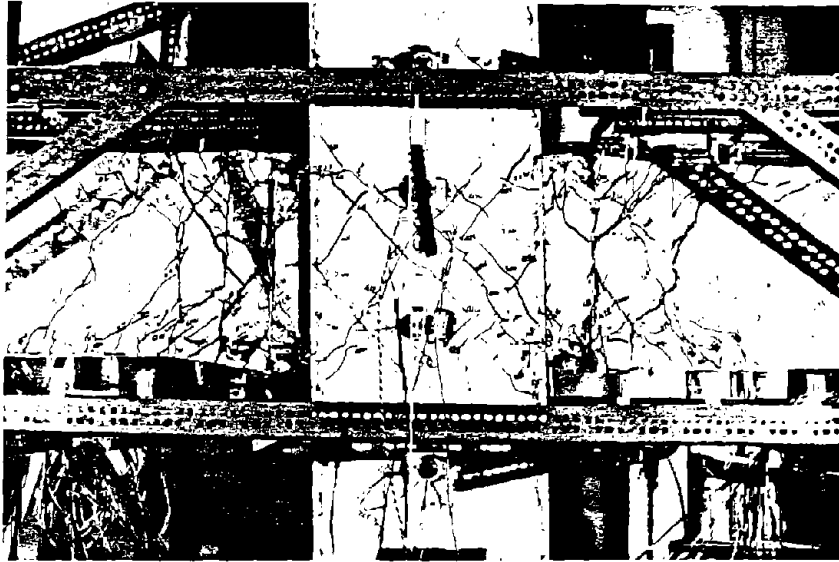Fig. 4.22   Beam deterioration of B-M-Z4 at 6 Δ_y, cycle 2.

52

Fig. 4.23 View of connection B-M-Z4 at 6 Δ_y, cycle 3.

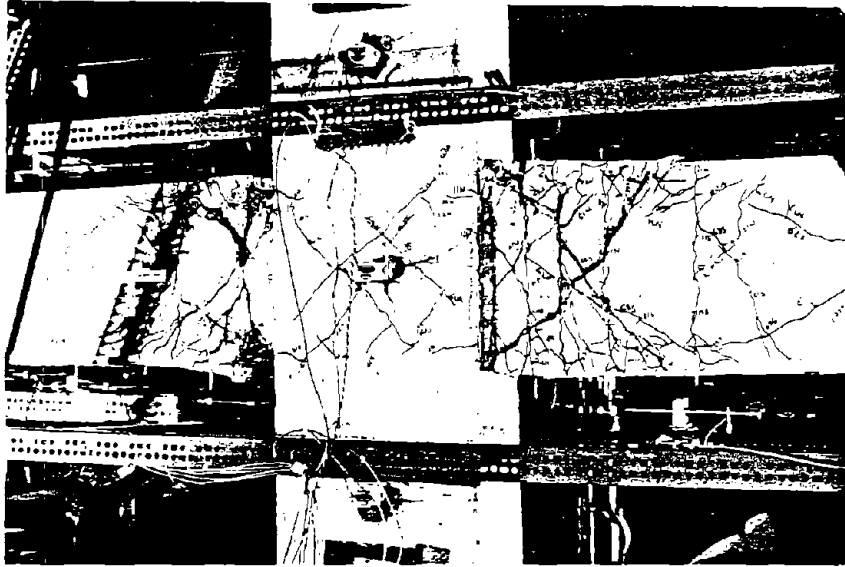Fig. 4.24 Shear crack opening of A-M-Z4 at 6 Δ_y, cycle 2.

Fig. 4.25 View of A-M-Z4 at 6 Δ_y, cycle 3.

The load-displacement plots for both monolithic zone 4 specimens, A-M-Z4 and B-M-Z4, are shown in Figs. 4.26 and 4.27. As seen in the figures, the behavior of both specimens was very similar and stable until extensive buckling of the beam rebar occurred in the plastic hinge region at 6 Δ_y. The experimental yield displacements for specimens A-M-Z4 and B-M-Z4 were 0.263 in. and 0.293 in., respectively. The ultimate displacement ductility achieved by both specimens was 6.
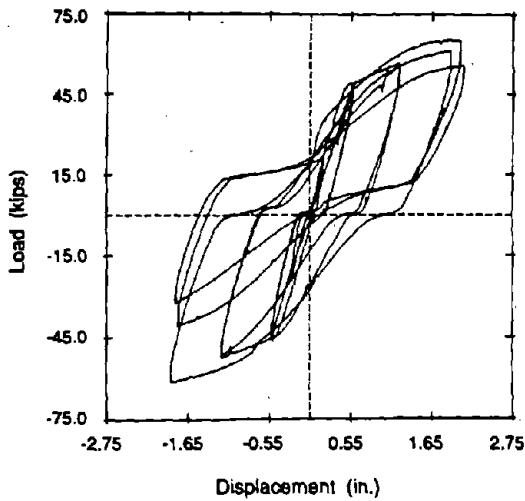
Fig. 4.26   Load displacement curves
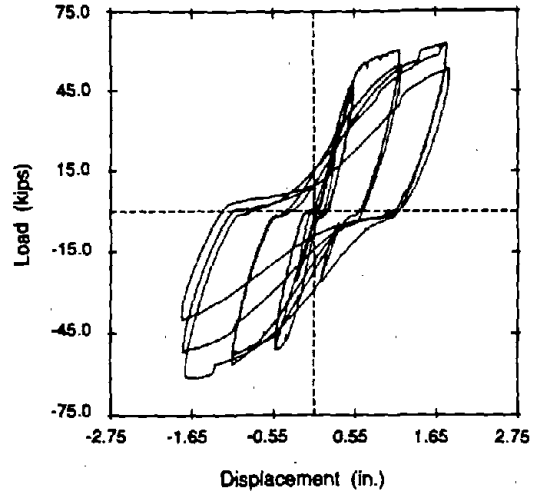   for specimen A-M-Z4.

Fig. 4.27   Load displacement curves
            for specimen B-M-Z4.

The experimental ultimate beam moments were 109 k-ft and 106 k-ft for A-M-Z4
and were 109 k-ft and 113 k-ft for B-M-Z4.   Again, these moments were computed
by multiplying the beam reactions as obtained from the load cells by the lever
arm.   These moments were achieved in the first cycle at 6 Δ_y and were measured
at the column face.

A comparison of the energy dissipated per cycle by the monolithic zone 4
specimens is given in Fig. 4.28.   The similarity in behavior between the two
monolithic zone 4 specimens can be clearly seen in Fig. 4.28.   The drop in energy
dissipation was significant in the second cycle at 6 Δ_y and therefore, a third
cycle at 6 Δ_y was performed.   The cumulative energy dissipated up to failure
was 597 k-in and 543 k-in. for specimens A-M-Z4 and B-M-Z4, respectively.
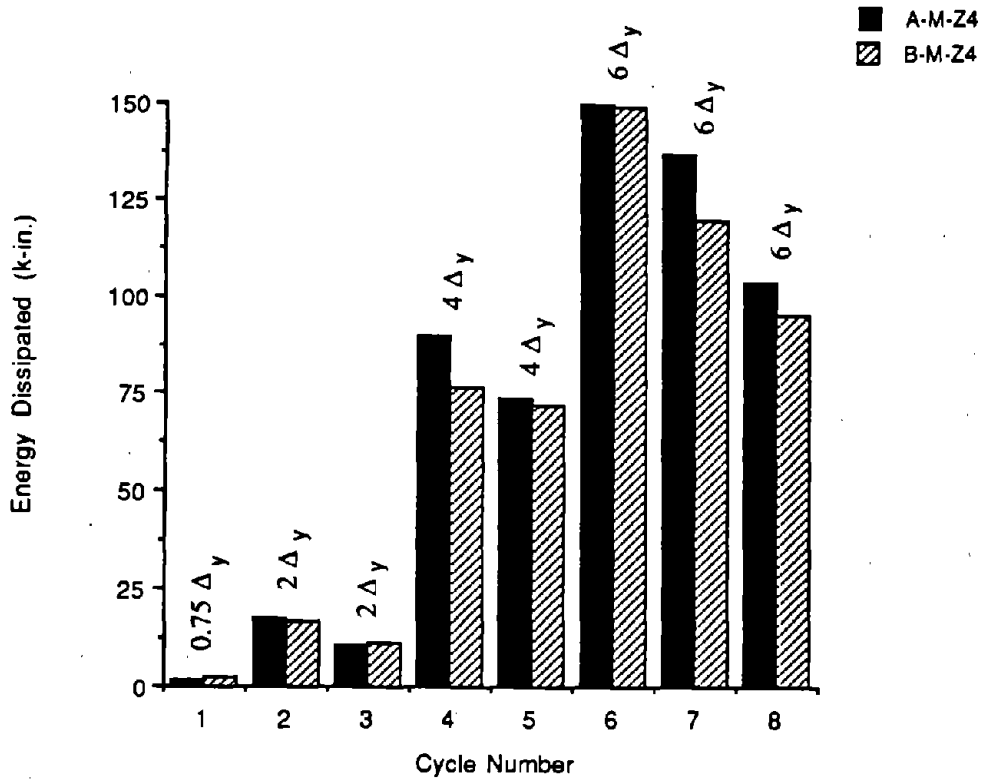
Fig. 4.28 Energy dissipated per cycle by the monolithic zone 4 specimens.

Rebar strains for both specimens are shown in Figs. 4.29 through 4.36. As indicated in these figures, strain data was lost in the plastic hinge region at 4 Δ_y, cycle 1 due to debonding of the strain gages from the rebars. The average length over which the rebars yielded was 21.0 in. (L/D - 1.31).

Fig. 4.29 Top rebar strains in north beam of A-M-Z4.

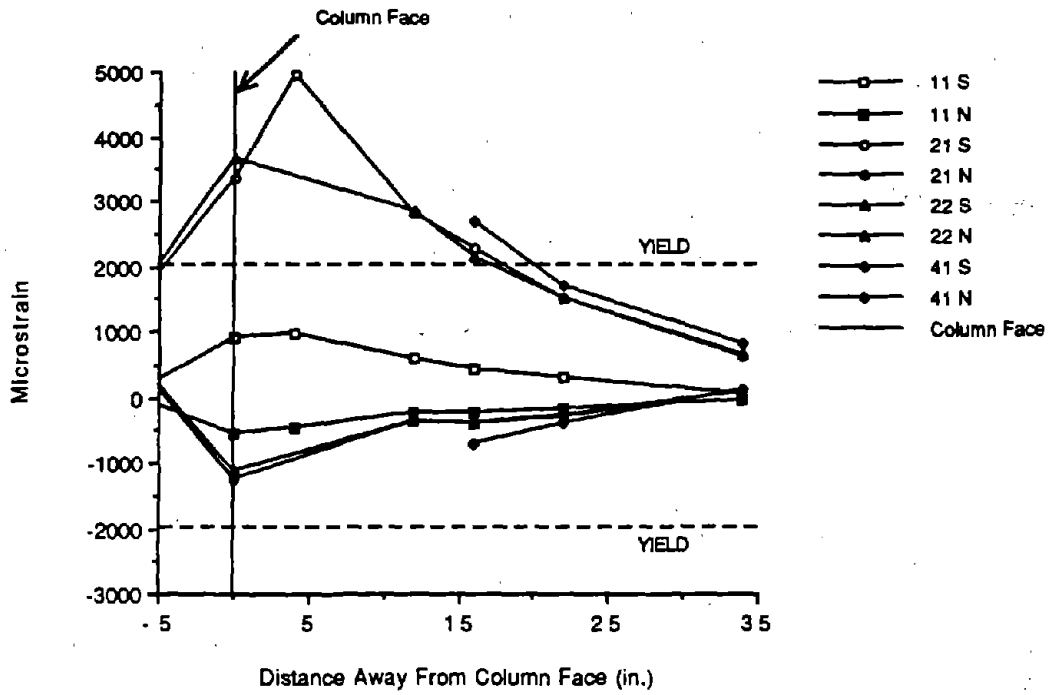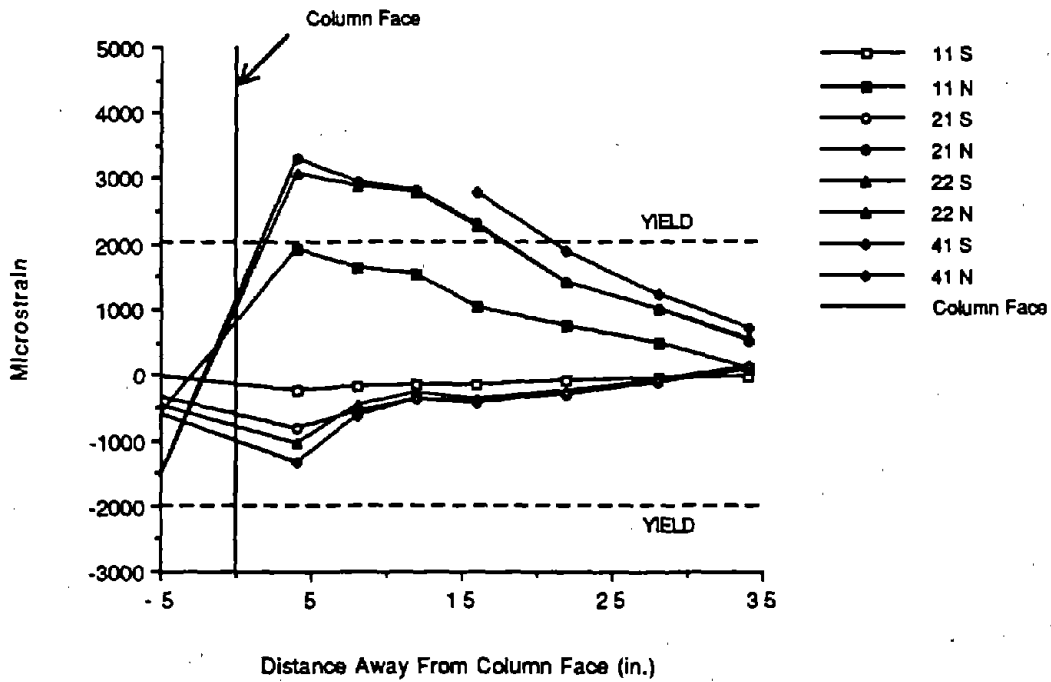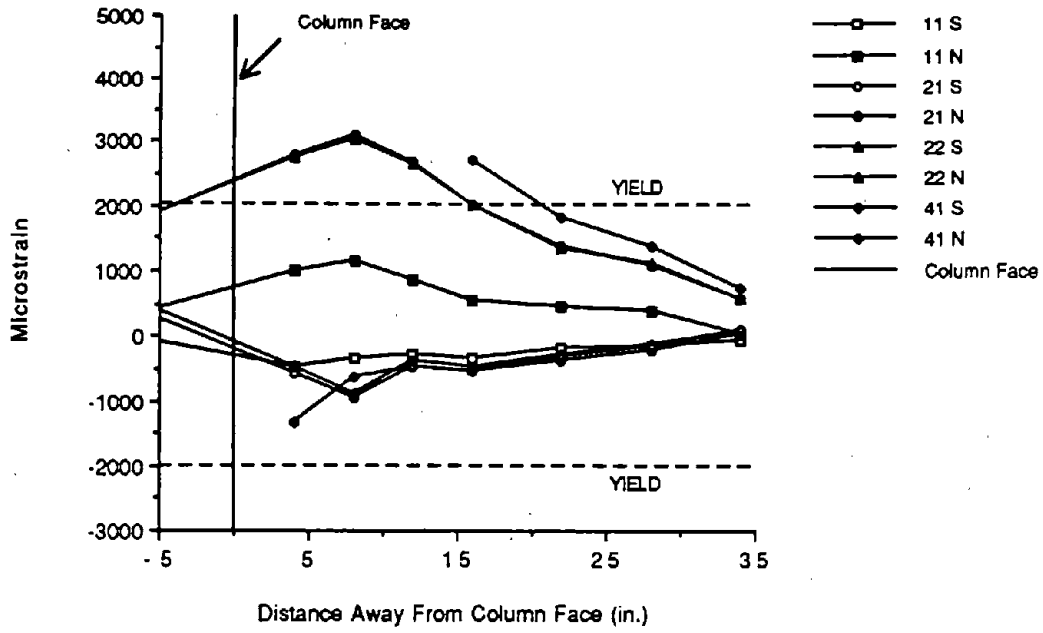Fig. 4.30 Bottom rebar strains in north beam for A-M-Z4.

57

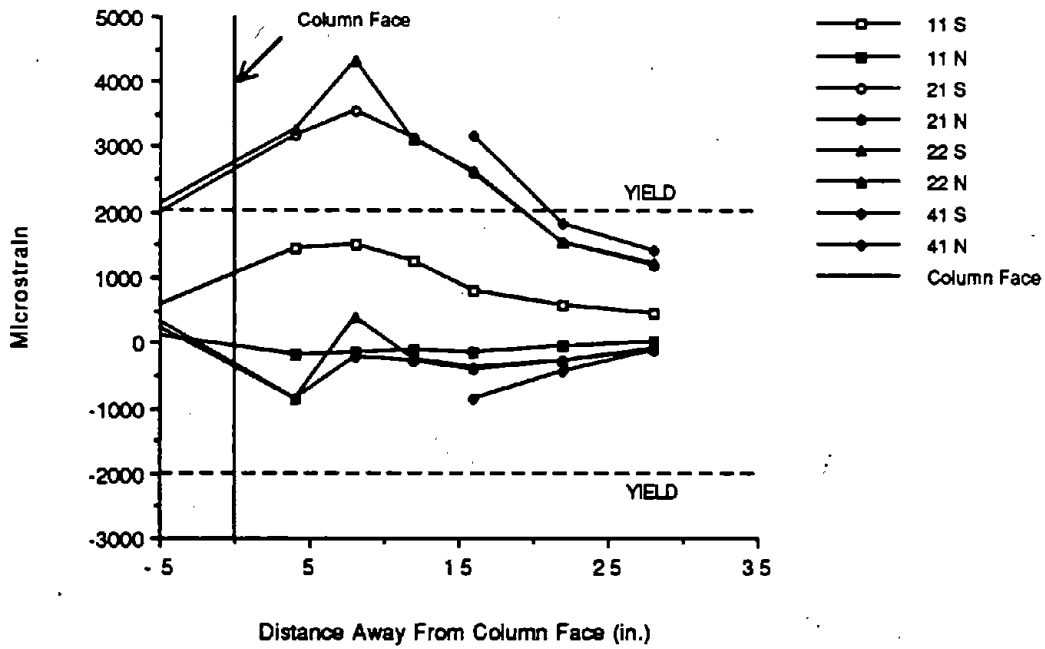Fig. 4.31 Top rebar strains in south beam for A-M-Z4.

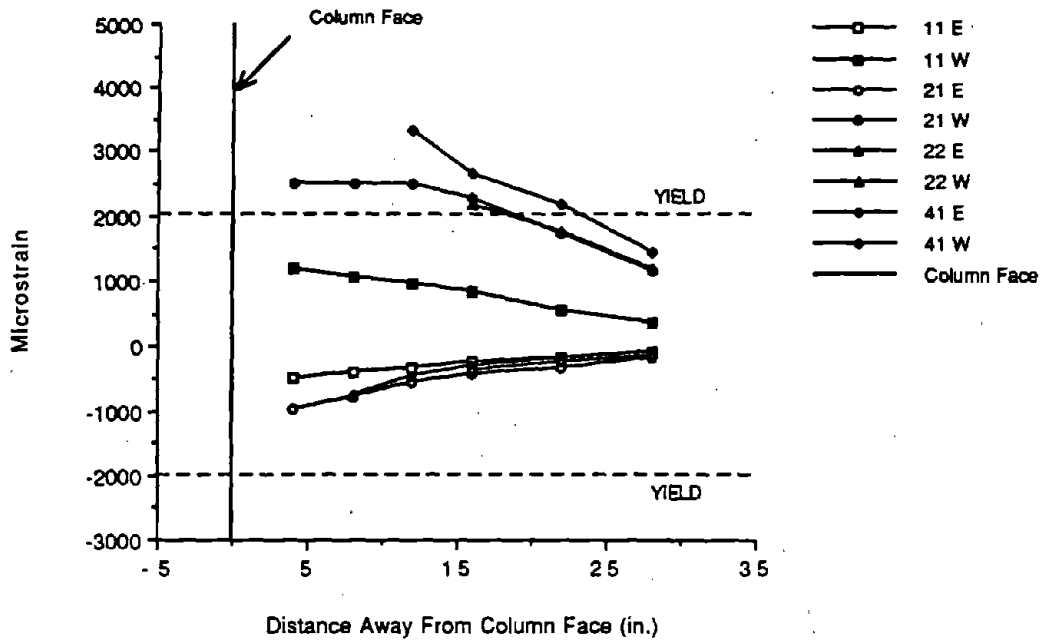Fig. 4.32 Bottom rebar strains in south beam for A-M-Z4.

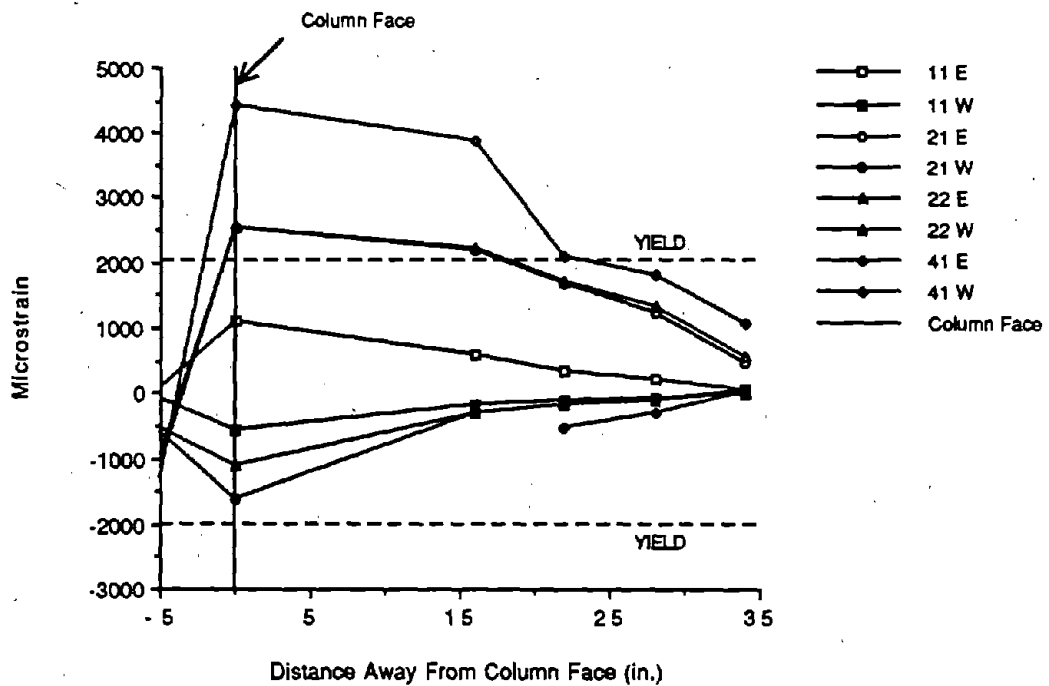Fig. 4.33 Top rebar strains in east beam for B-M-Z4.

Fig. 4.34 Bottom rebar strains in east beam for B-M-Z4.
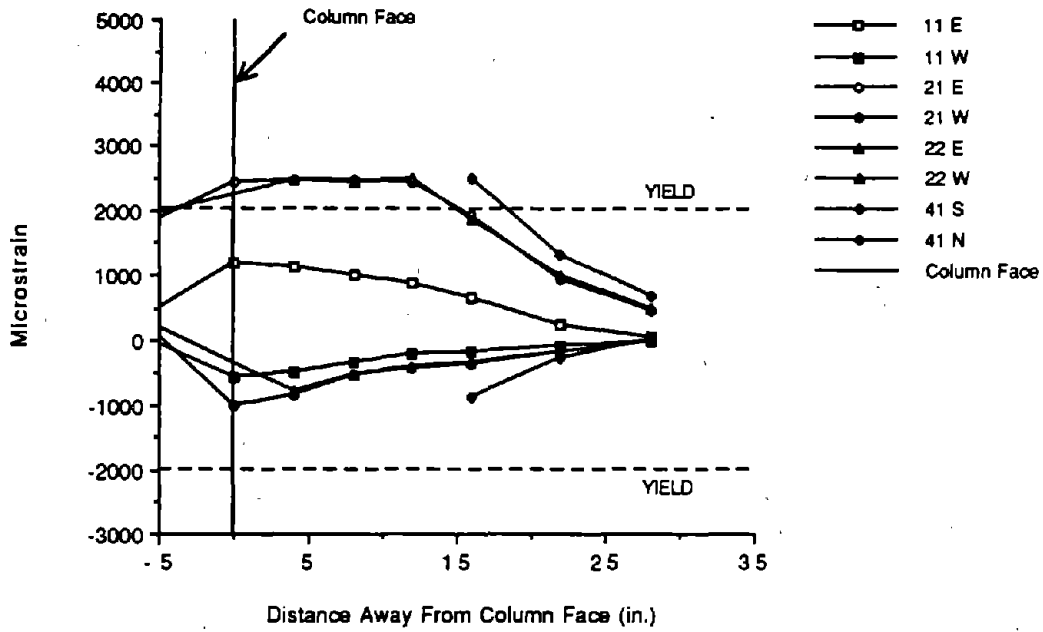
Fig. 4.35 Top rebar strains in west beam for B-M-Z4.
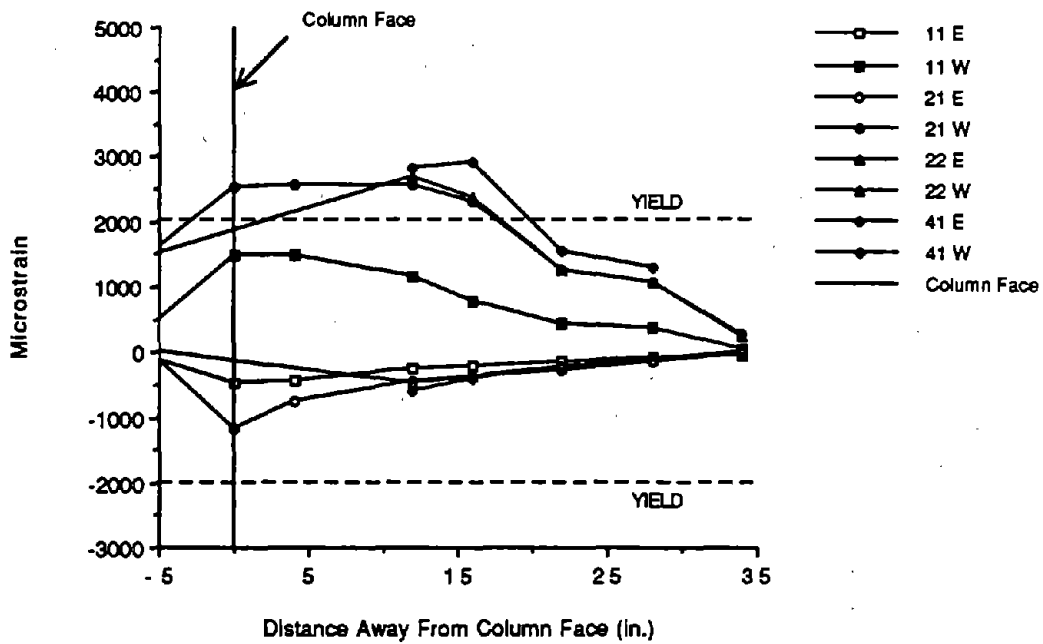
Fig. 4.36 Bottom rebar strains in west beam for B-M-Z4.

60

4.3   Post-tensioned Precast Specimens

Two identical specimens, A-P-Z4 and B-P-Z4, detailed as shown in Fig. 3.3 were tested. The load history for the post-tensioned specimens was the same as for the monolithic specimens, but with the addition of 3 cycles at 8 Δ_y, 2 cycles at 10 Δ_y, and 3 cycles at 12 Δ_y as is shown in Fig. 4.37. The additional cycles were required as the precast specimens did not fail at the same displacement ductility levels as the monolithic zone 4 specimens. The column was subjected to an axial load of 106.5 kips (0.1 f'$_c$ A$_g$ based on a 28-day concrete strength of 5915 psi). Both specimens were loaded in-plane in the N-S direction.
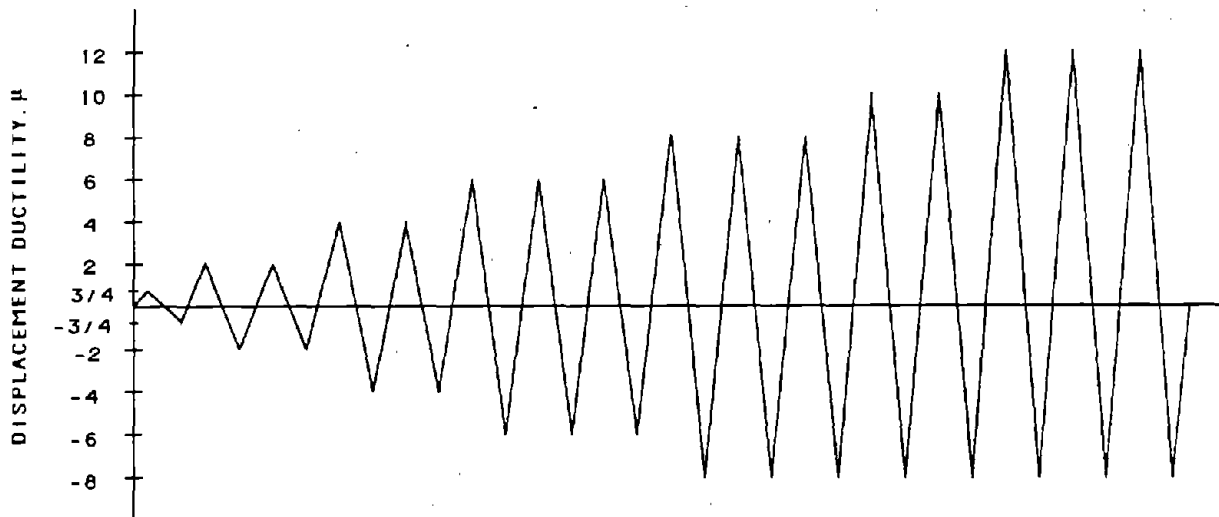
Fig. 4.37   Load sequence for the post-tensioned zone 4 specimens.

No cracks were observed in either specimen at 0.75 Δ_y. Only a few very minor shear and flexure cracks in the beams and columns were observed at 2 Δ_y. The construction joints showed signs of incipient crushing and widening at 4 Δ_y.

61

The crack pattern of specimen A-P-Z4 at 4 Δ_y is shown in Fig. 4.38. Crushing of the compression zones of the beams and widening of the gap between the beam and column were observed at 6 Δ_y as seen in Fig. 4.39. Spalling of the concrete in the beam occurred at 8 Δ_y at the column face. Slippage of the post-tensioning bar or the corrugated duct in the joint region was heard at this ductility level. Crushing of the beam and the opening between the beam and column at 8 Δ_y, cycle 2 are shown in Figs. 4.40 and 4.41, respectively. Due to the rotational limit of the test facility, the specimen could only be cycled to a maximum of 8 Δ_y in the north direction. Therefore, the subsequent cycles were 10 Δ_y or 12 Δ_y in the south direction and 8 Δ_y in the north direction.
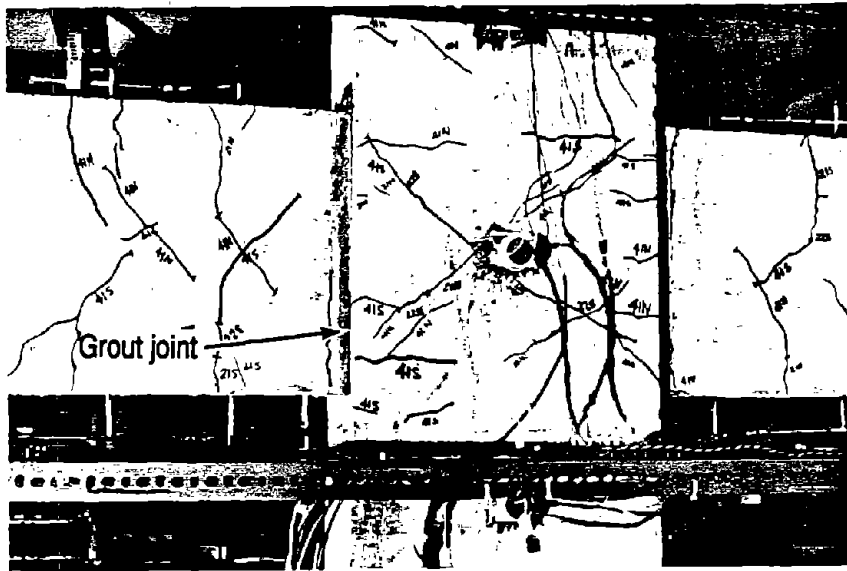
Fig. 4.38 Crack pattern of specimen A-P-Z4 at 4 Δ_y, cycle 1.
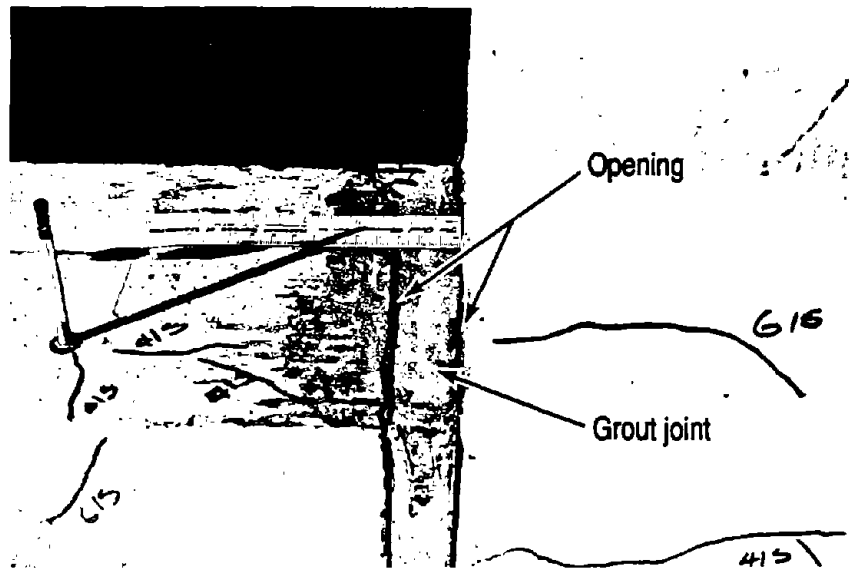
Fig. 4.39 Opening between the beam and column at 6 Δ_y, cycle 1.
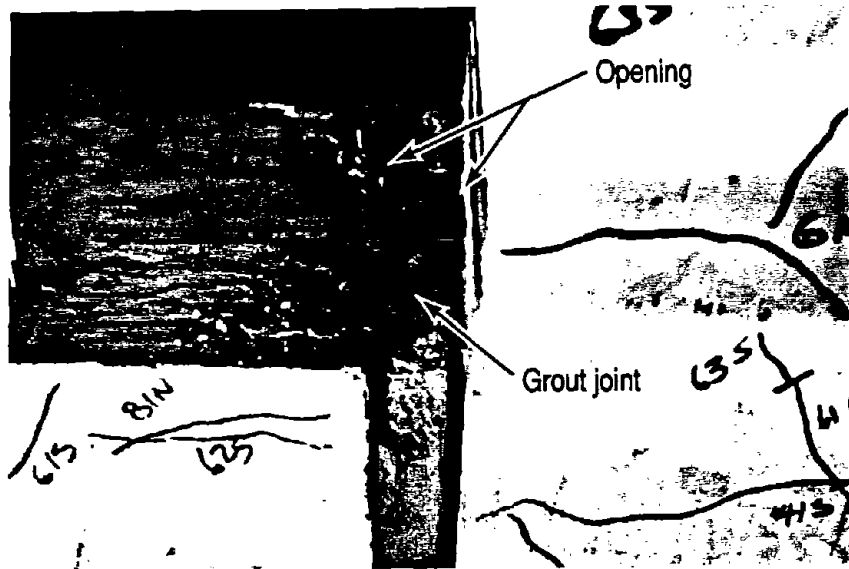
Fig. 4.40 Opening between the beam and column at 8 Δ_y, cycle 2.
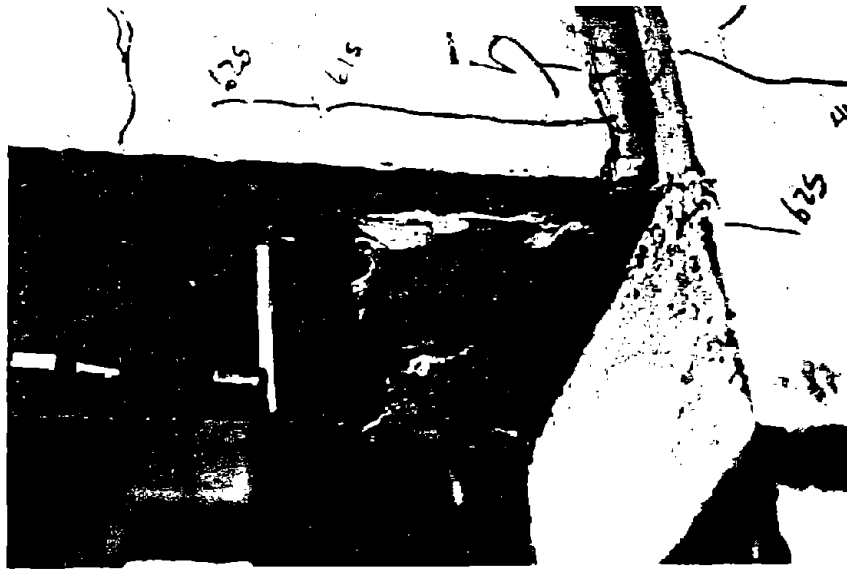
Fig. 4.41 Crushing of the beam at 8 Δ_y, cycle 2.

Only widening of the column to beam gap and continued crushing of the beams at the joints was observed at 10 and 12 Δ_y. The opening between the beam and column was 1/2 in. wide at 12 Δ_y. Crushing of the beams occurred over a region from the column face to approximately 6 in. away. Fig. 4.42 and 4.43 show the spall region and opening between beam and column of specimen A-P-Z4 at 12 Δ_y, respectively. The fiber reinforced grout held together very well throughout the entire test. The voids in the grout joint seen in Fig. 4.42 is due to poor rodding of the joint during the construction process.
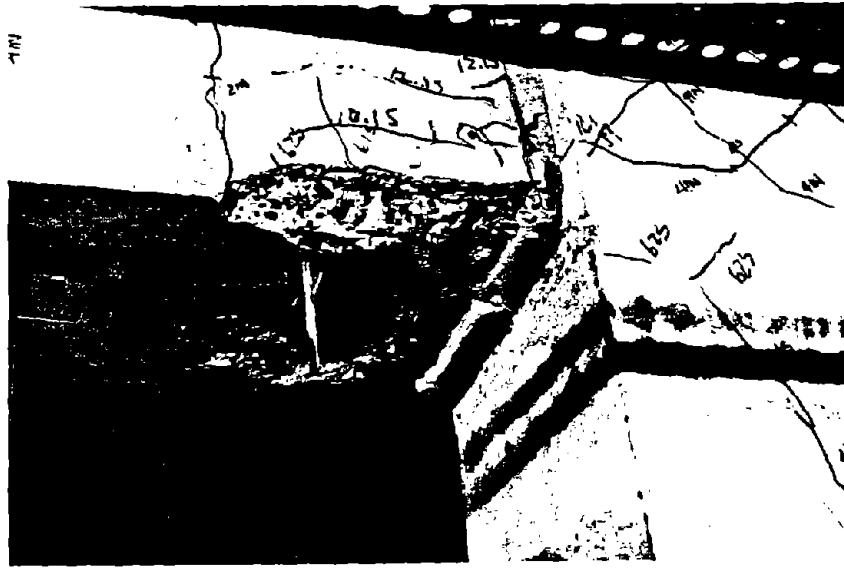
Fig. 4.42 Spall region of specimen A-P-Z4 at 12 Δ_y.
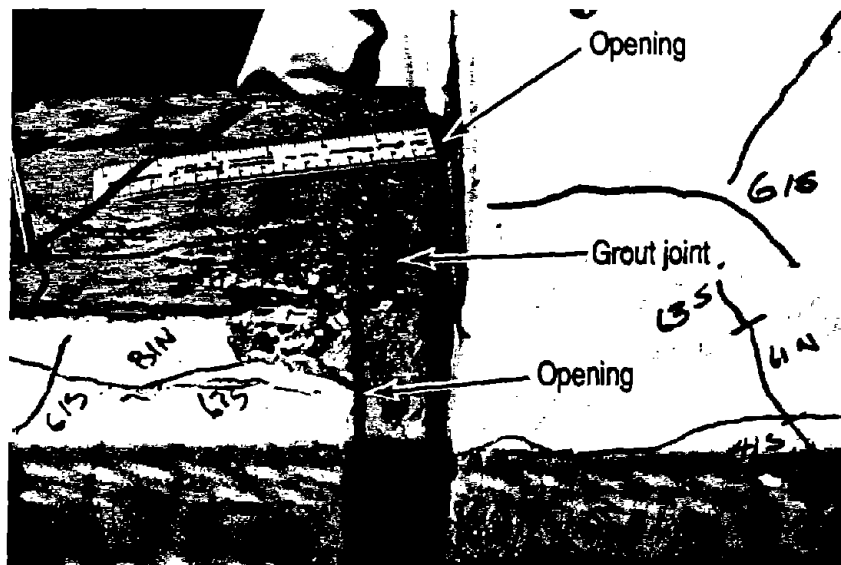
Fig. 4.43 Half inch opening between beam and column at 12 Δ_y.

The test was terminated at 12 Δ_y due to the rotational limit of the test facility. Since the ultimate moment was reached at 10 Δ_y, it was felt that further testing would not have yielded any more pertinent data. Specimen B-P-Z4 failed in the first cycle at 12 Δ_y based on the previously defined failure criteria. Although the specimen A-P-Z4 was not considered to have failed based on the failure criteria, the load in the specimen was within 7% of the failure load at 12 Δ_y. In view of this and since the specimens were not loaded symmetrically at 10 Δ_y and at 12 Δ_y, μ_u for the post-tensioned specimens was conservatively considered to be 10.

The load displacement plots for both post-tensioned specimens are shown in Figs. 4.44 and 4.45. The behavior of the connections was stable throughout the test. The flat portions of the hysteresis curves at approximately zero displacement in the latter part of the tests were due to the re-opening of the joint between the column and the beam. Once the opening was wide enough to accommodate the plastic elongation of the post-tensioning bar, the lateral load increased. The yield displacement was 0.160 in. for A-P-Z4 and was 0.179 in. for B-P-Z4.
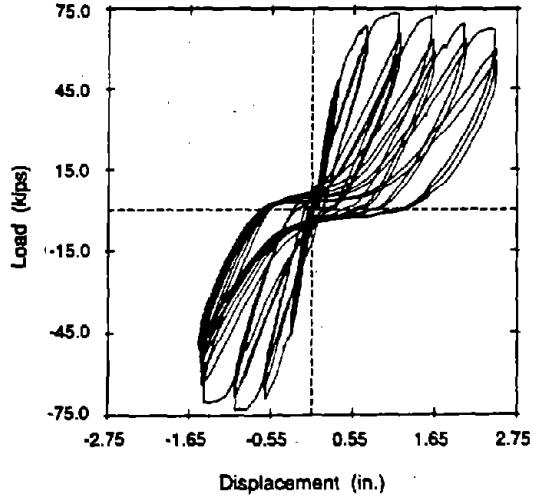
Fig. 4.44   Load displacement curves
            for specimen A-P-Z4.
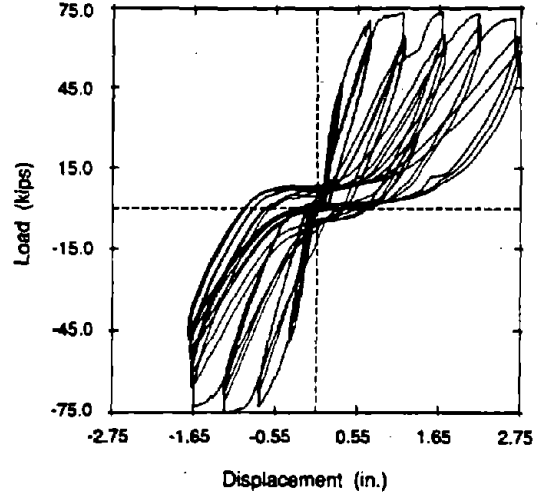
Fig. 4.45   Load displacement curves
            for specimen B-P-Z4.

The experimental ultimate beam moments at the column face were 130 k-ft and 135 k-ft for A-P-Z4 and were 136 k-ft and 137 k-ft for B-P-Z4. In each of these specimens, the ultimate moment was attained in one of the beams in the first cycle at 8 Δ_y and the other was attained in the first cycle at 10 Δ_y.

As shown in Figs. 4.44 and 4.45 by the narrow hysteresis loops and as found in previous studies, the ability of the post-tensioned connection to dissipate energy is very low. This low energy dissipation is reflected in Fig. 4.46. The cumulative energy dissipated up to the third cycle at 6 Δ_y for specimen A-P-Z4 and B-P-Z4 are 165 k-in and 181 k-in, respectively. The total energy dissipated by the post-tensioned connections up to failure, 10 Δ_y, cycle 2, was 438 k-in and 477 k-in for specimens A-P-Z4 and B-P-Z4, respectively.

67
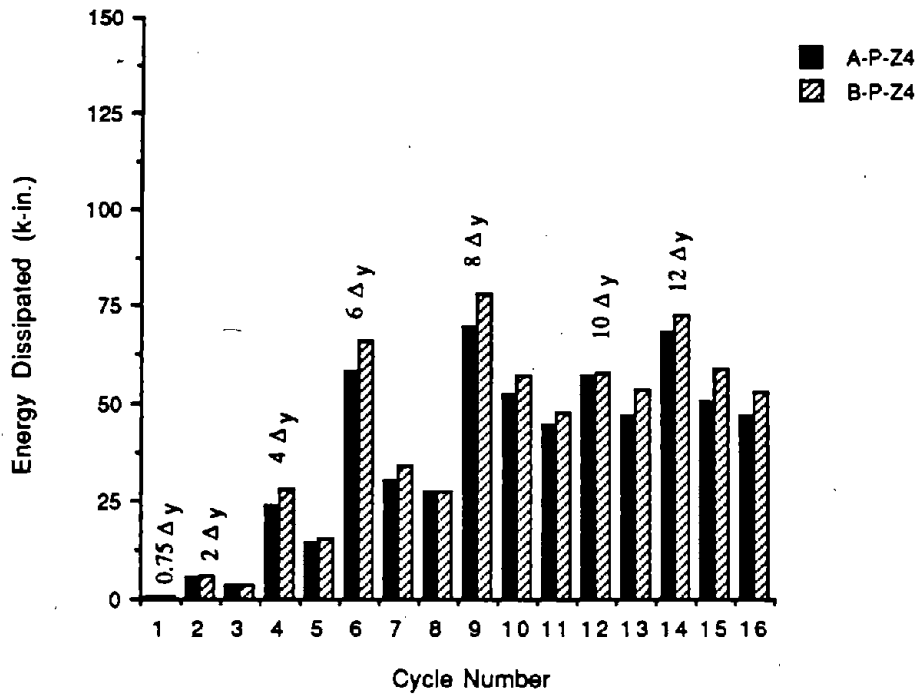
Fig. 4.46 Energy dissipated per cycle by the post-tensioned specimens.

Rebar strains for the post-tensioned specimens are given in Figs. 4.47 through 4.62. As seen in these figures, the beam rebars only yielded in the latter stages of the test. The strain gage data showed that the beam rebars only attained strains that were slightly above the rebar yield strain. This would indicate that the post-tensioning bar provided the main resistance to the applied loads, as expected. In Figs. 4.47 through 4.62, the term "northeast" refers to a rebar in the north beam on the east side of the beam and "southwest" refers to a rebar in the south beam on the west side of the beam, etc. Recall that there are only four #3 rebars in each of the beams, i.e., one in each corner of the beam. The average length over which these rebars yielded is 10.7 in. or 0.67 D where D is the depth of the beam.

68

Fig. 4.47   Top northeast rebar strains for A-P-Z4.

Fig. 4.48   Bottom northeast rebar strains for A-P-Z4.

Fig. 4.49   Top northwest rebar strains for A-P-Z4.

Fig. 4.50   Bottom northwest rebar strains for A-P-Z4.

70
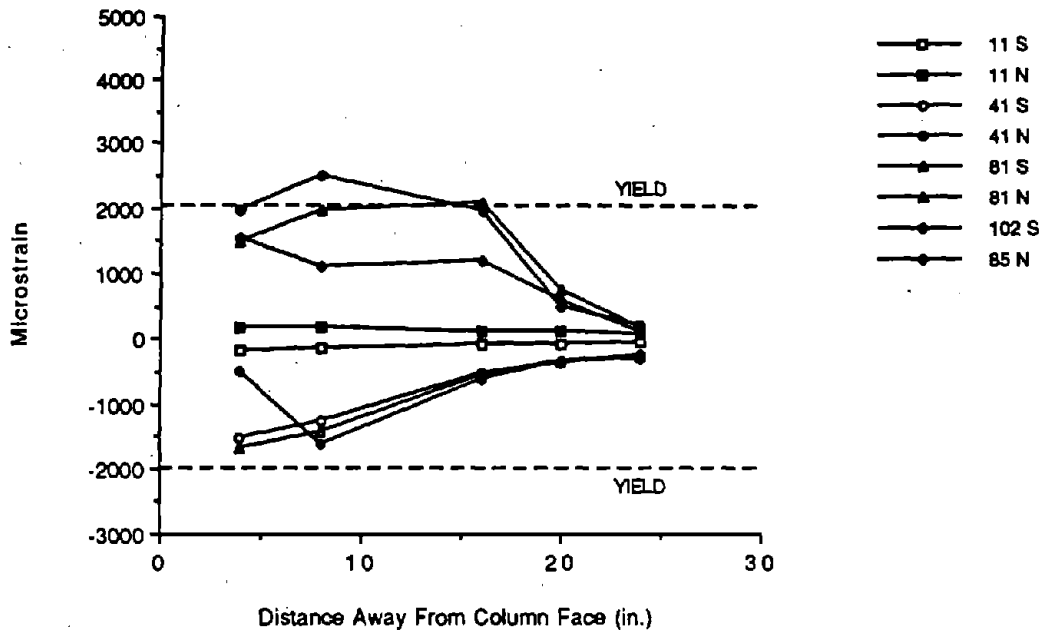
Fig. 4.51   Top southeast rebar strains for A-P-Z4.
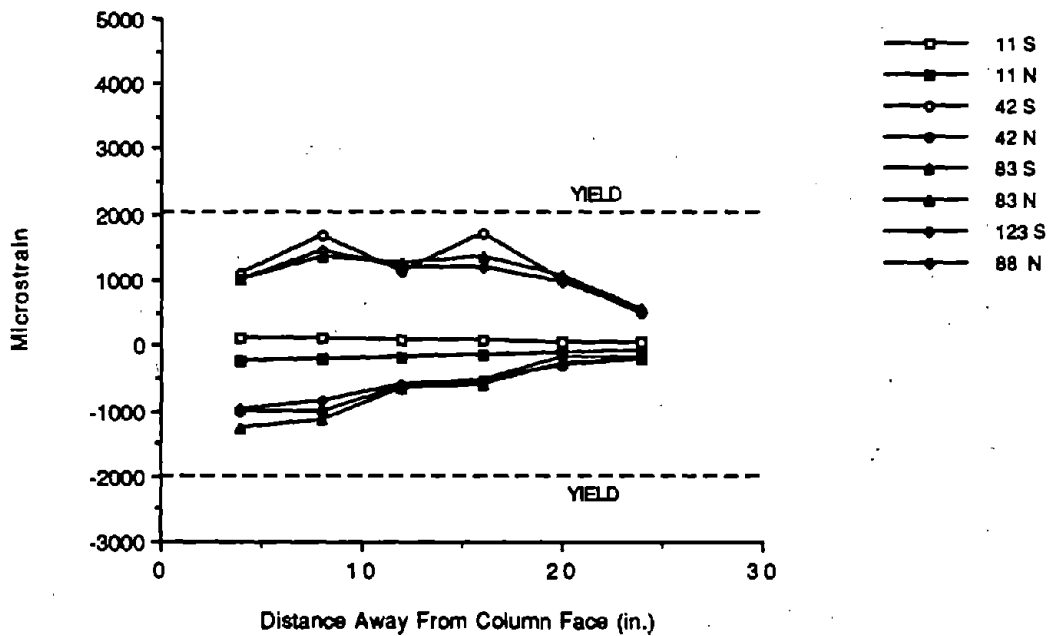
Fig. 4.52   Bottom southeast rebar strains for A-P-Z4.

71
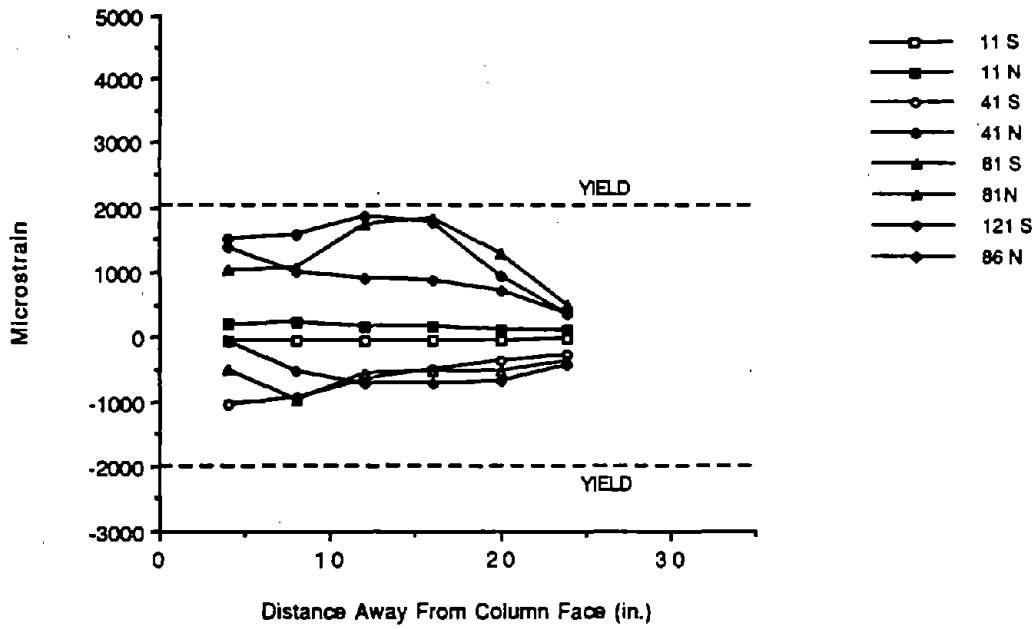
Fig. 4.53 Top southwest rebar strains for A-P-Z4.
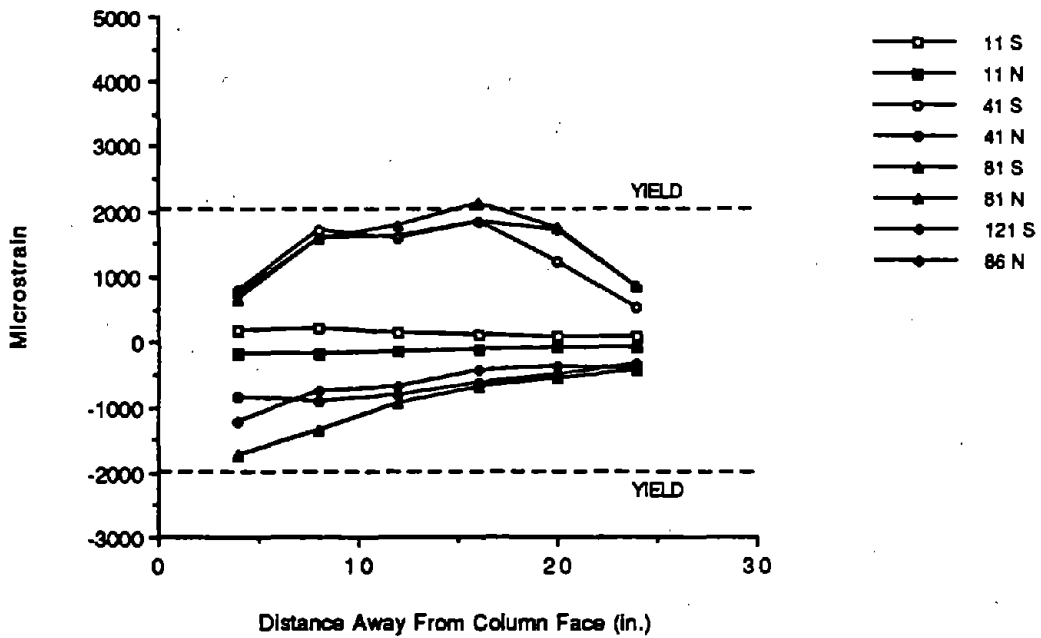
Fig. 4.54 Bottom southwest rebar strains for A-P-Z4.
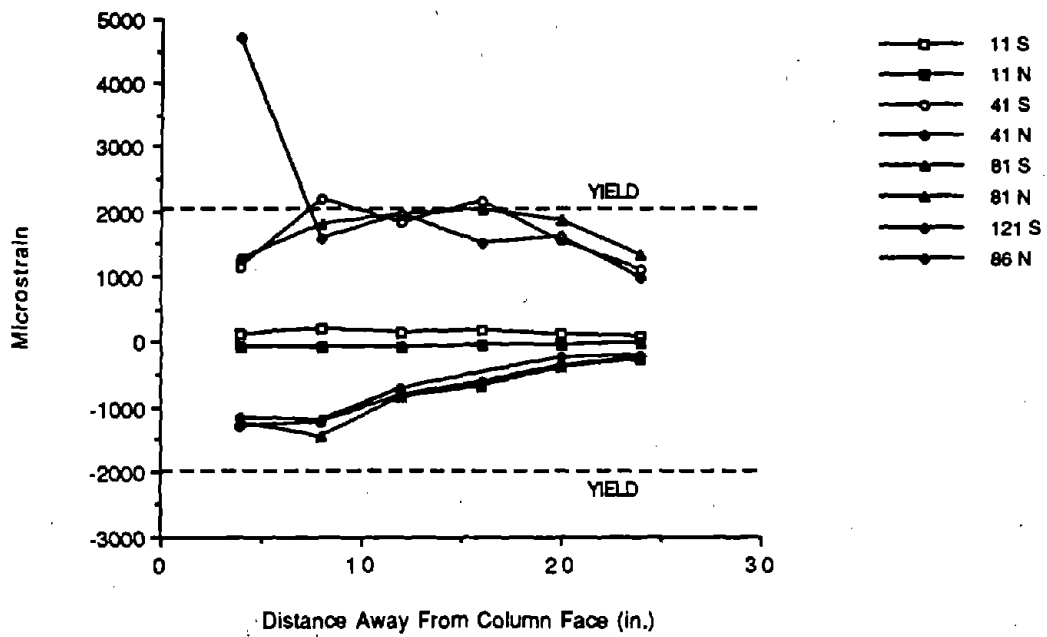
Fig. 4.55 Top northeast rebar strains for B-P-Z4.
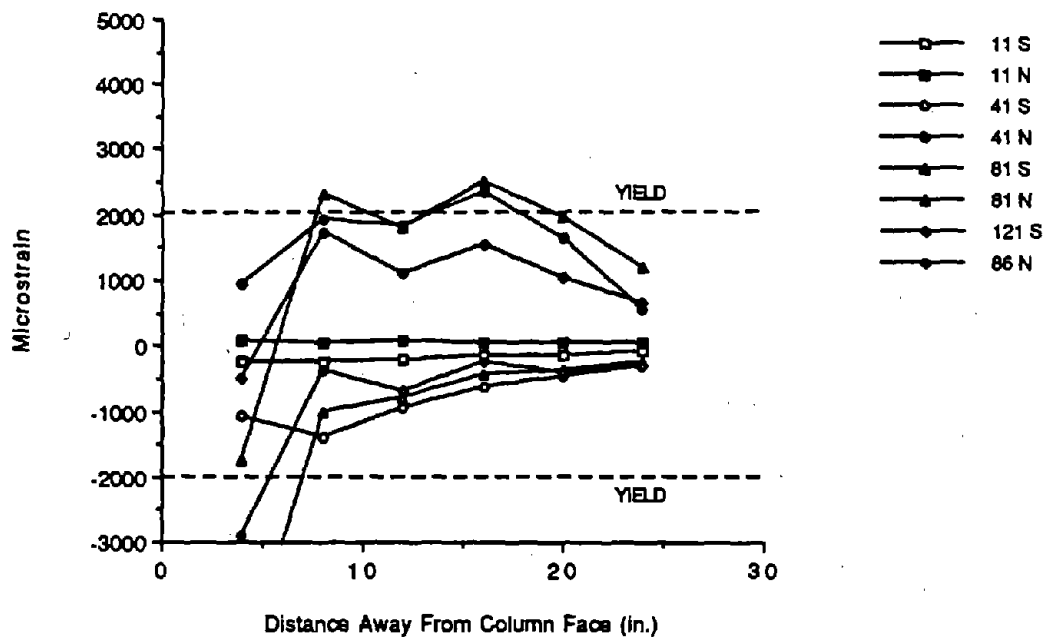
Fig. 4.56 Bottom northeast rebar strains for B-P-Z4.
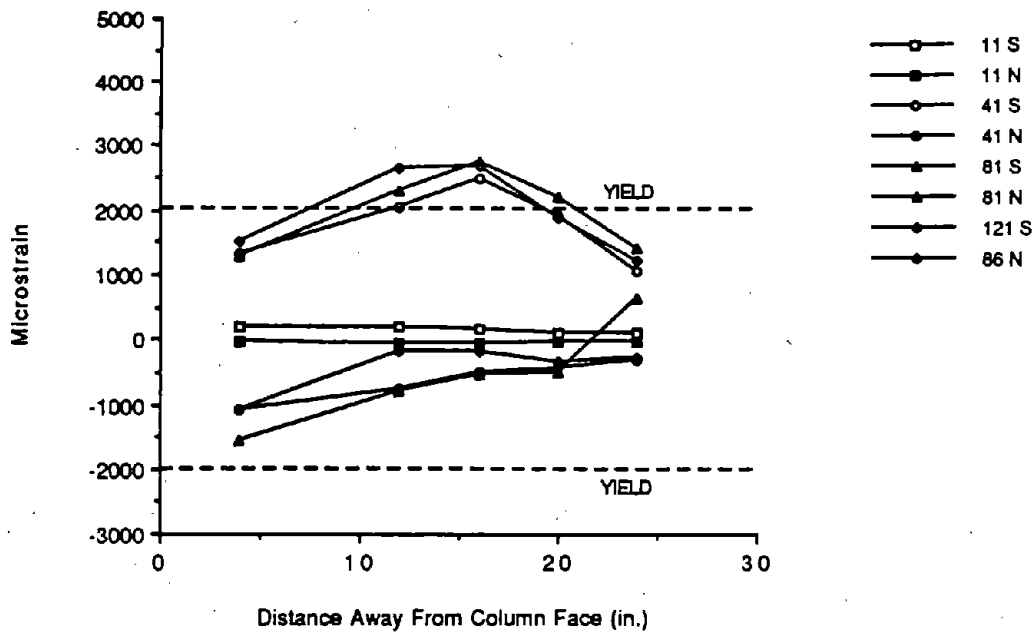
Fig. 4.57 Top northwest rebar strains for B-P-Z4.
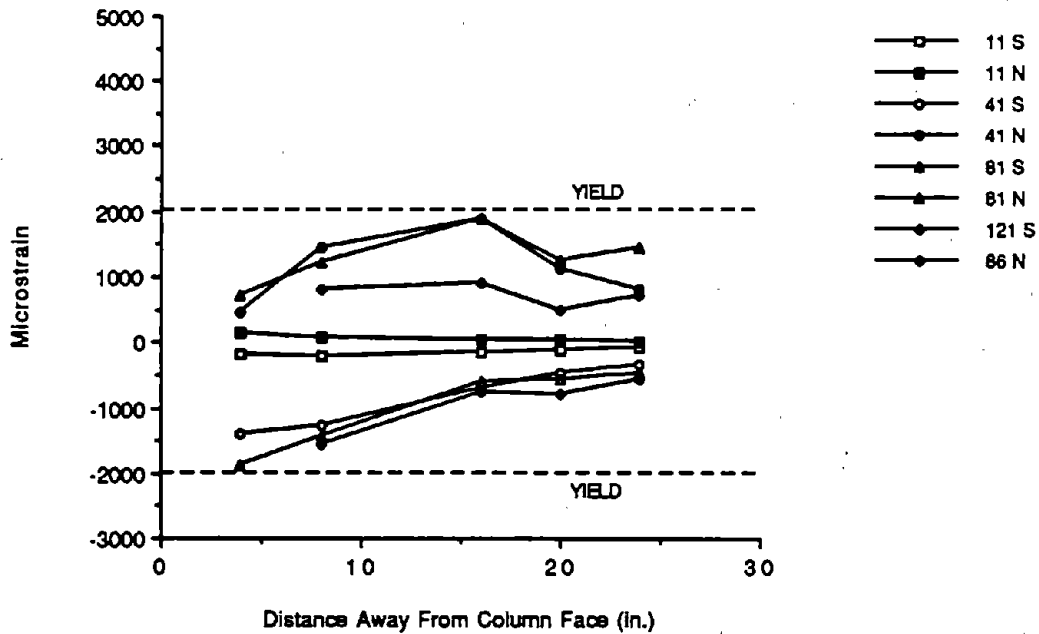
Fig. 4.58 Bottom northwest rebar strains for B-P-Z4.
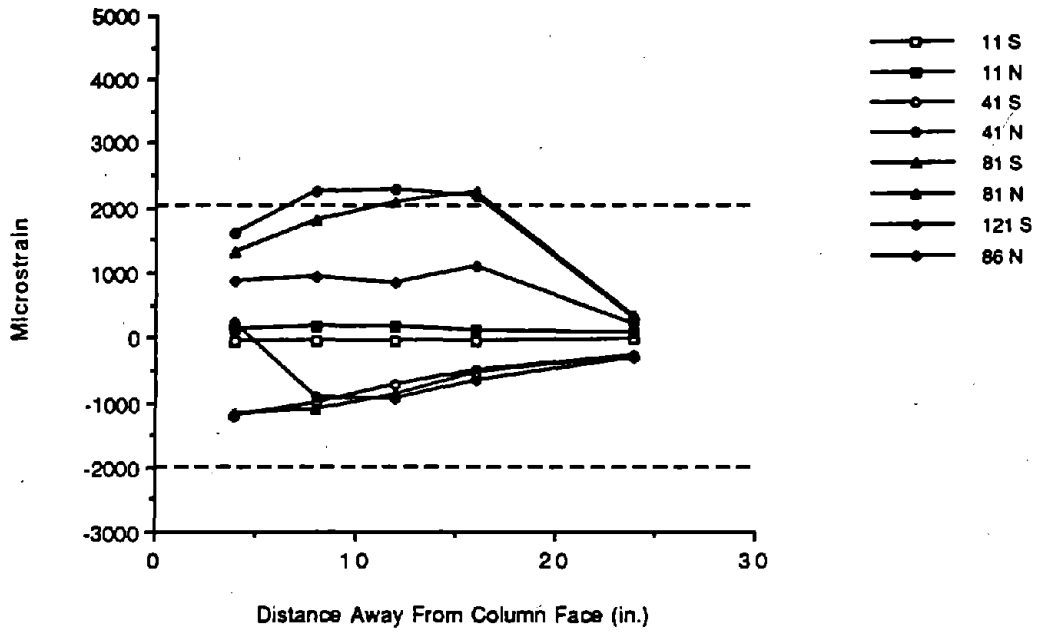
Fig. 4.59 Top southeast rebar strains for B-P-Z4.
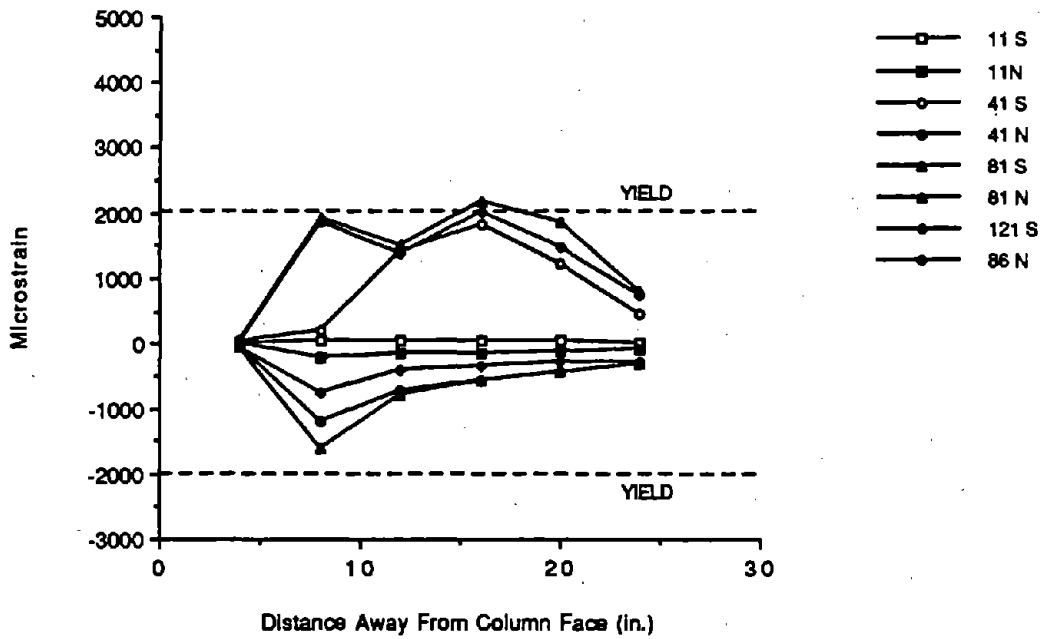
Fig. 4.60 Bottom southeast rebar strains for B-P-Z4.
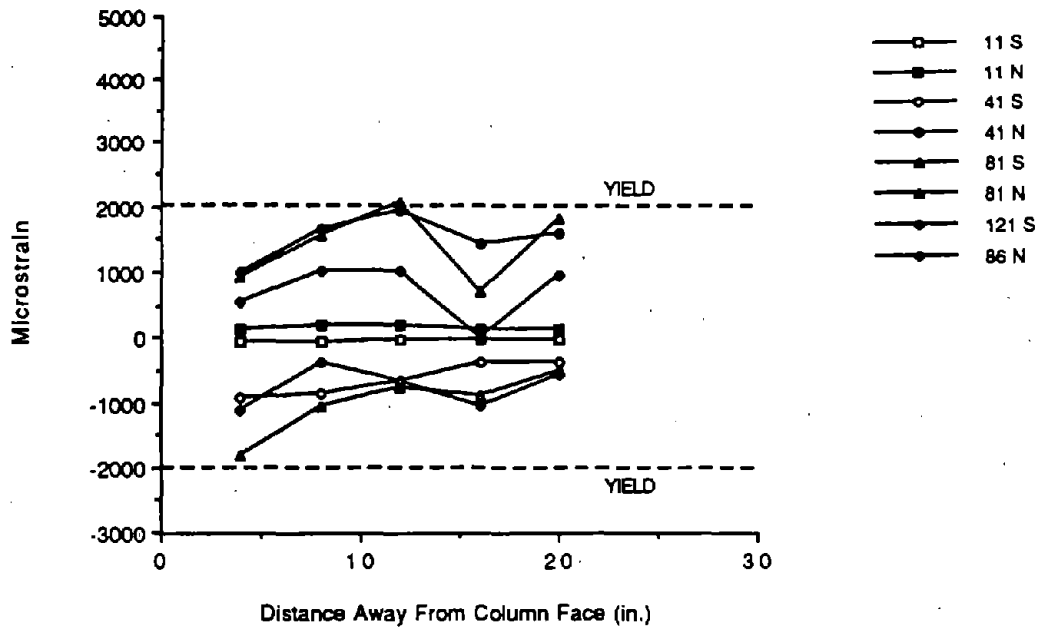
Fig. 4.61   Top southwest rebar strains for B-P-Z4.
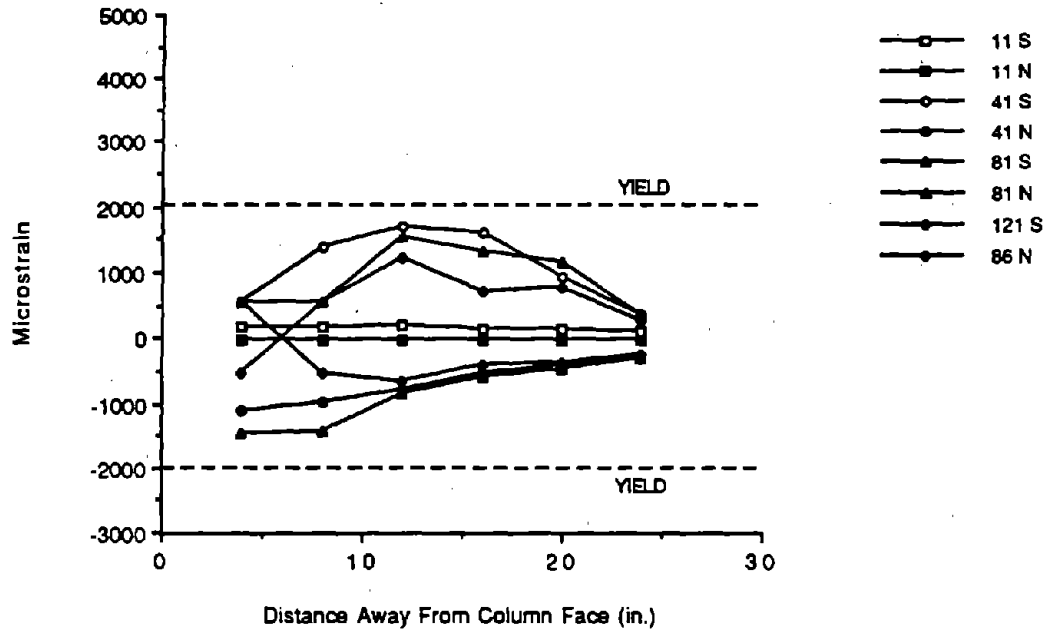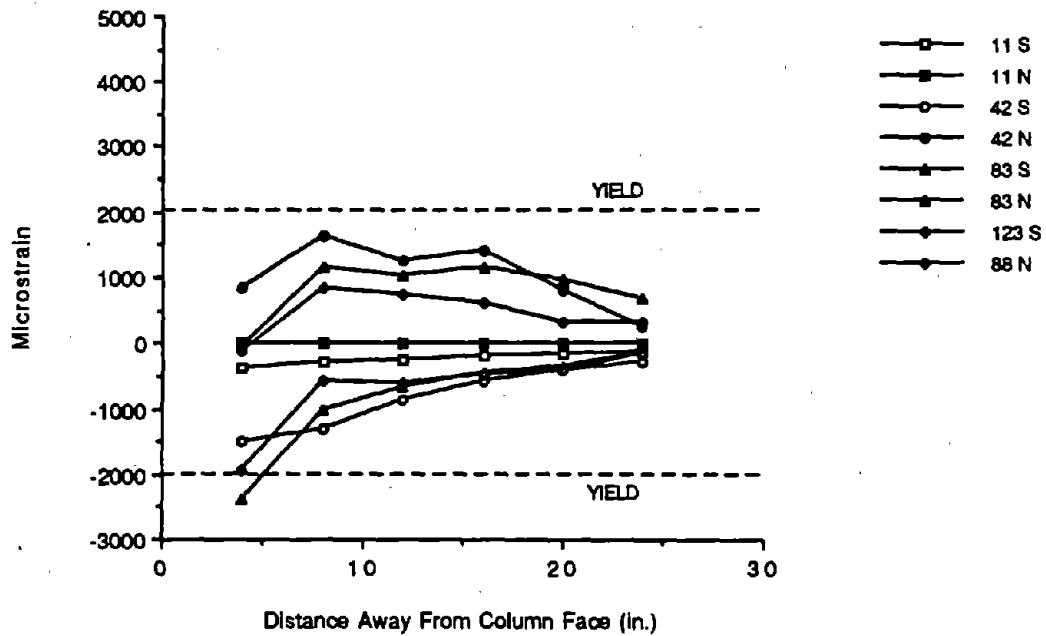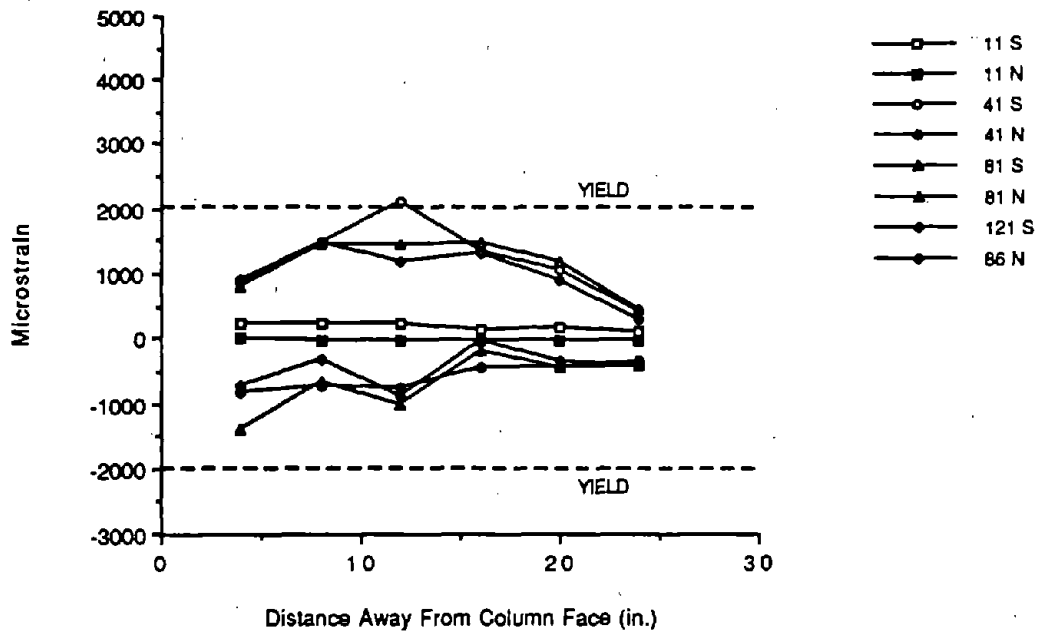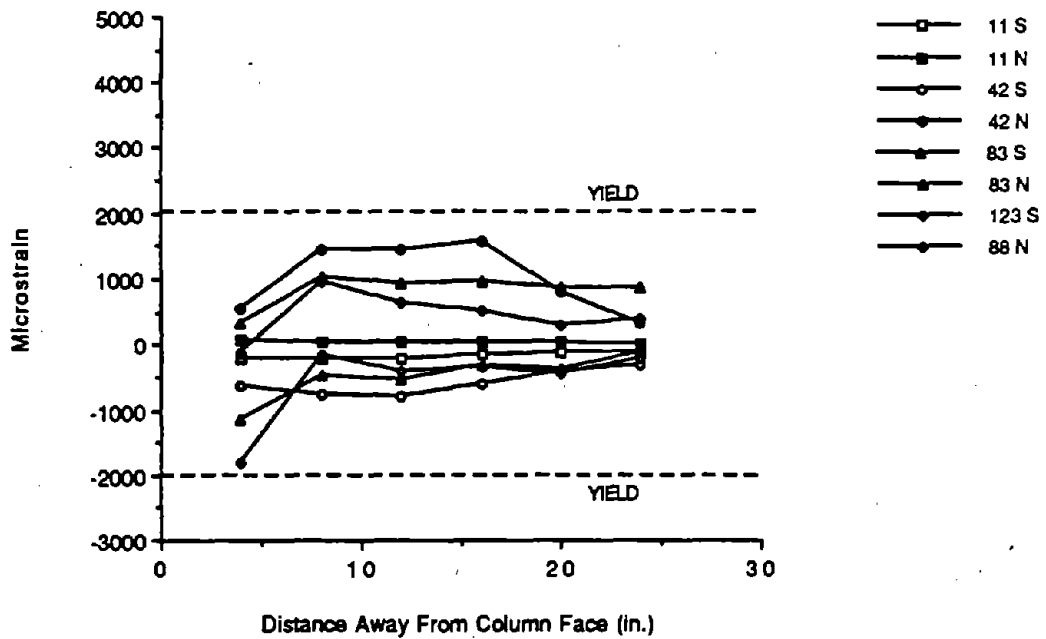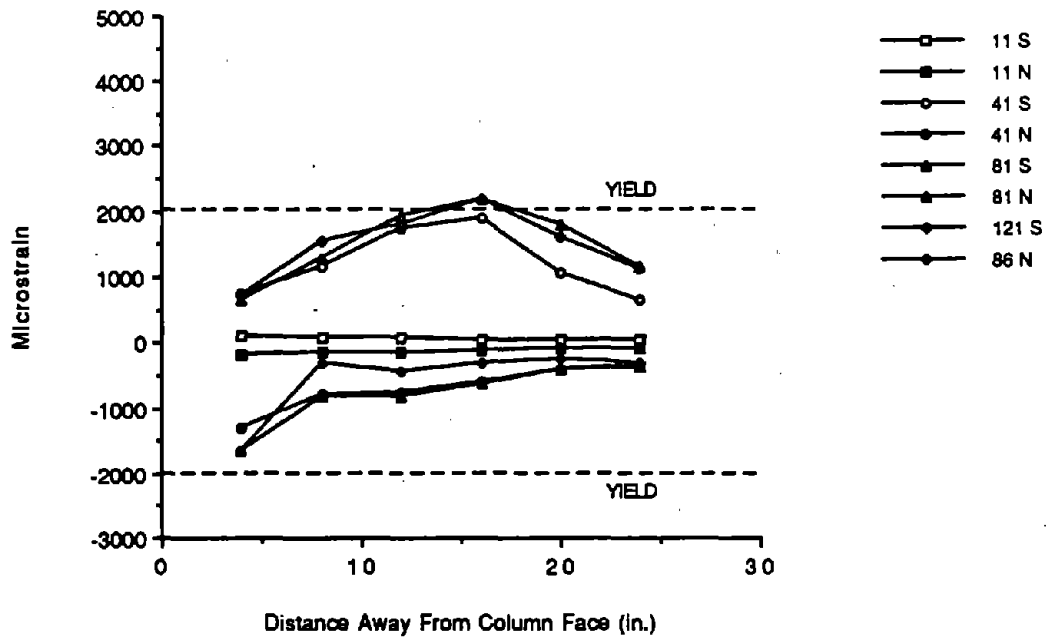

Fig. 4.62   Bottom southwest rebar strains for B-P-Z4.

5.0   DISCUSSION OF TEST RESULTS

5.1   Displacement Ductility

As expected, the ultimate displacement ductilities of the monolithic zone 2 specimens were lower than for the zone 4 specimens. The ultimate displacement ductilities, μ_u, and the ultimate story drifts for all the specimens are listed in Table 5.1. Story drift is defined as the ratio of the story displacement to the story height.

Table 5.1   Yield Displacement and Displacement Ductility.

Specimen	f'_c[1] (psi)	Exp. Yield Displacement (in.)	μ_u	Connection Stiffness (k/in.)	Ult. Story Drift (%)
A-M-Z2	6314	0.359	4	44	2.76
B-M-Z2	5962	0.371	6	38	4.28
A-M-Z4	4452	0.263	6	121	3.02
B-M-Z4	4675	0.293	6	103	3.38
A-P-Z4	5891	0.160	10	204	3.07
B-P-Z4	6450	0.179	10	216	3.44

[1]   These strengths were obtained at the time of the specimen tests.   See Table 3.2 for the 28-day strengths.

From the results of the monolithic zone 2 specimen tests, it would appear that the ultimate ductility is somewhat variable for connections failing in the joint region, and for which shear is the predominantly mode of failure.   This is, however, based on 2 tests and more tests will have to be performed to confirm this finding.

77

Although the post-tensioned specimens achieved higher displacement ductilities than the monolithic specimens, the ultimate story drifts were essentially equal for both sets of zone 4 specimens. This was because the post-tensioned specimens were stiffer than the monolithic zone 4 specimens. As shown in Table 5.1, the post-tensioned specimens were approximately twice as stiff as their companion monolithic specimens and five times as stiff as the monolithic zone 2 specimens. The initial elastic flexural stiffness was obtained from the load-displacement plot for the first cycle to 0.75 Δ_y on the initial excursion. A regression analysis was used to determine the stiffness of the subassemblage. Figs. 5.1 - 5.6 show the load displacement plots for the initial excursion at 0.75 Δ_y with the regression line superimposed. The connection stiffnesses in Table 5.1 were obtained from the slopes of these regression lines.
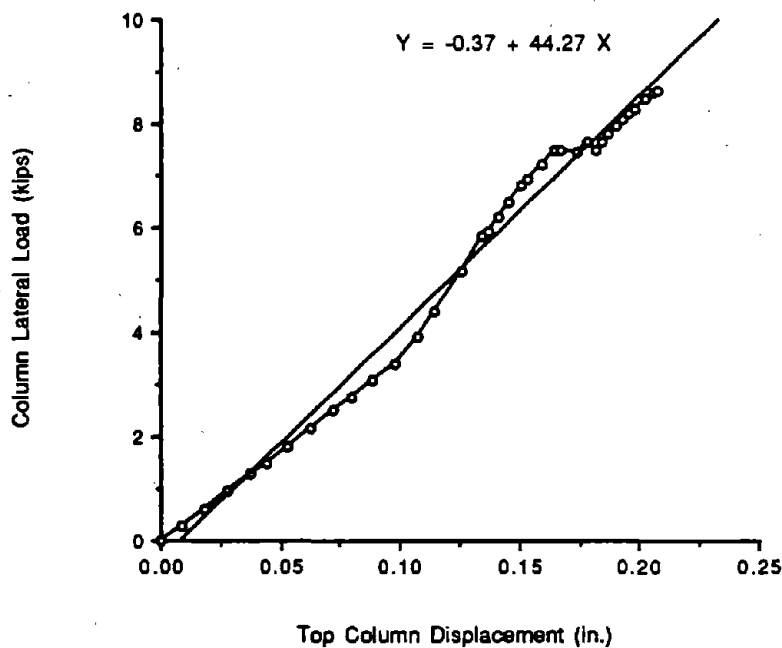
Fig. 5.1 Initial elastic flexural stiffness for A-M-Z2.
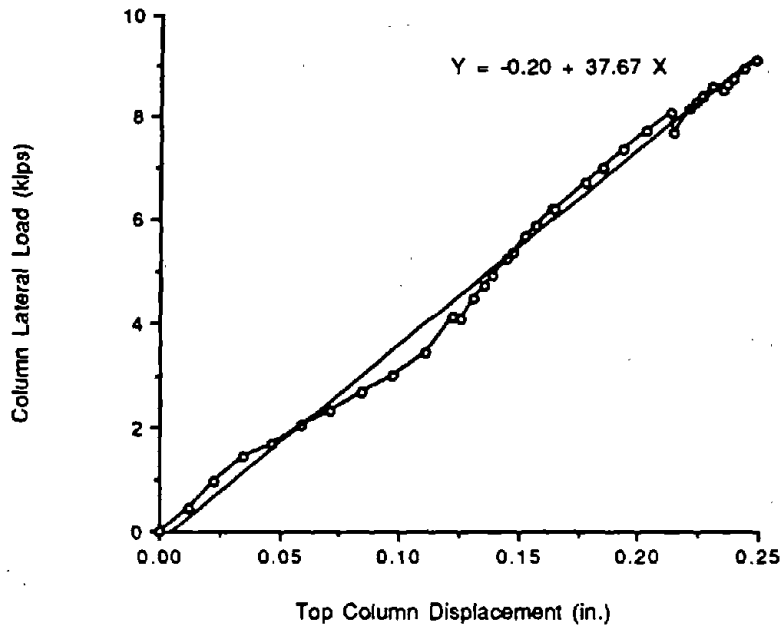
Fig. 5.2 Initial elastic flexural stiffness for B-M-Z2.
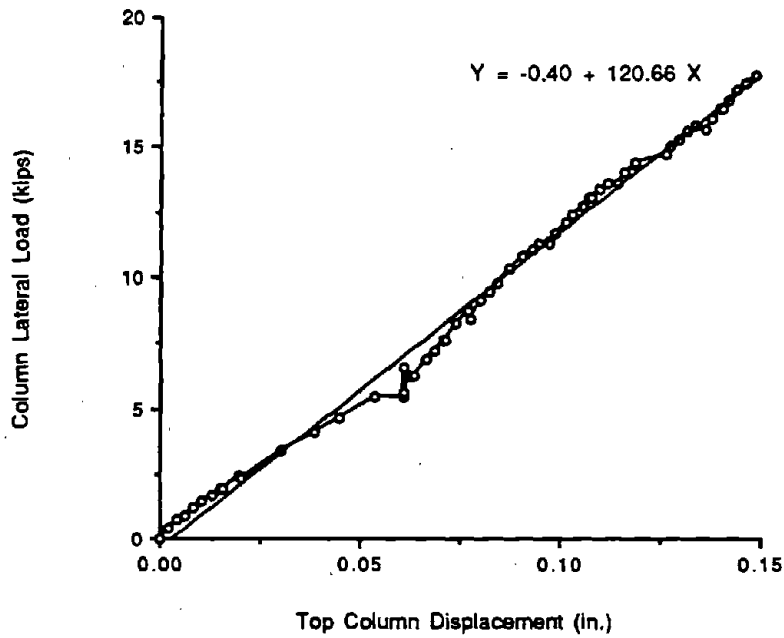
Fig. 5.3 Initial elastic flexural stiffness for A-M-Z4.

79
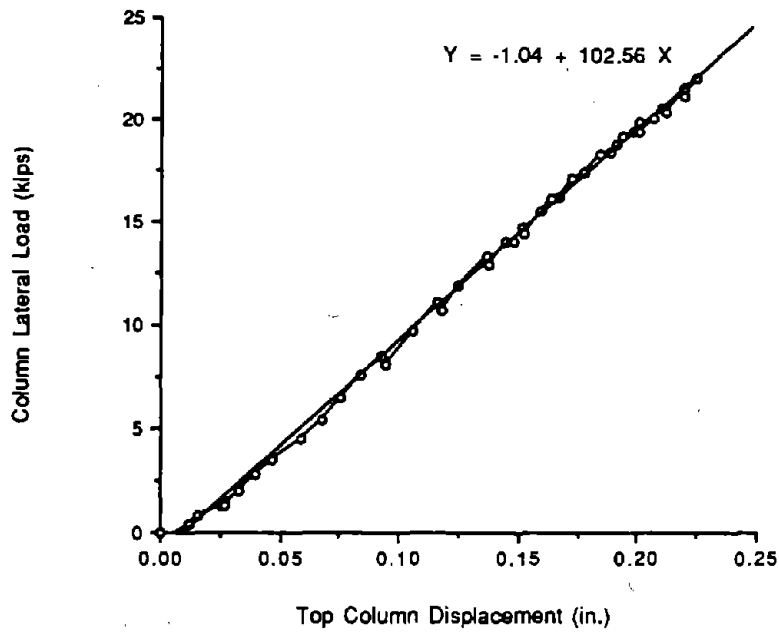
Fig. 5.4 Initial elastic flexural stiffness for B-M-Z4.
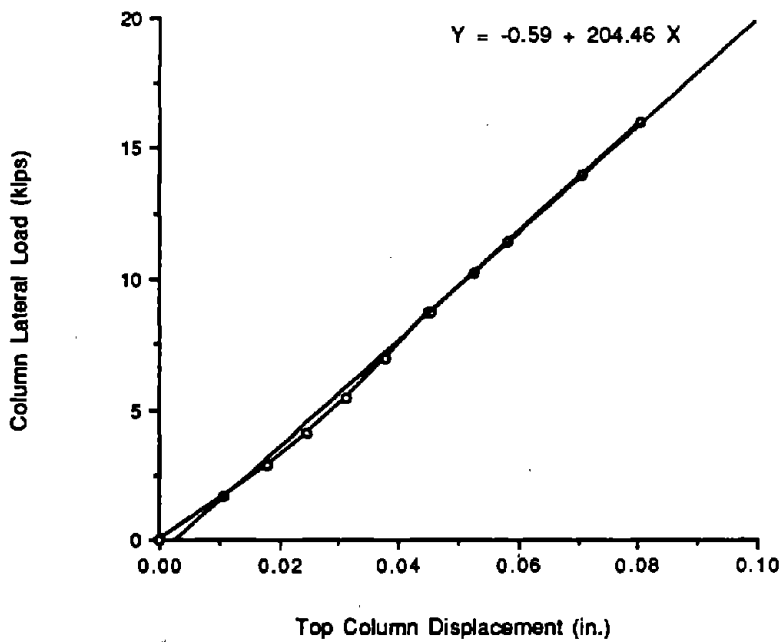
Fig. 5.5 Initial elastic flexural stiffness for A-P-Z4.

80

$$Y = -0.57 + 216.46 \ X$$
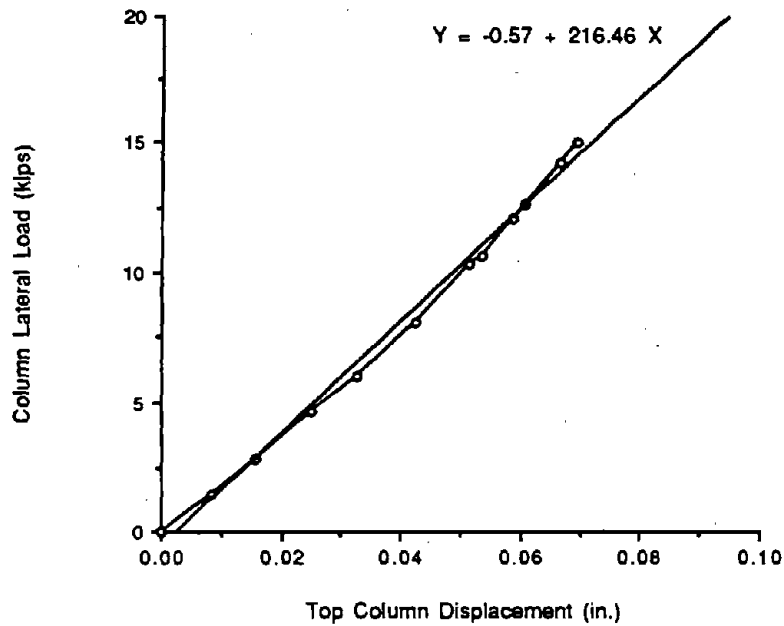
Fig. 5.6 Initial elastic flexural stiffness for B-P-Z4.

5.2 Ultimate Moments

The calculated and experimental beam moments are given in Table 5.2. The calculated values were based on an ultimate concrete strain of 0.003 and actual material properties. A factor of 1.25 was applied to the yield stress to account for steel strain hardening for the monolithic specimens. No factor was applied to the yield stress for the post-tensioned specimens to account for strain hardening as the yield stress of the post-tensioning bars was 148.5 ksi and the ultimate stress was 159.7 ksi. The experimental beam moments were obtained by multiplying the peak beam load as recorded by the load cell by the lever arm.

Table 5.2   Comparison of the Ultimate Beam Moments.

Specimen	f'_c[1] (psi)	Calculated Ultimate Moment (k-ft)	Experimental Ultimate Moment[2] (k-ft)	Avg. Exp. Mom. Calc. Ult. Mom.
A-M-Z2	6314	50.0	51 & 59	1.10
B-M-Z2	5962	50.0	52 & 55	1.07
A-M-Z4	4452	97.0	109 & 106	1.11
B-M-Z4	4675	97.0	109 & 113	1.14
A-P-Z4	5891	114.0	130 & 135	1.16
B-P-Z4	6450	114.0	136 & 137	1.20

[1]   These strengths were obtained at the time of the specimen tests.   See Table 3.2 for the 28-day strengths.

[2]   These moments are moments at the column face. There are two values because the specimens were interior joints.

The average of the four experimental ultimate beam moments for the monolithic zone 2 specimens is 54 k-ft. This value is 8.5% higher than the calculated ultimate moment. However, it should be noted that it was the deterioration of the column joint region which led to the eventual failure of the connection and not beam degradation. The ultimate moment for the column using actual material properties with an axial load of 51.15 kips is 69 k-ft.

The average of the four experimental ultimate moments for the monolithic zone 4 specimens is 109 k-ft and 134 k-ft for the post-tensioned specimens. These values are 12.4% and 17.5% higher than the calculated moments for the monolithic and post-tensioned specimens, respectively. The higher value for the post-tensioned specimens as compared with the monolithic specimens could in part be

82

a result of strain hardening of the post-tensioning bars which was not taken into account.

5.3 Joint Stress

The joint shear stresses for monolithic specimens A-M-Z2 and B-M-Z2 were 1.62 ksi and 1.64 ksi, respectively. These stresses were computed using actual material properties and the following equations:

$$V_{u \, col} = (M_{bm \, 1} + M_{bm \, 2}) / H \tag{5.1}$$

$$V_{u \, jt} = f_y A_{st} + f_y A_{sb} - V_{u \, col} \tag{5.2}$$

$$v_n = V_{u \, jt} / \phi A_{cv} \tag{5.3}$$

$$A_{cv} = b_E d$$

$V_{u \, col}$ = Shear force in column

$V_{u \, jt}$ = Shear force in joint

v_n = Joint shear stress

A_{cv} = Effective shear area

$M_{bm \, 1,2}$ = Moment in beams

H = Story height

f_y = Yield stress of steel

A_{st} = Area of top beam steel

A_{sb} = Area of bottom beam steel

ϕ = Undercapacity factor (ϕ = 1 was used)

b_E = Width taken to outside of column for confined sections

= Width measured to the outside of the ties, for all other sections

d = Distance to the centroid of steel

These stresses are greater than $20 \sqrt{f_c'}$ which is the maximum allowable joint stress recommended by ACI-ASCE Committee 352. A lack of sufficient transverse confinement led to joint failure in the monolithic zone 2 specimens prior to the onset of beam failure.

The calculated joint shear stress using actual material properties for the monolithic zone 4 specimens is approximately one third of the maximum recommended shear stress of $20 \sqrt{f_c'}$. This low joint stress was evidenced by the excellent performance of the joint for the duration of the test. The joint shear stress for the post-tensioned specimens is approximately 2/3 of the maximum recommended shear stress. The experimental value may be less than this calculated value due to slippage of the post-tensioning bar and/or duct in the column region.

5.4 Energy Dissipation

A comparison of the energy dissipated, as defined in Section 4.1, on a per cycle basis up to 6 Δ_y, cycle 3 is given in Fig. 5.7 for all the specimens. The energy dissipated at various stages in the test is given in Table 5.3. As seen in Fig. 5.7 and Table 5.3, the energy dissipated by the post-tensioned specimens was closer in range to the energy dissipated by the monolithic zone 2 beam-column connections.

84
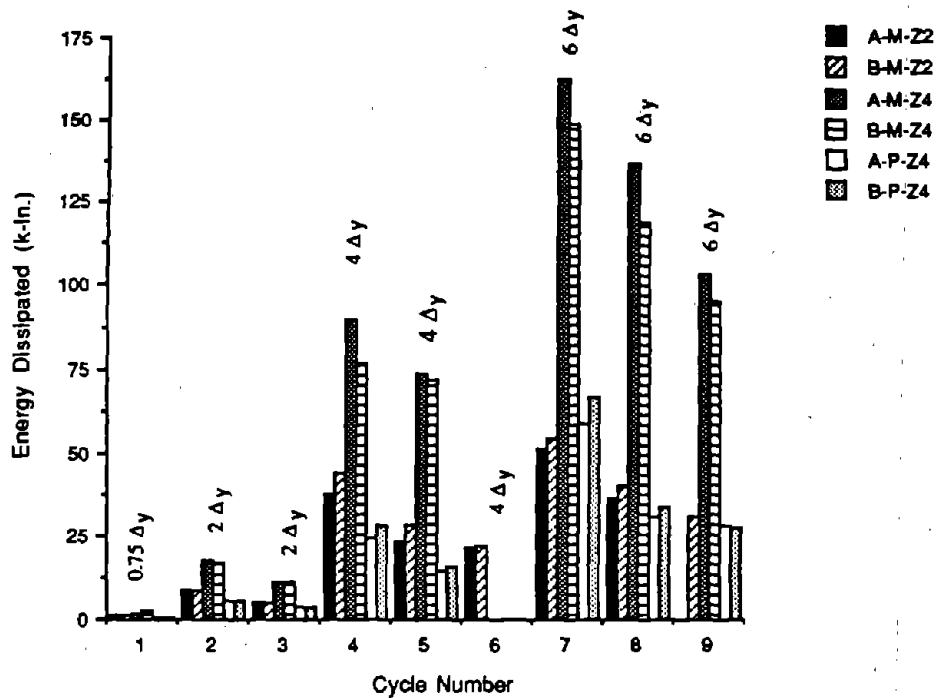
Fig. 5.7 Comparison of the cyclic energy dissipated up to 6 Δ_y, cycle 3 for all the specimens.

Table 5.3 Comparison of the Energy Dissipation.

| Specimen | μ_u | Cumulative Energy Dissipated (k-in) | | |
		to Failure (k-in)	to 6 Δ_y, cycle 3 (k-in)	to 12 Δ_y (k-in)
A-M-Z2	4	77	165[1,2]	-
B-M-Z2	6	204	212[2]	-
A-M-Z4	6	597	597	-
B-M-Z4	6	543	543	-
A-P-Z4	10	438	165	507
B-P-Z4	10	477	181	550

1   Cumulative energy dissipated through 6 Δ_y, cycle 2.

2   For purposes of comparison, the energy dissipated in the third cycle at 4 Δ_y was not included in this summation as the zone 4 specimens did not undergo this particular cycle.

On a per cycle basis, the energy dissipated by the post-tensioned specimens was approximately 30% of the energy dissipated by the monolithic specimens. The average of the total energy dissipated by the post-tensioned connections was approximately 20% lower than the energy dissipated to failure by the monolithic zone 4 specimens.

As stated in Chapter 4, the ultimate displacement ductility for the post-tensioned specimens was conservatively considered to be 10. If the ultimate displacement ductility was considered to be 12 instead of 10, the summation of energy dissipated up to the first cycle at 12 Δ_y would be 507 k-in and 550 k-in for specimens A-P-Z4 and B-P-Z4, respectively. The average of these two values is approximately 10% lower than the average of the total energy dissipated by the monolithic zone 4 specimens to failure.

5.5 Plastic Hinge Length

The plastic hinge length was defined as the length over which the curvature exceeded the yield curvature. Axial displacement was obtained at 3 locations along the top and bottom faces of each beam to determine the extent of plastic hinging. The experimental plastic hinge lengths for the monolithic zone 2 specimens were 11.36 in. (L/D - 1.14) and 11.52 in. (L/D - 1.15) for A-M-Z2 and 11.36 in. (L/D - 1.14) and 10.45 in. (L/D - 1.05) for B-M-Z2. These plastic hinge lengths were obtained from LVDT data. The plastic hinge lengths as calculated using rebar strains were 17.2 in. (L/D - 1.72) and 19.2 in. (L/D - 1.92) for A-M-Z2 and 21 in. (L/D - 2.10) and 19.3 in. (L/D - 1.93) for B-M-Z2).

The experimental plastic hinge lengths as obtained from LVDT data for the monolithic zone 4 specimens were at least 16 in. (L/D > 1.0) Determination of the exact plastic hinge length from LVDT data was not possible due to a lack of LVDTs beyond 16 in. from the column face. The plastic hinge lengths as calculated using rebar strains were 27.5 in. (L/D - 1.72) for both beams of A-M-Z4 and 34 in. (L/D - 2.13) and 28.75 in. (L/D - 1.80) for B-M-Z4.

Unfortunately, the experimental plastic hinge length for the post-tensioned specimens could not be determined. This was because the opening between the beam and column was not monitored during the tests, and the readings obtained from the LVDTs could not be corrected to account for this movement. The strain data from the regular (unstressed) reinforcement was not be used for computing the beam curvature. This was because the post-tensioning bars provided the moment resisting capacity of the connections as noted in Chapter 4.

However, it is noted that the average extent of the rebar yield was 10.7 in. (L/D - 0.67) for the precast specimens as compared to 21 in. (L/D - 1.31) for the monolithic zone 4 specimens. Therefore, based on observations during the tests and from the low strains in the precast beam reinforcement, it would appear that the plastic hinge lengths were less for the post-tensioned specimens than for the monolithic specimens.

NOTE:
1 in. - 25.4 mm
1 kip - 4.448 kN
1 k-in. - 112.98 N-m
1 ksi - 6.895 MPa

6.0 SUMMARY AND CONCLUSIONS

6.1 Summary

In Phase I of the precast concrete beam-column connection study at NIST, six specimens were tested. Two of the specimens were monolithic concrete connections designed to UBC (1985) seismic zone 2 criteria. The other four specimens were designed to UBC (1985) seismic zone 4 criteria. Two of the zone 4 specimens were monolithic specimens while the remaining two were precast concrete with post-tensioned beam-column connections. The precast elements were connected by two post-tensioning bars. The construction joint between the beam and column was filled with a fiber reinforced grout and the post-tensioning ducts were grouted after tensioning.

Results from the monolithic tests are used as a benchmark reference for both present and future precast concrete tests. The objective of the test program was to develop an economical moment-resistant precast beam-to-column connection for seismically active regions. The following section presents the conclusions drawn from the results of the Phase I tests.

6.2 Conclusions

Failure of the monolithic zone 2 specimens occurred in the joint region due to a combination of high joint stresses and inadequate confinement. The monolithic zone 4 specimens failed as a result of beam hinging and deterioration. Failure of the post-tensioned specimens was characterized by plastic elongation, 1/2 in.,

of the post-tensioning bars and crushing and spalling of the concrete cover in the beams. Joint shear stresses for the zone 4 specimens were below the recommended value of $20 \sqrt{f_c'}$.

The ultimate displacement ductilities for the monolithic zone 2 specimens were 4 and 6. These ductilities corresponded to story drifts of 2.8% and 4.3%. The ultimate displacement ductility for the post-tensioned specimens were higher than for their companion monolithic specimens - 10 vs. 6. However, since the post-tensioned specimens were stiffer than the monolithic specimens, the story drift at failure for the zone 4 post-tensioned and monolithic specimens were almost identical. The story drifts for the zone 4 specimens ranged from 3% - 3.4%. The post-tensioned specimens were approximately twice as stiff as the monolithic zone 4 specimens and fives times as stiff as the monolithic zone 2 specimens.

The post-tensioned connections were slightly stronger than the monolithic specimens. The ultimate beam moments were on the average 18% greater than the calculated moments for the post-tensioned specimens and 13% greater for the monolithic zone 4 specimens. The monolithic zone 2 specimens achieved ultimate beam moments that were on the average 8% greater than the calculated moment.

When comparing the energy dissipated per cycle, the behavior of the post-tensioned specimens was more similar to the monolithic zone 2 specimens than to the monolithic zone 4 specimens. On a per cycle basis, the post-tensioned specimens dissipated about 30% of the energy dissipated by the monolithic zone 4 specimens. However, since the post-tensioned specimens achieved higher displacement ductilities than the monolithic specimens, the average of the total

energy dissipated up to failure by the post-tensioned specimens was approximately 80 % of that for the monolithic specimens. The average of the total energy dissipated up to failure by the monolithic zone 2 specimens is about 33% of that dissipated by the monolithic zone 4 specimens.

Based on the results of the Phase I test program, it would appear that a post-tensioned precast concrete beam-column connection is a viable solution for precast concrete connections in high seismic regions. Acceptance of this type of connection by the engineering community will depend on more research data and a better understanding of connection behavior. It will also depend on the criteria used for acceptance; one based on energy dissipation and/or one based on ductility demand.

NOTE:
1 in. = 25.4 mm
1 kip = 4.448 kN
1 k-in. = 112.98 N-m
1 ksi = 6.895 MPa

REFERENCES

1. Applied Technology Council, "Design of Prefabricated Concrete Buildings for Earthquake Loads", Berkeley, CA, 1981.

2. Bhatt, P. and Kirk D. W., "Tests on an Improved Beam Column Connection for Precast Concrete", American Concrete Institute Journal, Detroit, MI, November-December, 1985, pp. 834-843.

3. Blakeley, R. W. G. and Park, R., "Seismic Resistance of Prestressed Concrete Beam-Column Assemblies", American Concrete Institute Journal, Detroit, MI, September, 1971, pp. 677-692.

4. Bull, D. K. and Park, R., "Seismic Resistance of Frames Incorporating Precast Prestressed Concrete Beam Shells", Prestressed Concrete Institute Journal, Chicago, IL, July-August 1986, pp. 54-93.

5. Cheok, G. S. and Stone, W. C., "Behavior of 1/6-Scale Model Bridge Columns Subjected to Cyclic Inelastic Loading", NBSIR 86-3494, National Bureau of Standards, Gaithersburg, MD, November, 1986.

6. Clarke, J. L., "The Behavior of a Precast Beam-Column Joint", Precast Concrete, United Kingdom, October, 1978, pp. 503-504.

7. Clough, D. P., "Design of Connections for Precast Prestressed Concrete Buildings for the Effects of Earthquake", Technical Report No. 5, Prestressed Concrete Institute, Chicago, IL, March, 1985.

8. French, C. W., et. al., "Connections Between Precast Elements - Failure Within Connection Region", ASCE Journal of Structural Engineering, New York, NY, December, 1989, pp. 3171-3192.

9. French, C. W., et. al., "Connections Between Precast Elements - Failure Outside Connection Region", ASCE Structural Journal, New York, NY, February, 1989, pp. 316-340.

10. Hawkins, N. M. and Englekirk, R. E., "U.S.-Japan Seminar on Precast Concrete Construction in Seismic Zones", Prestressed Concrete Institute Journal, Chicago, IL, March-April, 1987, pp. 75-85.

11. Imai, H. and Kanoh, Y., "Standard for Performance Evaluation of Rebar Joints", Proceedings of the US/Japan Seminar on Precast Concrete Construction in Seismic Zones, Vol. 2, Tokyo, Japan, October, 1986, pp. 137-156.

12. International Conference of Building Officials, Uniform Building Code, Whittier, CA., 1985.

13. Kanoh, Y., "Review of Japanese Precast Concrete Frame Structures Used as Building Structures", Seminar on Precast Concrete Construction in Seismic Zones, Japan Concrete Institute, Japan, 1986, pp. 35-54.

93

14. Martin, L. D. and Korkosz, W. J., "Connections for Precast Prestressed Concrete Buildings", Technical Report No. 2, Prestressed Concrete Institute, Chicago, IL, March, 1982.

15. Pillai, S. U. and Kirk, D. W., "Ductile Beam-Column Connection in Precast Concrete", American Concrete Institute Journal, Detroit, MI, November-Decemeber, 1981, pp. 480-487.

16. Reinhardt, H. W. and Stroband, J., "Load Deformation Behaviour of the Cutting Dowel Connection", Mechanical & Insulating Properties of Joints of Precast Reinforced Concrete Elements, Proceedings of the RILEM-CEB-CIP Symposium, Vol. I, Greece, September, 1978, pp. 197-208.

17. Seckin, M. and Fu, H. C., "Beam-Column Connections in Precast Reinforced Concrete Constrution", American Concrete Institute Structural Journal, Detroit, MI, May-June, 1990, pp. 252-261.

18. Soubra, K. S., et. al., "Fiber Reinforced Concrete Connections for Earthquake Resistant Design of Precast Reinforced Concrete Structures", Report No. UMCE 89-13, University of Michigan, Ann Arbor, MI, October, 1989.

19. Stanton, J. F., et. al, "Moment Resistant Connections and Simple Connections", Research Project No. 1/4, Prestressed Concrete Institute, Chicago, IL, 1986.

20. Wilby, C. B., "Structural Behavior of a Special Type of Joint for Connecting Precat Concrete Members", Mechanical & Insulating Properties of Joints of Precast Reinforced Concrete Elements, Proceedings of the RILEM-CEB-CIP Symposium, Vol. II, Greece, September, 1978, pp. 489-501.

21. Woodward, K. and Rankin, F, "The NBS Tri-Directional Test Facility", NBSIR 84-2879, National Bureau of Standards, Gaithersburg, MD, 1984.

U.S. DEPARTMENT OF COMMERCE
NATIONAL INSTITUTE OF STANDARDS AND TECHNOLOGY

NIST-114A
(REV. 3-90)

BIBLIOGRAPHIC DATA SHEET

1. **PUBLICATION OR REPORT NUMBER**
NISTIR 4433

2. **PERFORMING ORGANIZATION REPORT NUMBER**

3. **PUBLICATION DATE**
OCTOBER 1990

4. **TITLE AND SUBTITLE**

Performance of 1/3-Scale Model Precast Concrete Beam-Column Connections Subjected to Cyclic Inelastic Loads

5. **AUTHOR(S)**

Geraldine S. Cheok and H. S. Lew

6. **PERFORMING ORGANIZATION (IF JOINT OR OTHER THAN NIST, SEE INSTRUCTIONS)**

U.S. DEPARTMENT OF COMMERCE
NATIONAL INSTITUTE OF STANDARDS AND TECHNOLOGY
GAITHERSBURG, MD 20899

7. **CONTRACT/GRANT NUMBER**

8. **TYPE OF REPORT AND PERIOD COVERED**

9. **SPONSORING ORGANIZATION NAME AND COMPLETE ADDRESS (STREET, CITY, STATE, ZIP)**

NIST CATAGORY #140

10. **SUPPLEMENTARY NOTES**

11. **ABSTRACT (A 200-WORD OR LESS FACTUAL SUMMARY OF MOST SIGNIFICANT INFORMATION. IF DOCUMENT INCLUDES A SIGNIFICANT BIBLIOGRAPHY OR LITERATURE SURVEY, MENTION IT HERE.)**

An experimental study of the behavior of precast concrete beam-column connections subjected to cyclic inelastic loading was initiated at the National Institute of Standards and Technology. The study was initiated to provide data for the development of a rational design procedure for such connections in high seismic regions. The objective of the study is to develop a moment resistant precast concrete connection that is economical and easily constructed. Results of the experimental tests of both monolithic and precast beam-column connections are described. The monolithic concrete specimens were designed to 1985 UBC Seismic Zone 2 and 4 criteria. The design of the precast concrete specimens was similar to that for the monolithic specimen designed to UBC seismic zone 4. The results from the monolithic specimens provide a benchmark for comparison with the results from the precast tests.

The experimental program is divided into three phases. This report presents the findings of the first phase of the test program. Comparisons of the performance of the monolithic beam-column joints with that of the precast joints in which the beam-to-column connection is provided by post-tensioning bars are presented. The effects of fiber reinforced grout between the beam and column are described. Comparisons are made between the energy dissipation, ductility, and failure mode for the two types of beam-column joints.

12. **KEY WORDS (6 TO 12 ENTRIES; ALPHABETICAL ORDER; CAPITALIZE ONLY PROPER NAMES; AND SEPARATE KEY WORDS BY SEMICOLONS)**

beam-column; buildings; connections; cyclic loadings; interior joints; joints; moment resistant; precast concrete; post-tensioned; reinforced concrete.

13. **AVAILABILITY**

| X | UNLIMITED |

FOR OFFICIAL DISTRIBUTION. DO NOT RELEASE TO NATIONAL TECHNICAL INFORMATION SERVICE (NTIS).

ORDER FROM SUPERINTENDENT OF DOCUMENTS, U.S. GOVERNMENT PRINTING OFFICE,
WASHINGTON, DC 20402.

| X | ORDER FROM NATIONAL TECHNICAL INFORMATION SERVICE (NTIS), SPRINGFIELD, VA 22161.

14. **NUMBER OF PRINTED PAGES**
104

15. **PRICE**
A06

ELECTRONIC FORM